POLITECNICO DI MILANO

Corso di Laurea Magistrale in Ingegneria Biomedica

Scuola di Ingegneria Industriale e dell'Informazione

Dipartimento di Elettronica, Informazione e Bioingegneria

Tesi di Laurea Magistrale

MECHANICS OF ARTICULAR CARTILAGE: DERIVATION AND NUMERICAL IMPLEMENTATION OF A VISCOELASTIC MODEL WITH STATISTICAL FIBRE DISTRIBUTION

Relatore: Prof. Pasquale VENA

Autore:

Gianluca GABELLINI

Matricola n. 765583

ANNO ACCADEMICO 2012–2013

ROYAL INSTITUTE
OF TECHNOLOGY

Viscoelastic modelling of articular cartilage

Gianluca Gabellini

Supervisor: T. Christian Gasser, Ph.D.

Master's Degree Project

Stockholm, Sweden 2013

KTH School of Engineering Sciences

Department of Solid Mechanics

Royal Institute of Technology

SE-100 44 Stockholm - Sweden

To my parents

Abstract

Articular cartilage is a multiphasic biological material characterized by complex mechanical properties. The solid phase is composed of a soft matrix reinforced by a three-dimensional network of collagen fibres and is particularly challenging to model as it exhibits non-linear anisotropic inhomogeneous viscoelastic response. In this work, a constitutive relation that accounts for these features was developed, while the fluid phase and related phenomena (i.e. poroelasticity) were disregarded. The model was developed in the framework of finite elasticity, as articular cartilage typically exhibits large deformations under physiological load. The elastic strain energy potential was defined as the superposition of an isotropic term associated with the ground matrix and an anisotropic term related to the collagen reinforcement. The fibre network was modelled in statistical terms using a probability density function from the literature, that provides at each point the probability of finding a fibre oriented in a given direction. The information about a single direction was enclosed into a so-called structure tensor, which was then integrated over the unit sphere to get its directional average, weighted by the probability distribution. Collagen fibres carry the load only when they are stretched. Hence, the contribution of compressed fibres to the average structure tensor was suitably modified to include the information about their distribution without influencing the strain energy potential. The intrinsic viscoelastic response was modelled adding a quasi-linear viscoelastic formulation for the collagen fibres, while the matrix was assumed to be elastic. This approach generates an overall non-linear viscoelastic response for the tissue, which is observed in experimental tests. The constitutive equations were linearised to derive the corresponding elasticity tensor and the model was implemented into a finite element analysis program that allows the definition of custom user subroutines. The averaging integrals where computed using the method of spherical designs, in which the result is approximated by a suitable sum over the unit sphere. The evolution equations were integrated using an efficient numerical scheme from the literature. In the last part of the work three representative numerical examples, based on published experimental data, where analysed with the aim of checking the physical response of the model. The results of these tests indicate that the model is capable of predicting the response of articular cartilage under tensile load both in terms of local stress and deformation and in terms of viscoelastic behaviour. Moreover, they suggest that the model is also able to account for the fibre contribution in compression, whereas at the current state it is not suitable for the analysis of the time-dependent response of the tissue in such configuration due to the important role of fluid-related viscoelasticity, not included in the model. The main outcomes of this work are the definition of a very general constitutive model, that can serve as a framework for further enhancements, and in particular the innovative definition of the contribution of compressed fibres to the structure tensor.

***Keywords*:** cartilage; collagen; composites; hyperelasticity; viscoelasticity; FEM

Acknowledgments

First, I would like to acknowledge my supervisor at KTH Christian Gasser. He was an inspiration, a guide and a priceless source of help throughout my project. I would also like to thank professor Pasquale Vena for his valuable suggestions and his support during all the stages of this work.
Last but not least, I would like to thank my parents for the unconditional support and the constant encouragement that made this possible.

Gianluca Gabellini
Milano, April 2014

Contents

List of Figures

Sommario

La cartilagine articolare (CA) è un strato relativamente sottile di tessuto connettivo che ricopre le superfici di contatto delle ossa nelle articolazioni. Le sue funzioni principali sono la riduzione dell'attrito e la trasmissione del carico, ma allo stesso tempo agisce come ammortizzatore e distribuisce i carichi su una superficie relativamente ampia prevenendo pericolose concentrazioni di sforzo.
La CA viene facilmente danneggiata in seguito a traumi o semplicemente a causa dell'usura nel tempo. Un'area lesionata viene solitamente sostituita da tessuto cicatriziale perché la CA fatica a rigenerarsi: le cellule non sono libere di migrare nella zona danneggiata e la mancanza di vascolarizzazione ne rallenta il metabolismo. L'artrosi, una malattia cronica che causa una perdita progressiva di tessuto cartilagineo, è divenuta la più alta spesa sanitaria negli Stati Uniti anche a causa dell'invecchiamento della popolazione [8]. Le procedure cliniche adottate comunemente vanno dal trattamento conservativo alla rimozione chirurgica di tessuto danneggiato, ma a lungo termine è solitamente necessario applicare una protesi [16]. Negli ultimi anni è stato proposto di utilizzare tessuto ingegnerizzato cresciuto in laboratorio. Sebbene promettente, questa soluzione richiede che CA ingegnerizzata e naturale abbiano le stesse proprietà meccaniche per evitare la comparsa di carichi non fisiologici potenzialmente pericolosi per il tessuto sano che circonda l'impianto. Per assicurarsi che questo avvenga, è necessario affiancare alle analisi sperimentali modelli costitutivi come quello presentato in questo lavoro. Data la complessità della CA infatti i test sperimentali non sono da soli sufficienti per lo studio della relazione tra struttura e funzione [29].

Dal punto di vista meccanico la CA è un materiale poroso composto da una matrice solida rinforzata da collagene e da una fase liquida. Il movimento del fluido interstiziale attraverso la matrice porosa causa dissipazione d'energia. Tale fenomeno, definito *viscoelasticità estrinseca*, è solitamente trascurabile in tensione [35]. Questo lavoro si concentra sulla fase solida della CA e di conseguenza la fase liquida viene trascurata, sebbene influenzi il com-

portamento del tessuto in compressione. Il collagene è organizzato in una complessa rete tridimensionale di fibre. Il comportamento del tessuto è determinato non solo dalle proprietà meccaniche di tali fibre ma anche dalla loro disposizione [37]. In particolare si individuano tre zone principali lungo lo spessore della CA: *superficiale*, *centrale* e *profonda* [40]. Nella prima le fibre sono disposte in prevalenza parallelamente alla superficie articolare; nella zona intermedia la distribuzione è casuale; nella zona profonda le fibre sono principalmente perpendicolari all'interfaccia con l'osso sottostante. Il collagene è responsabile anche di quella che viene definita *viscoelasticità intrinseca* (chiamata semplicemente viscoelasticità nel seguito), la quale determina il comportamento tempo-dipendente del tessuto in trazione. Numerosi modelli analitici e numerici sono stati proposti per la CA. Le elevate deformazioni a cui è sottoposto il tessuto sotto carichi fisiologici rende in primo luogo necessaria una trattazione in grandi deformazioni [9] [32]. La fase solida è stata modellata sia come continuo [31] sia a partire dai costituenti [9] [32]. In generale il secondo approccio garantisce una migliore rappresentazione del rinforzo fibroso e del suo contributo. Similmente la viscoelasticità delle fibre di collagene è stata modellata con formulazioni lineari [57], quasi-lineari [26] e non lineari [43]. In particolare la formulazione quasi-lineare rappresenta una scelta comune in letteratura per i tessuti biologici con rinforzati da collagene [21] [62] e specificamente per la CA [32].

In questo contesto il presente lavoro ha come obiettivo generale la definizione di un modello costitutivo di tipo continuo per la fase solida della CA che sia in grado di riprodurne le proprietà anisotrope e non omogenee e le caratteristiche tempo-dipendenti, che possa essere integrato con modelli per la fase liquida. I tre obiettivi specifici sono la definizione di una quantità strutturale che tenga conto della distribuzione del collagene nel tessuto, l'introduzione di formulazione viscoelastica valida intorno all'equilibrio termodinamico e l'implementazione del corrispondente modello numerico.

Modello costitutivo

I tessuti biologici rinforzati da collagene possono essere trattati con una formulazione basata sugli invarianti della deformazione e sulla sovrapposizione di un potenziale isotropo associato alla matrice e uno trasversalmente isotropo associato alle fibre. Le fibre vengono suddivise in famiglie e le informazioni sulla direzione di ciascuna di esse vengono racchiuse in un co-

siddetto *tensore strutturale* [25]. Tuttavia la complessa rete tridimensionale di collagene che caratterizza la CA può essere modellata più efficacemente come un'unica famiglia di fibre statisticamente distribuita intorno ad un asse polare. A questo scopo è stato proposto in [13] di ridefinire il tensore strutturale calcolandone una *media direzionale* sulla sfera unitaria, approccio adottato in questo lavoro.
Il tensore tensore strutturale assume la seguente espressione:

$$\mathbf{H} = \frac{1}{4\pi}\int_0^{2\pi}\int_0^{\pi} \rho(\Theta)\mathbf{M}(\Theta,\Phi)\otimes\mathbf{M}(\Theta,\Phi)\sin\Theta\, d\Theta\, d\Phi = \frac{1}{4\pi}\int_{\mathbb{S}^2}\rho(\mathbf{M})\mathbf{A}(\mathbf{M})\, dS$$

dove $\mathbf{A}(\mathbf{M}) = \mathbf{M}\otimes\mathbf{M}$ è il contributo al tensore strutturale associato alla direzione $\mathbf{M}$ e ρ è la funzione di probabilità che caratterizza la distribuzione di fibre nella configurazione a riposo. In accordo con [13] è stata scelta una distribuzione trasversalmente isotropa attorno al proprio asse polare, sufficiente a rappresentare la disposizione delle fibre nelle tre zone in cui viene suddivisa la CA.
La configurazione iniziale è stata considerata priva di sforzi e il tessuto incomprimibile. Quest'ipotesi rende necessaria la definizione della sola parte deviatorica del potenziale, in quanto la parte volumetrica è determinata a partire dalle condizioni al contorno. Il potenziale deviatorico è determinato da un contributo legato alla matrice e da uno legato alle fibre. In accordo con molti lavori in letteratura [24] [13] [1], la matrice è stata rappresentata per semplicità come materiale neo-hookeano isotropo. Il potenziale delle fibre è invece stato suddiviso in un contributo isotropo che tiene conto delle diverse proprietà meccaniche rispetto alla matrice, ed uno anisotropo che rappresenta le proprietà trasversalmente isotrope delle fibre. Per il primo è stato nuovamente scelto un modello neo-hookeano con parametri diversi da quelli della matrice; il secondo incorpora le informazioni sulle fibre attraverso il tensore strutturale definito in precedenza:

$$\bar{\Psi}^{\infty}_{f_a}(\bar{\mathbf{C}},\mathbf{H}) = \frac{1}{2}c_{f_a}(\mathbf{H}:\bar{\mathbf{C}}-1)^2 = \frac{1}{2}c_{f_a}(\bar{I}_4-1)^2$$

dove c_{f_a} è una costante, $\bar{\mathbf{C}}$ è la parte deviatorica tensore di deformazione di Cauchy-Green e $\bar{I}_4$ è un invariante di tale tensore e rappresenta l'allungamento medio delle fibre nel punto in cui il potenziale viene calcolato.
La scelta di un legame quadratico ha lo scopo di replicare un fenomeno tipico dei tessuti biologici definito *reclutamento*: le fibre di collagene sono ondulate a riposo e il carico necessario a distenderle è trascurabile rispetto a quello che trasmettono una volta orientate

nella direzione della sollecitazione. Questo si traduce in un incremento di pendenza nella curva carico-deformazione che può essere modellato efficacemente per mezzo di un legame non-lineare. In particolare è riportato in letteratura che un polinomio di secondo ordine è in generale sufficiente a riprodurre il comportamento del tessuto in casi d interesse, come ad esempio quello della cartilagine ingegnerizzata, la quale non presenta forti non linearità in grandi deformazioni [51].
Infine è stato ipotizzato che le fibre siano in grado di sostenere carichi solamente in tensione, in accordo con la letteratura [34] [13] [9]. Di conseguenza le fibre contribuiscono al potenziale solamente quando la deformazione nella direzione del loro asse è positiva e il tensore strutturale deve essere modificato in modo da escludere le fibre in compressione. Sotto carichi fisiologici la variazione di rigidezza attraverso lo spessore del tessuto genera un complesso stato di deformazione e implica che in ogni punto alcune fibre siano tese ed altre compresse. Ad ogni iterazione è dunque necessario controllare l'allungamento in ogni direzione e ricalcolare l'integrale sulla sfera unitaria. Il contributo al tensore strutturale nella direzione delle fibre compresse deve essere tale da generare un allungamento unitario nello stato di deformazione corrente. In questo modo il corrispondente contributo all'energia risulta nullo. Ciò implica che questo contributo non possa essere definito *a priori*, ma debba essere legato al tensore di deformazione. La definizione del contributo del tensore strutturale associato ad ogni specifica direzione è stata modificata come segue:

$$\mathbf{A} = \begin{cases} \frac{1}{3}\bar{\mathbf{C}}^{-\mathbf{1}} & \text{if } \bar{\lambda}^2_{\mathbf{M}} \leq 1 \\ \mathbf{M} \otimes \mathbf{M} & \text{if } \bar{\lambda}^2_{\mathbf{M}} > 1 \end{cases}$$

dove $\bar{\lambda}^2_{\mathbf{M}}$ rappresenta l'allungamento in direzione $\mathbf{M}$. L'approccio qui descritto è equivalente ad integrare il tensore strutturale su un'area efficace della sfera unitaria che racchiude solamente le fibre tese e a pesare il valore ottenuto per la deformazione con la frazione volume volumetrica di fibre tese. Il vantaggio sta nel fatto che non è necessario ricalcolare la superficie di integrazione e che tutta l'informazione è racchiusa nel tensore strutturale senza necessità di agire sulla definizione della deformazione.

La risposta viscoelastica è stata modellata attraverso il concetto delle variabili interne, i.e. come sovrapposizione di una risposta elastica all'equilibrio e di un certo numero di processi viscosi transienti. Si è ipotizzato che la viscoelasticità sia legata soltanto alla parte deviatorica

della deformazione in accordo con la letteratura [25]. Inoltre nel modello solo le fibre di collagene sono viscoelastiche, mentre i proteoglicani sono elastici. Questa scelta si basa sull'evidenza sperimentale che la CA mostra un marcato comportamento viscoelastico anche in tensione, dove il contributo del fluido e dei proteglicani è trascurabile [34]. In accordo con le ipotesi riportate, ed esprimendo il contributo viscoso in funzione di quello elastico all'equilibrio, la forma completa del potenziale deviatorico è la seguente

$$\bar{\Psi} = \bar{\Psi}_g(\bar{\mathbf{C}}) + (1 + \sum_{\alpha=1}^{m} \beta_\alpha^\infty)[\bar{\Psi}_{f_i}^\infty(\bar{\mathbf{C}}) + \bar{\Psi}_{f_a}^\infty(\bar{\mathbf{C}}, \mathbf{H})]$$

dove $\bar{\Psi}_g$ e $\bar{\Psi}_{f_i}^\infty$ rappresentano il contributo neo-hookean legato rispettivamente a matrice e fibre, mentre le costanti adimensionali $\beta_\alpha^\infty \in [0, \infty)$ legano la rappresentazione elastica e quella viscosa. Tale approccio è valido intorno all'equilibrio termodinamico. La relazione sopra riportata estende la viscoelasticità lineare al campo delle grandi deformazioni tenendo conto della legame non lineare tra sforzo e deformazione. Ciascun elemento della sommatoria corrisponde nel caso lineare al contributo di un singolo elemento in un modello di Maxwell generalizzato. In questo modo si tiene conto del fatto che il rilassamento non avviene in un unico istante ma in un intervallo di tempo. È possibile definire tanti processi di rilassamento quanti necessari per riprodurre accuratamente il comportamento di un materiale. In questo lavoro sono stati definiti tre elementi, essendo riportato in letteratura che questo è sufficiente per approssimare correttamente il comportamento della CA [35] [58]. La relazione usata per le fibre di collagene è di tipo quasi-lineare. Questo implica che in un test di rilassamento degli sforzi la funzione di rilassamento (ovvero lo sforzo normalizzato sullo sforzo massimo al termine della rampa di carico) è indipendente dal livello di deformazione applicato. Sperimentalmente è stato dimostrato che questo non avviene nel caso della CA [2]. Tuttavia, la sovrapposizione di una matrice elastica e di un rinforzo viscoelastico quasi-lineare genera un comportamento tempo-dipendente globalmente non lineare per il tessuto, come già indicato in [62]. A bassi livelli di deformazione, dove la risposta è dominata dalla matrice, l'effetto viscoso è limitato. Quest'ultimo aumenta progressivamente verso livelli di deformazione maggiori dove più fibre sono attive e il carico è sostenuto prevalentemente dalle fibre di collagene.

Implementazione numerica

Data la complessità di geometrie, proprietà del tessuto e condizioni di carico, non è in generale possibile calcolare una soluzione analitica per il modello qui presentato ed è perciò necessario introdurre dei metodi di soluzione numerici. Il metodo degli Elementi Finiti ha dimostrato di essere particolarmente efficace nella modellazione di tessuti biologici ed è comunemente utilizzato in letteratura. Il legame costitutivo è stato dunque implementato in linguaggio FORTRAN e aggiunto come *subroutine* in un software di simulazione tramite il quale è poi stata eseguita l'analisi ad Elementi Finiti.

La soluzione delle equazioni costitutive viene calcolata in configurazione deformata. Sono dunque state derivate le corrispondenti espressioni per il tensore strutturale e per gli sforzi generati dalla particolare espressione scelta per il potenziale. Inoltre la soluzione del sistema di equazioni differenziali che governa il modello viene calcolata applicando metodi numerici iterativi e risolvendo una sequenza di problemi lineari. Dato che il modello opera nel campo delle grandi deformazioni, questo ha richiesto la linearizzazione del legame tra sforzo e deformazione e la definizione del corrispondente *tensore di elasticità*. Inoltre la deformazione viene ricalcolata ad ogni iterazione, perciò il numero e la direzione delle fibre tese (i.e. attive) può variare durante il processo di riduzione dell'errore, andando di fatto a modificare la soluzione esatta. Questo aumenta il tempo di calcolo e può causare problemi di convergenza. Per questa ragione il valore dell'allungamento calcolato all'istante precedente è stato utilizzato durante tutte le iterazioni, assumendo che le variazioni di tempo e carico siano sufficientemente piccole da rendere la differenza trascurabile.

Il tensore strutturale viene integrato sfruttando un efficiente algoritmo suggerito in [9], basato sul cosiddetto *t-design*, che definisce il sottoinsieme di punti sulla sfera unitaria in cui l'integrale viene valutato. Il numero e la posizione dei punti cambia in funzione del grado di precisione richiesto che è a sua volta funzione della distribuzione scelta per rappresentare le fibre. Una serie di test numerici di compressione sono stati utilizzati per determinare il minimo grado t che garantisce convergenza. È infatti importante limitare l'ordine di integrazione in quanto un suo aumento incrementa sensibilmente la dimensione del problema e la quantità di memoria richiesta alla macchina su cui è eseguita l'analisi.

L'algoritmo di discretizzazione dell'integrale di convoluzione che definisce il contributo viscoso e di aggiornamento di sforzi e tensore elastico è basato su un approccio consolidato in letteratura per la viscoelasticità in grandi deformazioni [60] [21] [14].

Il modello è stato implementato secondo un approccio variazionale misto, che definisce ap-

prossimazioni separate per pressione e deformazione volumetrica evitando di incorrere in problemi numerici causati dall'ipotesi di incomprimibilità. Inoltre l'applicazione del metodo dei lagrangiani aumentati garantisce che il processo di soluzione venga iterato finché l'ipotesi di incomprimibilità non è correttamente rispettata.

Risultati

Il modello è stato utilizzato per riprodurre dei test sperimentali di rilassamento dello sforzo in tensione e compressione descritti in [35]. I risultati mostrano un'asimmetria tra le due prove, dovuta al maggior contributo del collagene in trazione e in accordo con evidenze sperimentali. Per quanto riguarda la trazione, la previsione del modello è in perfetto accordo con i dati riportati in [35] sia per quanto riguarda i valori di sforzo che l'evoluzione del rilassamento, come mostrato in figura 1a. In compressione invece il modello produce un valore di sforzo all'equilibrio leggermente maggiore di quanto misurato sperimentalmente, mentre sottostima la componente viscosa che nei dati sperimentali tiene conto anche del contributo del fluido. I risultati indicano comunque che il contributo delle fibre in compressione non può essere trascurato. Tale contributo appare tuttavia sovrastimato nel modello, il che può essere attribuito almeno in parte alla distribuzione scelta per rappresentare il collagene. Essa infatti definisce una zona superficiale (in cui le fibre sono attivate in compressione dall'effetto di Poisson) più spessa di quella che si osserva nel tessuto reale. Una prova di rilassamento caratterizzata da una deformazione applicata maggiore dimostra invece la non linearità viscoelastica del modello. In figura 1b la funzione di rilassamento cambia al variare dello spostamento massimo applicato, mentre la risposta viscoelastica lineare è per definizione indipendente dal livello di deformazione.

Un secondo test analizza l'effetto delle fibre sotto carico di compressione. I risultati mostrano innanzi tutto un andamento quadratico dello sforzo che può essere addebitato ad un sostanziale contributo delle fibre, dato che se il ruolo della matrice fosse predominante l'andamento sarebbe simile a quello di un materiale neo-hookeano. Il fatto che i risultati siano in accordo con test sperimentali simili [44] rinforza l'idea che il contributo del collagene in compressione non sia trascurabile. La non omogeneità della distribuzione lungo lo spessore, rappresentata dal tensore strutturale, genera inoltre una deformazione non omogenea del campione. I risultati, riportati in Figura 2, mostrano che nonostante la superficie articolare (superiore) non sia vincolata nella direzione radiale, le fibre disposte parallelamente ad es-

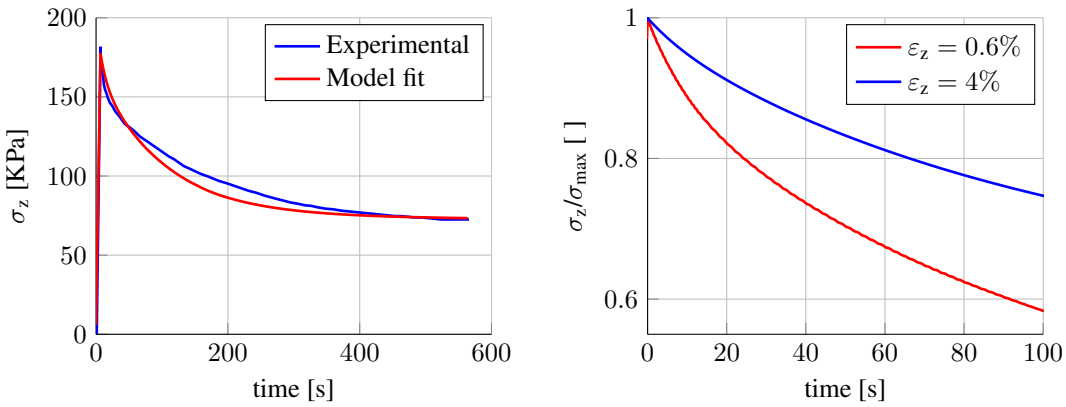

(a) Tensile relaxation test **(b)** Relaxation function

Figura 1: (a) Confronto tra le previsioni del modello e dati sperimentali riportati in [35] per una prova di rilassamento degli sforzi in trazione. I risultati sono espressi in sforzo nominale assiale vs tempo. (b) Effetto del livello di deformazione sulla funzione di rilassamento degli sforzi.

sa ne impediscono la deformazione radiale, che si concentra quindi nella parte inferiore in accordo con [11] per poi azzerarsi in corrispondenza del substrato osseo. Un confronto tra primo e il secondo sforzo principale mostra inoltre che a causa delle rotazioni indotte dalla deformazione sulle fibre, il tessuto perde la proprietà di isotropia trasversale locale garantita nella configurazione iniziale dalla particolare distribuzione scelta per il collagene.

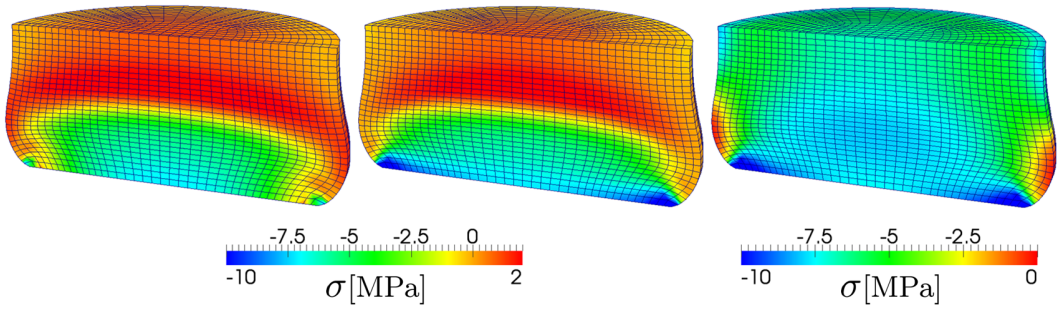

Figura 2: Distribuzione di primo, secondo e terzo sforzo principale di Cauchy in provino cilindrico di cartilagine sotto compressione non confinata in corrispondenza dello spostamento $u = 0.35$mm. La superficie superiore è quella articolare, mentre quella inferiore è attaccata ad un substrato osseo rigido.

Un ultimo test basato su prove sperimentali di carico e scarico in compressione descritte in [44] analizza l'effetto della frequenza di carico sul modello. Nonostante le costanti viscoelastiche siano state modificate nel tentativo di compensare l'assenza del fluido, l'area di isteresi è minore di quella registrata sperimentalmente. I risultati sono migliori alla frequenza di carico maggiore dato che il fluido non ha il tempo di spostarsi nel tessuto. Allo stesso modo la funzione di rilassamento, sebbene sia adattata in questo esempio alla rappresentazione di evoluzioni più rapide nel tempo, non riesce a riprodurre l'influenza del diverso

comportamento del fluido a diverse frequenze di carico. Tuttavia si comporta correttamente relativamente alle costanti viscoelastiche imposte e genera minor isteresi a frequenza di carico maggiore, andamento qualitativamente in accordo con i risultati riportati in [44].

Discussione e conclusioni

Il tensore strutturale generalizzato introdotto in questo lavoro estende il campo di applicabilità di quello proposto in [13] alla modellazione di tessuti con proprietà meccaniche non omogenee e privi di direzioni preferenziali per il rinforzo fibroso e rappresenta un contributo innovativo nello studio di questa classe di tessuti biologici. Il rovescio della medaglia è rappresentato da un aumento del costo computazionale del modello dovuto alla necessità di ripetere l'integrazione in ogni punto del tessuto ad ogni istante temporale. L'aumento di complessità è tuttavia necessario nel caso della CA e può essere richiesto in altre applicazioni per ottenere previsioni più accurate. Data la generalità dell'approccio proposto infatti la CA rappresenta solo una delle possibili applicazioni del modello, che è compatibile con qualunque espressione per il potenziale elastico che tenga conto della presenza di un tensore strutturale e con qualunque distribuzione di fibre, sia essa un'espressione analitica o un insieme di valori tabulati da prove sperimentali. A tal proposito si sottolinea che nel caso specifico di questo lavoro i parametri costitutivi sono stati stimati a partire dai risultati di test sperimentali sulla CA ma non sono basati su misurazioni dirette; allo stesso modo la distribuzione proposta per il collagene riproduce solo qualitativamente quella osservata sperimentalmente. Le ultime osservazioni unitamente alla mancanza della fase liquida implicano che una comparazione quantitativa diretta dei risultati con dati sperimentali non è possibile. Tuttavia il modello produce un comportamento fisicamente corretto per la fase solida della CA e risultati qualitativamente in accordo con le previsioni teoriche e la letteratura. In particolare esso è in grado di riprodurre la risposta del tessuto a un carico di trazione sia in termini di sforzi e deformazioni locali che in termini di comportamento viscoelastico; il contributo delle fibre può essere riprodotto anche in compressione, mentre allo stato attuale il comportamento tempo-dipendente non può essere correttamente simulato in tale configurazione. I risultati dei test numerici indicano anche che il modello è in grado di riprodurre il comportamento viscoelastico non lineare osservato per la CA.

Dal punto di vista numerico il modello sfrutta efficienti algoritmi dalla letteratura. Tuttavia il fatto che il tensore strutturale sia implementato come funzione della deformazione all'istante

precedente richiede la definizione di un alto numero di variabili in memoria, il che si traduce in un rallentamento nel calcolo della soluzione e in una possibile limitazione sulla dimensione massima del problema qualora l'analisi venga effettuata su un normale PC. Inoltre si è osservata una diminuzione nell'ordine di convergenza dell'algoritmo numerico di soluzione nel caso di carichi di compressione relativamente elevati, fenomeno che può essere attribuito alle instabilità generate dal progressivo collasso delle fibre in compressione.

Il modello presenta alcune limitazioni e necessita di ulteriori sviluppi. Dal lato modellistico un possibile miglioramento è rappresentato dall'uso di dati sperimentali per la definizione dei parametri costitutivi e della distribuzione del collagene. Dal lato computazionale la derivazione di una linearizzazione che tenga conto esplicitamente della dipendenza del tensore strutturale dalla deformazione migliorerebbe le prestazioni del modello. Ultimo è più importante sviluppo è rappresentato dall'introduzione di una formulazione dei fenomeni poroelastici generati dalla presenza di fluido interstiziale che renda il modello adatto a descrivere il comportamento della CA in compressione.

Chapter 1

Introduction

Articular cartilage is introduced in this chapter. After a brief overview of its characteristics and functions, the clinical problems that represent the motivation for this work are presented. The mechanical properties of the tissue are described with focus on those included in the model developed in the following chapters. A review of constitutive models for articular cartilage from the literature leads to the definition of the objectives of this work.

1.1 Problem background

Cartilage is a soft connective tissue found in different areas of the bodies of humans and other animals, such as joints, nose and ear, bronchial tubes, rib cage and intervertebral discs. Cartilage is composed of specialized cells called *chondrocytes* that produce a large amount of extracellular matrix (ECM). They are bound in spaces called *lacunae* with up to eight chondrocytes per lacuna. Since cartilage is an avascular tissue, the cells are supplied by diffusion, which is improved by the pumping effect of compressive physiological loads. ECM is made of collagen fibres, proteoglycans and elastin fibres, which will be described with respect to their mechanical properties in section 1.2. The relative amounts of these three components determines the classification of cartilage in three families: elastic cartilage, hyaline cartilage and fibrocartilage.

Articular cartilage (AC) is a relatively thin layer ($\approx 1 - 3\mathrm{mm}$) of hyaline cartilage covering articulating surfaces of bones. Its main functions are reducing the friction and transmitting the load between bones in contact. It also distributes external loads over a relatively large surface, thus preventing potentially dangerous stress concentration. In addition, it acts as a damper and dissipates energy under dynamic loads.

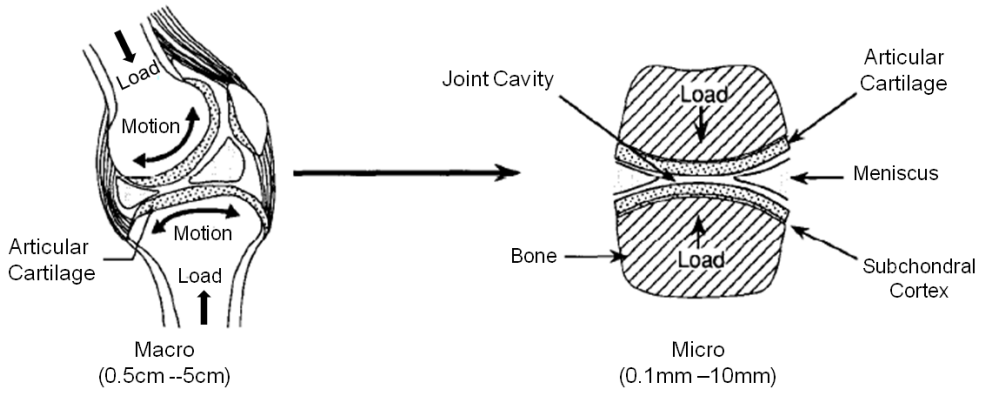

Figure 1.1: Representation of articular cartilage in the knee joint. Adapted from [42].

Damage and degeneration of AC are a major problem that affects millions of people in the world. Cartilage structure and functions can easily be harmed as a result of traumatic events (e.g. sport accidents), post-traumatic events (e.g. previous joint injuries) or simply wear and tear over time.

Arthritis, a degenerative condition that causes progressive loss of cartilage thickness and integrity, is now the leading cause of chronic disability and the highest medical cost in the United States due to increasing ageing of the population. It affects about 50 million people in the United States only, with an approximate cost of 130 billion dollars per year [8]. Around the world approximately 250 million people suffer from osteoarthritis of the knee [63].

Though AC damage is not life threatening, it does strongly affect the quality of life causing pain, swellings, strong barriers to mobility and severe restrictions to the patient's activities. AC damage is difficult to heal: chondrocytes, bound in lacunae, cannot migrate to damaged areas; moreover, the lack of blood supply and the slow metabolic activity of the cells makes natural repair response slow and insufficient. As a result, the damaged portion is often replaced by fibrocartilage scar tissue. This is clearly visible in Figure 1.2, which shows two pictures taken with a fibre-optic camera during an arthroscopy procedure. Cartilage repair procedures developed by surgeons and scientists in the last decade range from conservative treatments (e.g. physical therapy or intra-articular injections) to removal of damaged tissue with open surgery, but ultimately a total joint replacement is usually needed [30] [16]. Bioengineering techniques have been proposed to grow tissue engineered AC *in vitro* and use it to repair or replace the damaged tissue *in vivo*.

For this solution to be effective the engineered tissue should replicate AC explants' mechanical properties. However, they are not only the result of the properties of the single constituents, but also of their organization and mutual interaction. Hence, growing the right

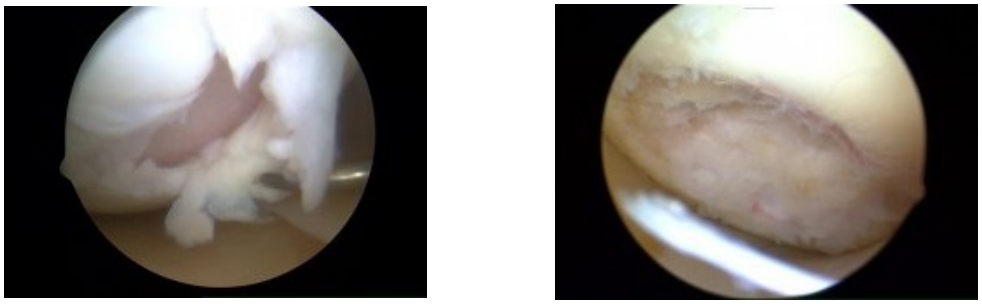

Figure 1.2: Severe articular cartilage damage on a medial femoral condyle (left) and ineffective formation of scar tissue in a damaged area (right).

components in the right proportions does not guarantee that the final product will be AC tissue [7]. On the other hand a mismatch with the properties of physiological tissue would generate abnormal and potentially dangerous loads on the cells surrounding the implant. Hence, it is important to develop experimental and numerical tools to compare the properties of engineered and natural AC. Experimental studies alone cannot capture the contribution of each constituent to the macroscopic properties of the tissue. In this scenario, the development of constitutive models, such as the one described in this work, plays an important role in better understanding structure-function relations: structural models account for composition and structure of the tissue and reproduce the load carrying mechanism of each constituent, increasing the predictive potential compared with other approaches. For a detailed review of the potential of continuum mechanics in understanding the mechanics of clinical applications, the reader is referred to [29].

1.2 Mechanical properties of articular cartilage

AC is a biphasic material composed of a solid porous matrix saturated with interstitial fluid. The porous matrix consists of collagen, mainly type II, proteoglycans and extracellular matrix (describing other proteins).

Collagen accounts for about 60–70% of dry weight and it is arranged in a network of fibres [38]. Density and orientation of these fibres and the cross links between them influence primarily the tensile and shear modulus of AC, but they are involved in the compressive response as well [4].

Approximately 30% of the dry weight is composed of proteoglycans, which are complex macromolecules consisting of a ‘core protein’ linked to specific polysaccharides called glycosaminoglycans [38]. Proteoglycans influence primarily the compressive response, as the

glycosaminoglycan links in solution form negatively charged ions that cause the solid matrix to swell and resist compression.
Interstitial fluid accounts for 70–85% of the total wet weight [38]. The movement of the fluid through the porous matrix under external compressive loads causes a drag force between the two phases and consequently significant energy dissipation. This flow-dependent viscoelastic behaviour is typically negligible in tension [35].
The present work focuses on the mechanical behaviour of the solid phase of the tissue, which is described in more detail below with focus on the role of the fibre reinforcement. On the other hand fluid-related phenomena are disregarded.

AC exhibits strong tension-compression asymmetry in experimental tests [54] [34], which is explained by the selective role of the constituents in the two loading configurations.
In particular, the tensile stiffness is highly strain dependent, and it is determined mainly by collagen. In the unloaded configuration collagen fibres are wavy. Hence, for small deformations they realign in the direction of the load rather than stretch, and consequently they do not bear load. For larger deformations, the external load has to stretch the fibres, generating higher tensile stress due to the higher stiffness of collagen compared to the soft matrix [66]. This phenomenon, known as *fibres engagement*, is common for soft biological tissues with collagen reinforcement [29] and determines a global non-linear response and the presence of a toe-region in the stress-strain curve.

AC exhibits also a strongly anisotropic and inhomogeneous response under physiological load, which can be related to the complex organization of the three-dimensional collagen network. Recent works [37] have shown that the macroscopic response of cartilage cannot be directly related to the mechanical properties of the individual fibrils at microscale, but that the tissue strength depends on their arrangement at higher levels. Fibres in immature AC are mostly oriented parallel to the articular surface throughout the depth, but tissue growth and remodelling causes the pattern of the fibres to change with age [61] [49]. In mature AC, the distribution of collagen fibres becomes highly anisotropic and depth-dependent. In particular three main layers can be identified, which are commonly referred to as superficial, middle and deep zone [40]. These layers differ in terms of fibres thickness, density and orientation leading to depth-dependent mechanical properties for the tissue. The superficial zone is the thinnest one and is characterized by high density of small diameter collagen fibres mostly

arranged in parallel to the articular surface, enhancing in-plane mechanical properties. In the middle zone the fibres are thicker and oriented randomly. Hence, the mechanical response of this layer is approximately isotropic. In the deep zone the fibres are characterized by largest diameter and are arranged mostly perpendicularly to the subchondral bone. A plane known as *tidemark* divides the deep zone from a calcified area that is sometimes described as the fourth layer of the tissue and constitutes a transition layer between AC and subchondral bone. The depth-dependent orientation of the fibrous reinforcement is illustrated in Figure 1.3.

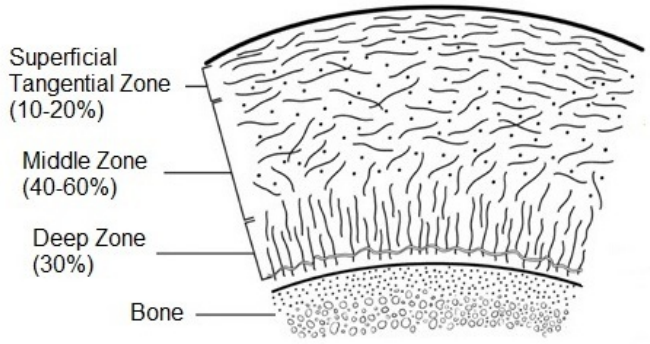

Figure 1.3: Representation of the AC layers and fibre orientations through the thickness.

Intrinsic viscoelasticity (referred to as viscoelasticity hereafter) has been shown to have a significant influence on the transient behaviour of AC in experimental studies [26] [27].
In particular, AC exhibits a viscoelastic response also in tensile testing [34] [67], where fluid pressure is negligible and the contribution from the proteoglycans matrix is likely low because of its small tensile stiffness compared to that of the fibrillar matrix. Hence, these results indicate the dominant role of collagen for the observed viscoelastic properties in tensile testing and more in general suggest the importance of collagen fibres in the transient response of the tissue. Moreover, the viscoelastic shear modulus of AC has been reported to increase with collagen cross-links [34].
On the other hand, the viscoelasticity of proteoglycans is not well documented and has anyway a minor role in tension, as stated above, and also in compression, where the transient response is dominated by flow-dependent viscoelasticity [35].
Relaxation tests have shown that AC exhibits a non-linear viscoelastic behaviour in tension [2], i.e. a dependence of the time evolution on the value of the displacement applied and kept constant during the test.

1.3 Constitutive modelling of articular cartilage

A constitutive model of the solid phase of AC should be able to reproduce tension-compression asymmetry, depth dependent mechanical properties, intrinsic viscoelasticity and finite multidimensional strains that characterize the response of the tissue to typical load *in vivo*.

Firstly, these requirements suggest the use of anisotropic finite deformation (i.e. non-linear) constitutive equations, which are in fact used in most models found in the literature, e.g. [32] [9] [47]. Another common assumption is that collagen fibres have zero compressive modulus and carry the load only in tension [34] [32] [9] [47]. Moreover, fibre engagement has been modelled both implicitly, through a non-linear expression for the potential energy, and explicitly by mean of an engagement function [1].

The fibre reinforcement in soft biological tissues has often been modelled by means of the so-called *superposition method*, in which the potential is the linear combination of an isotropic term describing the non-fibrous matrix and one or more anisotropic terms associated with each family of fibres, whose directional information is represented through the definition of a so-called *structure tensor*.
While this method is effective for tissues where a finite number of families of fibres can be identified (e.g. one family for tendon and ligaments [62] and two families for the adventitial layer of blood vessels [23]), it cannot capture the complexity of the fibre arrangement in AC. Attempts have been made to adapt this approach by defining a framework of secondary fibre directions on top of the one defined by the principal fibre directions [31].
A better approach to describe the complex fibre arrangement of AC is to treat the composite material in statistical terms, i.e. defining a probability distribution density function that provides at each material point the probability of finding a fibre oriented in a given direction [33].
Gasser *et al.* [13] proposed to account for fibres with statistical orientation by calculating the directional average of the structure tensor. For tissues in which families of fibres can be identified, it is sufficient to perform only one integration to define a scalar parameter that accounts for fibre dispersion about the preferred orientation of a specific family. In turn, the degree of dispersion is used to modulate the level of response, assuming that if the tissue is stretched in the preferential direction of a family, all the fibres in that family undergo tension and therefore bear load. This approach was for AC by Pierce [46], who introduced a discrete

real fibre distribution extracted from the imaging method described in [36].
An alternative constituent-based approach has been adopted for AC in several works, e.g. [3] [9] [51]: at each material point the potential associated with the fibres in each direction is computed and integrated over the unit sphere weighted by a normalized fibre distribution function. This procedure corresponds to a directional average of the fibre potential. In this case, the deformation features in the integral, which therefore cannot be calculated *a priori*. As a consequence, an analytical use of this potential is impossible.
In particular, Federico and Gasser [9] introduced a three dimensional statistical distribution function that accounts for both the depth-dependent preferential orientation and the dispersion of the fibres. This function was used as an example in this work and is described in detail in section 3.3. In [9] the numerical evaluation of the integrals is performed using the method of spherical design, that was adopted for the model presented in the following chapters and it is discussed in section 3.6.2.

The intrinsic viscoelasticity of collagen fibres has been modelled with linear [57], quasi-linear [26] and non-linear viscoelastic formulations [43].
One of the first attempts was made by Hayes and Mockros [18], who used a generalized Kelvin model (a series of Kelvin models). The choice of a linear viscoelastic model is justified by its simplicity, but it can hardly reproduce the time dependent response of AC. Moreover, it is only suitable under the assumption of small deformations. The quasi-linear viscoelastic (QLV) model, originally proposed by Fung [12], is a common choice in the literature for fibre reinforced tissues [21] [62] and specifically for AC [32]. This approach preserves the linearity in time but introduces the non-linear relation between stress and strain typical of highly deformable materials. Hence, it is suitable in the framework of finite deformations. Holzapfel and Gasser [21] developed a time discretisation procedure that eases the finite element implementation of this model. This method is based on the concept of internal variables, presented in section 2.5. The derivation for the model developed here is reported in section 3.6.3. A fully non-linear viscoelastic formulation increases the level of complexity of the model, but it is motivated by experimental evidence of non-linear time dependent behaviour of the tissue (see section 1.2).
An alternative approach is represented by a constituent-based model in which specific viscoelastic parameters are defined for each constituent, as proposed by Vena *et al.* [62] for ligaments. The study showed that a mixture of quasi-linear viscoelastic constituents generates

a non-linear response for the whole tissue, as it is discussed in more detail in section 3.2.2, suggesting a possible explanation for the non-linear viscoelastic behaviour of soft biological tissues as well as a convenient way to model it. This approach was later adopted to model the specific case of AC [32].
Recently, Gasser [14] developed an invariant-based framework for finite strain viscoelasticity that describes the viscoelastic continuum as the superposition of a Maxwell body and an elastic body having two independent reference configurations. This formulation coincides with the standard quasi-linear models when linearised around the thermodynamic equilibrium, but it is valid also for configurations away from it.

1.4 Objective

The long-term goal of the present work was to introduce a hyperelastic constitutive model for the solid phase of AC that accounts for the anisotropic structural arrangement of the collagen fibres reinforcement and provides a general approach compatible with a viscoelastic formulation valid away from the thermodynamic equilibrium (e.g. [14]) and ultimately with the numerical implementation of the fluid-related response of the tissue.
The primary objective was to introduce an invariant-based viscoelastic formulation of the free-energy function presented in [9], that represents distributed fibres in a continuum sense and that accounts for their directional characteristics as well as their intrinsic viscoelastic behaviour. The specific aims are (1) including the three-dimensional information on the fibre distribution into a purely structural quantity, i.e. a generalized structure tensor similar to the one in [13] but suitable for AC, (2) incorporating a viscoelastic formulation valid around the thermodynamic equilibrium and capable of reproducing the non-linear time-dependent behaviour of the tissue in tension, (3) deriving the corresponding numerical model and implementing an efficient solution procedure.

Chapter 2

Continuum mechanical framework

In this chapter an overview of the main aspects of continuum mechanics at large deformations is provided, as it represents the theoretical foundation of the model developed in this work. Starting from the definition of basic quantities like strains and stresses, the focus moves towards the specific case of biological tissues through the concepts of hyperelasticity, incompressibility and fibre reinforcement, concluding with viscoelasticity at large deformations. Finally the concept of *elasticity tensor* is introduced, which is fundamental for the numerical implementation of the model.

2.1 Motion and deformation gradient

A deformable body, within the framework of 3D Euclidean space $\mathbb{R}^3$, can be described as a set of interacting particles embedded in the domain $\Omega \in \mathbb{R}^3$. Among all possible configurations assumed by the body during its motion, one is chosen as *reference* and denoted as Ω_0. In this configuration, every point in the body is uniquely identified by the position vector

$$\mathbf{X} = X_I \mathbf{E}_I \qquad I = 1, \dots, 3 \tag{2.1}$$

where $\{\mathbf{E}_1, \mathbf{E}_2, \mathbf{E}_3\}$ is the basis of the underlying coordinate system. For simplicity, the orthogonal cartesian basis is used. The motion of the body to the so-called *current configuration* Ω^φ can be described as the combination of the motion of all its points

$$\mathbf{x} = x_i \mathbf{e}_i \qquad i = 1, \dots, 3 \tag{2.2}$$

where $\{\mathbf{e}_1, \mathbf{e}_2, \mathbf{e}_3\}$ is the basis of the current configuration. In this work it assumed that the two sets of base vectors are coincident, i.e. $\mathbf{E}_I \equiv \mathbf{e}_i$, which is convenient since all the possible motions take place within the Euclidean space.
In the following, capital letters are used to identify entities related to the reference (also called *material* or *Lagrange*) configuration, and small letters for those related to the current (also called *spatial* or *Eulerian*) reference.
The simplification used in the linear theory that the two sets of coordinates $\mathbf{X}_I$ and $\mathbf{x}_i$ are also coincident cannot be used in the context of finite elasticity due to the large displacements involved.

To describe the deformation process locally, a tensor $\mathbf{F}$ is introduced which maps a material line element of the initial configuration d$\mathbf{X}$ in the reference configuration, to a line element d$\mathbf{x}$ in the current configuration.

$$d\mathbf{x} = \mathbf{F}d\mathbf{X} \quad \text{or} \quad dx_i = F_{iJ}dX_J \tag{2.3}$$

In the equation above $\mathbf{F}$ represents a gradient and it is therefore known as *deformation gradient*. Thus, the components of $\mathbf{F}$ are given by the partial derivatives $x_{i,J} = \partial x_i/\partial X_J$:

$$\mathbf{F} = \frac{\partial x_i}{\partial X_J}\mathbf{e}_i \otimes \mathbf{E}_J \quad \text{or} \quad F_{iJ} = \frac{\partial x_i}{\partial X_J} \tag{2.4}$$

The inverse of the deformation gradient $\mathbf{F}^{-1}$ defines the inverse relation

$$d\mathbf{X} = \mathbf{F}^{-1}d\mathbf{x} \tag{2.5}$$

It is now possible to express the transformation of differential surface elements, which is given by *Nanson's formula* (see e.g. [25])

$$d\mathbf{a} = \mathbf{n}da = J\mathbf{F}^{-\mathrm{T}}\mathbf{N}dA = J\mathbf{F}^{-\mathrm{T}}d\mathbf{A} \tag{2.6}$$

where $J = \mathrm{det}\mathbf{F}$ and $\mathbf{N}$ and $\mathbf{n}$ are the normal vectors corresponding to dA and da, respectively.
The transformation between volume elements, defined as the scalar product of infinitesimal

surface element and an infinitesimal vector, is immediately given by

$$dv := dx \cdot da\mathbf{n} = \mathbf{F}d\mathbf{X} \cdot J\mathbf{F}^{-\mathrm{T}}dA\mathbf{n} = JdV \tag{2.7}$$

which shows that *J* represent a volume ratio. To exclude self-penetration of the body and ensure that the deformation gradient is non singular (i.e. invertible), $\mathbf{F}$ should then fulfil the following condition:

$$J = \mathrm{det}\mathbf{F} > 0 \tag{2.8}$$

The deformation gradient $\mathbf{F}$ represents the transformation of $d\mathbf{X}$ into $d\mathbf{x}$ and it includes the changes in modulus, direction and orientation. However, the deformation is related only to the change in length of an infinitesimal vector. Hence, the motion can be split into the sequence of a deformation and a rotation through a *polar decomposition*:

$$\mathbf{F} = \mathbf{R}\mathbf{U} \qquad \text{with} \quad \mathbf{R}^{\mathrm{T}} = \mathbf{R}^{-1}\,;\ \mathbf{U}^{\mathrm{T}} = \mathbf{U} \tag{2.9}$$

where the orthogonal tensor **R** is an isometric transformation that changes only direction and orientation of a vector and the positive definite symmetric tensor **U**, defined by the relation $\|d\mathbf{x}\| = \|\mathbf{U}d\mathbf{X}\|$, is known as the *right stretch tensor*.

2.2 Strain measures

Unlike displacements, strains are not measurable quantities. They are introduced to simplify analyses and are based on a concept, allowing many possible definitions. Those presented in this section represent the most common choices in solid mechanics and are based on the definition of rotation-independent deformation tensors.

The distance between two sufficiently close points $\mathbf{X}$ and $\mathbf{Y}$ in the reference configuration can be expressed as

$$\mathrm{d}\mathbf{X} = \mathrm{d}\varepsilon\mathbf{m}_0 \qquad \text{with} \qquad \mathrm{d}\varepsilon = |\mathbf{Y} - \mathbf{X}|\ ,\ \mathbf{m}_0 = \frac{\mathbf{Y} - \mathbf{X}}{|\mathbf{Y} - \mathbf{X}|} \tag{2.10}$$

where $\mathrm{d}\varepsilon$ is a scalar value and $\mathbf{m}_0$ is a unit vector (i.e. $|\mathbf{m}_0| = 1$).

The deformation gradient $\mathbf{F}$ can then be used to compute the corresponding vector $\mathrm{d}\mathbf{x}$ in the spatial configuration. In particular the application of $\mathbf{F}$ to the unit vector $\mathbf{m}_0$ provides a

measure of the stretch applied in the direction of $\mathbf{m}_0$

$$\boldsymbol{\lambda}_{\mathbf{m}_0}(\mathbf{X}) = \mathbf{F}(\mathbf{X})\mathbf{m}_0 \tag{2.11}$$

The vector $\boldsymbol{\lambda}_{\mathbf{m}_0}$ is the so-called *stretch vector* and its modulus λ is known as *stretch ratio*. The stretch ratio can be used to determine whether during the deformation a line element was compressed ($\lambda < 1$), unstretched ($\lambda = 1$) or extended ($\lambda > 1$).
It is then possible to define the *right Cauchy-Green deformation tensor* $\mathbf{C}$ through the square of the stretch ratio:

$$\lambda^2 = \boldsymbol{\lambda}_{\mathbf{m}_0} \cdot \boldsymbol{\lambda}_{\mathbf{m}_0} = \mathbf{Fa} \cdot \mathbf{Fa} = \mathbf{m}_0 \cdot \mathbf{F}^{\mathrm{T}}\mathbf{Fa} = \mathbf{m}_0 \cdot \mathbf{Ca} \tag{2.12}$$

$$\mathbf{C} = \mathbf{F}^{\mathrm{T}}\mathbf{F} \qquad \text{or} \qquad C_{IJ} = F_{iI}F_{iJ} \tag{2.13}$$

Using the properties of $\mathbf{U}$ and $\mathbf{R}$, $\mathbf{C}$ can be written as

$$\mathbf{C} = \mathbf{F}^{\mathrm{T}}\mathbf{F} = \mathbf{U}^{\mathrm{T}}\mathbf{R}^{\mathrm{T}}\mathbf{RU} = \mathbf{U}^{\mathrm{T}}\mathbf{U} = \mathbf{U}^2 \tag{2.14}$$

which confirms that $\mathbf{C}$ is purely a measure of the deformation.
Also, the right Cauchy-Green tensor is symmetric and positive definite $\forall \mathbf{x} \in \boldsymbol{\Omega}$:

$$\mathbf{C} = \mathbf{F}^{\mathrm{T}}\mathbf{F} = (\mathbf{F}^{\mathrm{T}}\mathbf{F})^{\mathrm{T}} = \mathbf{C}^{\mathrm{T}} \qquad \text{and} \qquad \mathbf{u} \cdot \mathbf{Cu} > 0 \quad \forall \mathbf{u} \neq \mathbf{0} \tag{2.15}$$

At this point a strain measure can be introduced to evaluate how much a given displacement differs locally from a rigid body displacement. The *Green-Lagrange strain tensor* $\mathbf{E}$ is derived from the change in the squared lengths:

$$\frac{1}{2}\left[(\lambda \mathrm{d}\varepsilon)^2 - \mathrm{d}\varepsilon^2\right] = \frac{1}{2}\left[(\mathrm{d}\varepsilon\mathbf{m}_0) \cdot \mathbf{F}^{\mathrm{T}}\mathbf{F}\,(\mathrm{d}\varepsilon\mathbf{m}_0) - \mathrm{d}\varepsilon^2\right] = \mathrm{d}\mathbf{X} \cdot \mathbf{E}\mathrm{d}\mathbf{X} \tag{2.16}$$

$$\mathbf{E} = \frac{1}{2}\left(\mathbf{F}^{\mathrm{T}}\mathbf{F} - \mathbf{I}\right) = \frac{1}{2}\left(\mathbf{C} - \mathbf{I}\right) \qquad \text{or} \qquad E_{IJ} = \frac{1}{2}\left(F_{iI}F_{iJ} - \delta_{IJ}\right) \tag{2.17}$$

The Green-Lagrangian strain tensor is a measure of how much $\mathbf{C}$ differs from $\mathbf{I}$ and therefore it equals zero when no deformation is acting on the body. Also, given the symmetry of $\mathbf{C}$ and $\mathbf{I}$, $\mathbf{E}$ is obviously symmetric.
It should be noted that the tensors $\mathbf{C}$ and $\mathbf{E}$ operate solely in material reference. Similarly, a deformation measure can be derived with respect to the spatial configuration. For this

purpose the *inverse stretch vector* $\boldsymbol{\lambda}^{-1}_{\mathbf{m}^\varphi}$ in the direction of $\mathbf{m}^\varphi$, for each $\mathbf{x} \in \Omega^\varphi$ might be define as:

$$\boldsymbol{\lambda}^{-1}_{\mathbf{m}^\varphi}(\mathbf{x}) = \mathbf{F}^{-1}(\mathbf{x})\mathbf{m}^\varphi \tag{2.18}$$

In analogy with the definitions for the reference configuration, the norm λ^{-1} of the inverse stretch vector $\boldsymbol{\lambda}^{-1}_{\mathbf{m}^\varphi}$ is known as *inverse stretch ratio* and the unit vector $\mathbf{m}^\varphi$ identifies the direction of the spatial line element $\mathrm{d}\mathbf{x}$, with $\mathrm{d}\mathbf{x} = \mathrm{d}\tilde{\varepsilon}\mathbf{m}^\varphi$.
The *left Cauchy-Green tensor* is defined trough the square of the inverse stretch ratio:

$$\lambda^{-2} = \lambda^{-1}_{\mathbf{m}^\varphi} \cdot \lambda^{-1}_{\mathbf{m}^\varphi} = \mathbf{F}^{-1}\mathbf{m}^\varphi \cdot \mathbf{F}^{-1}\mathbf{m}^\varphi = \mathbf{m}^\varphi \cdot \mathbf{F}^{-\mathrm{T}}\mathbf{F}^{-1}\mathbf{m}^\varphi = \mathbf{m}^\varphi \cdot \mathbf{b}^{-1}\mathbf{m}^\varphi \tag{2.19}$$

where **b** is the left Cauchy-Green tensor, given by

$$\mathbf{b} = \mathbf{F}\mathbf{F}^{\mathrm{T}} \qquad \text{or} \qquad b_{ij} = F_{iI}F_{jI} \tag{2.20}$$

As the corresponding tensor in material description, $\mathbf{b}$ is symmetric and positive definite $\forall \mathbf{x}^\varphi \in \Omega^\varphi$:

$$\mathbf{b} = \mathbf{F}\mathbf{F}^{\mathrm{T}} = (\mathbf{F}^{\mathrm{T}}\mathbf{F})^{\mathrm{T}} = \mathbf{b}^{\mathrm{T}} \qquad \text{and} \qquad \mathbf{u} \cdot \mathbf{b}\mathbf{u} > 0 \quad \forall \mathbf{u} \neq \mathbf{0} \tag{2.21}$$

The most used strain measure in the spatial configuration is the *Euler-Almansi tensor* **e**, which is defined using the change in square length similarly to the Green-Lagrange tensor in material reference (in fact **e** is the push-forward of the **E**). In particular, with the use of 2.19, the expression of the strain tensor is given by

$$\frac{1}{2}\left[\mathrm{d}\tilde{\varepsilon}^2 - (\lambda^{-1}\mathrm{d}\tilde{\varepsilon})^2\right] = \frac{1}{2}\left[\mathrm{d}\tilde{\varepsilon}^2 - (\mathrm{d}\tilde{\varepsilon}\mathbf{m}^\varphi) \cdot \mathbf{F}^{-\mathrm{T}}\mathbf{F}^{-1}(\mathrm{d}\tilde{\varepsilon}\mathbf{m}^\varphi)\right] = \mathrm{d}\mathbf{x} \cdot \mathbf{e}\mathrm{d}\mathbf{x} \tag{2.22}$$

$$\mathbf{e} = \frac{1}{2}\left(\mathbf{I} - \mathbf{F}^{-\mathrm{T}}\mathbf{F}^{-1}\right) = \frac{1}{2}\left(\mathbf{I} - \mathbf{b}^{-1}\right) \quad \text{or} \quad e_{ij} = \frac{1}{2}\left(\delta_{IJ} - F^{-1}_{Ii}F^{-1}_{Ij}\right) \tag{2.23}$$

2.3 Stress measures

In continuum mechanics, stress is a physical quantity that expresses the internal forces that neighbouring particles of a continuous material exert on each other. Quantitatively, the stress is expressed by the traction vector, defined as the traction force F between adjacent parts of the material across an imaginary separating surface, divided by the area of the surface. The

infinitesimal force acting on a surface element $d\mathbf{f}$ can be defined as

$$d\mathbf{f} = \mathbf{t}\mathrm{d}a = \mathbf{T}\mathrm{d}A \tag{2.24}$$

where $\mathbf{t}$ is defined with respect to the spatial configuration and it is known in the literature as the *Cauchy traction vector*, while the (*pseudo*) traction vector $\mathbf{T}$ is defined with respect to the material configuration and it is known as *first Piola-Kirchhoff traction vector*.
The well-known *Cauchy stress theorem* postulates the existence of tensor fields $\boldsymbol{\sigma}$ and $\mathbf{P}$ such that:

$$\mathbf{t}(\mathbf{x}, \mathbf{n}) = \boldsymbol{\sigma}(\mathbf{x})\mathbf{n} \qquad \text{or} \qquad t_i = \sigma_{ij} n_j \tag{2.25}$$

$$\mathbf{T}(\mathbf{X}, \mathbf{N}) = \mathbf{P}(\mathbf{X})\mathbf{N} \qquad \text{or} \quad T_i = P_{iI} N_I \tag{2.26}$$

where $\mathbf{N}$ and $\mathbf{n}$ are the normals corresponding to the surface elements dA and da, while the tensor $\boldsymbol{\sigma}$ denotes the symmetric *Cauchy (or true) stress tensor* and $\mathbf{P}$ denotes the *first Piola-Kirchhoff (or nominal) stress tensor*.
The stress tensors are related by the so-called *Piola transformation*, given by the substitution of (2.25) and (2.26) into (2.24) and the use of the Nanson's formula:

$$\mathbf{P} = J\boldsymbol{\sigma}\mathbf{F}^{-\mathrm{T}} \qquad \text{or} \qquad P_{iI} = J\sigma_{ij}F^{-1}_{Ij} \tag{2.27}$$

Another stress tensor acting on the spatial configuration and often used in computational mechanics is known as *Kirchhoff stress tensor* $\boldsymbol{\tau}$ and it is defined as

$$\boldsymbol{\tau} = J\boldsymbol{\sigma} \qquad \text{or} \qquad \tau_{ij} = J\sigma_{ij} \tag{2.28}$$

It should be noted that the first Piola-Kirchhoff stress tensor is in general non-symmetric, which complicates its use in computational mechanics. To overcome this problem, the so-called *second Piola-Kirchhoff stress tensor* $\mathbf{S}$ has been introduced, computed by performing the pull-back operation on the spatial tensor τ:

$$\mathbf{S} = \mathbf{F}^{-1}\boldsymbol{\tau}\mathbf{F}^{-\mathrm{T}} \qquad \text{or} \qquad S_{IJ} = F^{-1}_{Ii}F^{-1}_{Jj}\tau_{ij} \tag{2.29}$$

The stress tensor $\mathbf{S}$ does not have any physical interpretation in terms of surface tractions. Nevertheless, it is very useful in computational mechanics because it is symmetric and in

the definition of constitutive relation because it acts on the material reference and it is work conjugate to the Green-Lagrange strain tensor.
Finally, the second Piola-Kirchhoff stress tensor can be related to the Cauchy stress substituting (2.28) into 2.29:

$$\mathbf{S} = J\mathbf{F}^{-1}\boldsymbol{\sigma}\mathbf{F}^{-\mathrm{T}} = \mathbf{F}^{-1}\mathbf{P} = \mathbf{S}^{\mathrm{T}} \qquad \text{or} \qquad S_{IJ} = JF^{-1}_{Ii}F^{-1}_{Jj}\sigma_{ij} = F^{-1}_{Ii}P_{iJ} = S_{JI} \tag{2.30}$$

where the use of (2.27) reveals also the relation with the first Piola-Kirchhoff stress tensor

$$\mathbf{P} = \mathbf{F}\mathbf{S} \qquad or \qquad P_{iI} = F_{iJ}S_{JI} \tag{2.31}$$

2.4 Hyperelastic materials

A so-called hyperelastic material postulate the existence of a Helmotz free-energy function Ψ, which is defined per unit reference volume rather than per unit mass. If Ψ is only function of some strain tensor, the Helmotz free-energy function is referred to as the strain-energy function and both the terminologies will be use in this work.
A hyperelastic material is defined as a subclass of an elastic material whose response can be expressed as

$$\mathbf{P} = \frac{\partial \Psi(\mathbf{F})}{\partial \mathbf{F}} \quad \text{or} \quad \boldsymbol{\sigma} = J^{-1}\frac{\partial \Psi(\mathbf{F})}{\partial \mathbf{F}}\mathbf{F}^{\mathrm{T}} \tag{2.32}$$

with respect to the material or the spatial configuration respectively.
It is assumed throughout this work that the strain-energy function vanishes in the reference configuration, i.e. when $\mathbf{F} = \mathbf{I}$. Also, the strain-energy function should increase with the deformation to guarantee physical behaviour. Thus, the range of admissible functions is limited by the following two conditions:

$$\Psi = \Psi(\mathbf{I}) = 0; \quad \Psi = \Psi(\mathbf{F}) \geq 0 \tag{2.33}$$

It follows that the residual stress (i.e. the stress in the undeformed configuration) is assumed to be zero. The reference configuration is therefore defined as stress-free. The strain energy function should also be objective, i.e. translations and rotations should not affect the amount of energy stored in the body. This is represented by the restriction

$$\Psi(\mathbf{F}) = \Psi(\mathbf{Q}\mathbf{F}) \tag{2.34}$$

where $\mathbf{Q}$ is an orthogonal tensor. Hence, using the polar decomposition (2.9) and choosing the transpose of the proper orthogonal rotation tensor as a specific case for $\mathbf{Q}$, it is possible to write

$$\Psi(\mathbf{F}) = \Psi(\mathbf{R}^{\mathrm{T}}\mathbf{F}) = \Psi(\mathbf{R}^{\mathrm{T}}\mathbf{R}\mathbf{U}) = \Psi(\mathbf{U}) \tag{2.35}$$

Using (2.14) and (2.32) it is finally possible to write the potential energy and the stress tensor as a function of $\mathbf{C}$:

$$\Psi(\mathbf{F}) = \Psi(\mathbf{C}) \quad \Rightarrow \quad \mathbf{P} = \frac{\partial \Psi(\mathbf{C})}{\partial \mathbf{C}} \frac{\partial \mathbf{C}}{\partial \mathbf{F}} = 2\mathbf{F} \frac{\partial \Psi(\mathbf{C})}{\partial \mathbf{C}} \tag{2.36}$$

2.4.1 Incompressible hyperelastic materials

Materials that keep the volume constant throughout a motion are characterized by the *incompressibility* constraint, that can be expressed as

$$J = \mathrm{det}\mathbf{F} = 1 \quad \text{or} \quad J^2 = \mathrm{det}\mathbf{C} = 1 \tag{2.37}$$

It is possible to separate the volumetric part and the isochoric part of the free-energy function, which is convenient when incompressible materials are studied because they show strong differences between the bulk and the shear behaviour.
To do this, the deformation gradient $\mathbf{F}$ is decomposed into

$$\mathbf{F} = (J^{1/3}\mathbf{I})\bar{\mathbf{F}} \tag{2.38}$$

where $(J^{1/3}\mathbf{I})$ represents the dilatation part and $\bar{\mathbf{F}}$ the distorsional part, so that $\mathrm{det}\bar{\mathbf{F}} = 1$. The tensor $\bar{\mathbf{F}}$ can be defined as isochoric deformation gradient. Consequently the modified right and left Cauchy-Green tensors can be defined as

$$\mathbf{C} = \mathbf{F}^{\mathrm{T}}\mathbf{F} = J^{2/3}\bar{\mathbf{C}}, \quad \bar{\mathbf{C}} = \bar{\mathbf{F}}^{\mathrm{T}}\bar{\mathbf{F}} \tag{2.39}$$

$$\mathbf{b} = \mathbf{F}\mathbf{F}^{\mathrm{T}} = J^{2/3}\bar{\mathbf{b}}, \quad \bar{\mathbf{b}} = \bar{\mathbf{F}}\bar{\mathbf{F}}^{\mathrm{T}} \tag{2.40}$$

The free-energy function can then be written as

$$\Psi(\mathbf{C}) = U(J) + \bar{\Psi}(\bar{\mathbf{C}}) \tag{2.41}$$

where $U(J)$ and $\bar{\Psi}(\bar{\mathbf{C}})$ describe the volumetric and the isochoric contribution to the poten-

tial, respectively. If a much higher external work is required to generate dilatational than distorsional changes the material is defined nearly-incompressible. For this class of material (that include biological tissues) the compressibility effects are small and it is still possible to use the decoupled form of the potential. It should also be noted that for incompressible materials it is not necessary to define $U(J)$.

Accordingly, the second Piola-Kirchhoff stress tensor can be computed by mean of the additive split

$$\mathbf{S} = 2\frac{\partial \Psi(\mathbf{C})}{\partial \mathbf{C}} = 2\frac{\partial [U(J) + \bar{\Psi}(\bar{\mathbf{C}})]}{\partial \mathbf{C}} = \mathbf{S}_{vol} + \bar{\mathbf{S}} \tag{2.42}$$

It is necessary to compute the derivative of the modified right Cauchy-Green tensor $\bar{\mathbf{C}}$ relative to $\mathbf{C}$. Given the definition of J^2 in (2.37), the introduction of the standard expression for the derivative of the determinant of a second order tensor leads to

$$\frac{\partial J^2}{\partial \mathbf{C}} = \frac{\partial(\det(\mathbf{C}))}{\partial \mathbf{C}} = \det(\mathbf{C})[\mathbf{C}^{-1}]^T = J^2\mathbf{C}^{-1} \tag{2.43}$$

which gives

$$\frac{\partial J^2}{\partial \mathbf{C}} = 2J\frac{\partial J}{\partial \mathbf{C}} \quad \Longrightarrow \quad \frac{\partial J}{\partial \mathbf{C}} = \frac{J}{2}\mathbf{C}^{-1} \tag{2.44}$$

$$\frac{\partial J^{-2/3}}{\partial \mathbf{C}} = -\frac{2}{3}J^{-2/3}\frac{\partial J}{\partial \mathbf{C}} = -\frac{1}{3}J^{-2/3}\mathbf{C}^{-1} \tag{2.45}$$

Hence, the derivative of $\bar{\mathbf{C}}$ relative to $\mathbf{C}$ is given by

$$\frac{\partial \bar{\mathbf{C}}}{\partial \mathbf{C}} = \frac{\partial [J^{-2/3}\mathbf{C}]}{\partial \mathbf{C}} = J^{-2/3}\frac{\partial \mathbf{C}}{\partial \mathbf{C}} + \mathbf{C} \otimes \frac{\partial J^{-2/3}}{\partial \mathbf{c}} = J^{-2/3}\underbrace{\left[\mathbb{I} - \frac{1}{3}(\mathbf{C} \otimes \mathbf{C}^{-1})\right]}_{\mathbb{P}^{\mathrm{T}}} = J^{-2/3}\mathbb{P}^{\mathrm{T}} \tag{2.46}$$

where $\mathbb{I}$ is the fourth order identity tensor, defined as $\mathbf{A} = \mathbb{I} : \mathbf{A}$ (where $\mathbf{A}$ is a second order tensor) and $\mathbb{P}^{\mathrm{T}}$ defines the *projector tensor* (with respect to the reference configuration) $\mathbb{P} = \mathbb{I} - \frac{1}{3}(\mathbf{C}^{-1} \otimes \mathbf{C})$, which furnishes the deviatoric operator so that $[\mathbb{P} : (\cdot)] : \mathbf{C} = \mathrm{dev}(\cdot) : \mathbf{C} = 0$.

It is then possible to compute

$$\mathbf{S}_{vol} = 2\frac{\partial U(J)}{\partial J}\frac{\partial J}{\partial \mathbf{C}} = pJ\mathbf{C}^{-1} \tag{2.47}$$

$$\bar{\mathbf{S}} = 2\frac{\partial \Psi(\bar{\mathbf{C}})}{\partial \bar{\mathbf{C}}}\frac{\partial \bar{\mathbf{C}}}{\partial \mathbf{C}} = J^{-2/3}\mathbb{P} : \tilde{\mathbf{S}} = J^{-2/3}\mathrm{dev}\tilde{\mathbf{S}} \tag{2.48}$$

where $p = \partial U(J)/\partial J$ is the hydrostatic pressure and $\tilde{\mathbf{S}} = 2\partial\bar{\Psi}/\partial\bar{\mathbf{C}}$ is a (fictitious) isochoric second Piola-Kirchhoff stress. Under the hypothesis of incompressibility the hydrostatic pressure is a Lagrange multiplier and can only be determined from the boundary conditions.

The Cauchy stress can be compute through an inverse Piola transformation of (2.42)

$$\boldsymbol{\sigma} = J^{-1}\chi_*[\mathbf{S}] = \boldsymbol{\sigma}_{vol} + \bar{\boldsymbol{\sigma}} \quad \text{or} \quad \sigma_{ij} = J^{-1}F_{iI}F_{jJ}S_{IJ} \tag{2.49}$$

with

$$\boldsymbol{\sigma}_{vol} = p\chi_*[\mathbf{C}^{-1}] = p\mathbf{I} \tag{2.50}$$

$$\bar{\boldsymbol{\sigma}} = J^{-5/3}\chi_*[\mathbb{P}] : \chi_*[\tilde{\mathbf{S}}] = J^{-2/3}\mathbb{p} : \tilde{\boldsymbol{\sigma}} \tag{2.51}$$

where $\mathbb{p} = \mathbb{I} - \frac{1}{3}(\mathbf{I}\otimes\mathbf{I})$ furnishes the deviatoric operator in the spatial configuration, so that $[\mathbb{p} : (\cdot)] : \mathbf{I} = 0$ and $\tilde{\boldsymbol{\sigma}} = J^{-1}\chi_*[\tilde{\mathbf{S}}]$ is the (fictitious) isochoric Cauchy stress.

2.4.2 Isotropic hyperelastic materials

A material is considered *isotropic* if its response in a stress-strain test is the same in all direction. In other words, a hyperelastic material is isotropic relative to the reference configuration Ω_0 if a motion superimposed on any particularly translated and/or rotated leads to the same strain-energy function. This condition is guaranteed by the following equality

$$\Psi(\mathbf{F}) = \Psi(\mathbf{F}\mathbf{Q}^{\mathrm{T}}) \tag{2.52}$$

where $\mathbf{F}$ is the deformation gradient and $\mathbf{Q}$ is an orthogonal tensor, which in turn can be expressed as a function of the right Cauchy-Green tensor $\mathbf{C}$ as

$$\Psi(\mathbf{C}) = \Psi(\mathbf{Q}\mathbf{F}^{\mathrm{T}}\mathbf{F}\mathbf{Q}^{\mathrm{T}}) = \Psi(\mathbf{Q}\mathbf{C}\mathbf{Q}^{\mathrm{T}}) \tag{2.53}$$

According to the representation theorem for invariants, every strain energy function that possesses this property can be expressed as a set of independent invariants of its argument,

$$\Psi(\mathbf{C}) = \Psi(I_1(\mathbf{C}), I_2(\mathbf{C}), I_3(\mathbf{C})) \tag{2.54}$$

where $I_a(\mathbf{C}),\ a = 1, 2, 3$ are the standard invariants of the right Cauchy-Green tensor

$$I_1 = \text{tr}(\mathbf{C}), \quad I_2 = \frac{1}{2}\left[(\text{tr}(\mathbf{C}))^2 - \text{tr}(\mathbf{C}^2)\right], \quad I_3 = \det(\mathbf{C}) \tag{2.55}$$

Introducing the decoupled form of the potential and the incompressibility assumption (i.e. $I_3 = J^2 = 1$, see (2.37)), the isochoric part of the strain-energy can be written as a function of the first and the second invariant of the modified right Cauchy-Green tensor

$$\bar{\Psi}(\bar{\mathbf{C}}) = \bar{\Psi}(\bar{I}_1(\bar{\mathbf{C}}), \bar{I}_2(\bar{\mathbf{C}})) \tag{2.56}$$

The so called *neo-Hookean* model is the simplest representation of this class of materials and it extends the Hooke's law for linear materials to the range of large deformation. The expression of the isochoric strain-energy function reads

$$\bar{\Psi}(\bar{\mathbf{C}}) = c_1(\bar{I}_1 - 3) \tag{2.57}$$

where c_1 is a material parameter equal to half of the shear modulus in the reference configuration and $\bar{I}_1 = tr(\bar{\mathbf{C}})$ is the first invariant of the modified right Cauchy-Green tensor.

2.4.3 Fibre reinforced hyperelastic materials

Biological tissues are usually composed of a matrix material and one or more families of fibres that generate strong directional properties and anisotropic mechanical behaviour. It is assumed that the fibres have single preferred direction, that they are continuously distributed throughout the material and that they are the only source of anisotropy. Moreover, micro-mechanical aspects are disregarded.

A material reinforced by one family of fibres typically shows much higher stiffness in the fibre direction and is isotropic in all the directions orthogonal to the fibres. This symmetry properties is called transverse isotropy. For this class of materials, the stress at a material

point depends on the deformation gradient, but also on the direction of the fibres throughout the material, which can be described in the reference configuration by a unit vector field $\mathbf{a}_0(\mathbf{X})$, $|\mathbf{a}_0| = 1$. After the deformation, the fibres will have a new preferred direction, defined by a unit vector field $\mathbf{a}(\mathbf{x})$, $|\mathbf{a}| = 1$, but also a new length. Hence, the stretch λ defined in (2.11), that is related to the right Cauchy-Green tensor by (2.13), must also be determined. The fibre direction in the reference configuration must be included in the expression of the free energy. In particular, since the sense of $\mathbf{a}_0$ is immaterial, the potential is chosen as an even function of $\mathbf{a}_0$ and the second order tensor $\mathbf{H}$, known as *structure tensor*, is introduced as an argument:

$$\mathbf{H} = \mathbf{a}_0 \otimes \mathbf{a}_0, \qquad \Psi = \Psi(\mathbf{C}, \mathbf{a}_0 \otimes \mathbf{a}_0) \tag{2.58}$$

It should be noted that objectivity is trivially satisfied as the potential is function of quantities defined with respect to the reference configuration.
It can be shown (e.g. see [25]) that the requirement for transverse isotropy becomes

$$\Psi(\mathbf{C}, \mathbf{a}_0 \otimes \mathbf{a}_0) = \Psi(\mathbf{Q}\mathbf{C}\mathbf{Q}^{\mathrm{T}}, \mathbf{Q}\mathbf{a}_0 \otimes \mathbf{a}_0\mathbf{Q}^{\mathrm{T}}) \tag{2.59}$$

Similarly to the case of isotropy, it is also possible to write the potential using a set of independent invariants, but it is necessary to define two additional invariants in order to fulfil (2.59) (a complete description is given in [56]):

$$I_4(\mathbf{C}, \mathbf{a}_0) = \mathbf{a}_0 \cdot \mathbf{C}\mathbf{a}_0 = \lambda^2 \,, \quad I_5(\mathbf{C}, \mathbf{a}_0) = \mathbf{a}_0 \cdot \mathbf{C}^2\mathbf{a}_0 \tag{2.60}$$

The invariants above describe the properties of the fibres and their interaction with other material constituents.

The same approach can be extended to materials with more than one family of fibres by introducing similar invariants for each family and additional expression describing the anisotropy generated by the interaction of different families.

2.5 Viscoelasticity at finite deformation

In this section a three-dimensional viscoelasticity framework based on the concept of *internal variables* is described, that is suitable for highly deformable materials. This approach is

convenient for the definition of numerical models using the finite element method and it can be applied to highly deformable materials for small perturbation away from the equilibrium state. For these reasons it is commonly used in the literature, e.g. see [52] [20].

Internal variables describe aspects of the internal structure of materials associated with dissipative effects, and they are introduced as phenomenological variables constructed mathematically within a macroscopic framework (similarly to the 'dashpot elements' in linear viscoelastic models). They influence strain and stresses, and they are often referred to as *history variables* ($\mathbf{\Gamma}_\alpha$) since their evolution reflects the history of the deformation. The current state of a viscoelastic material can then be described by the deformation gradient and the current values of a set of internal variables (note that strain is independent of past values of history variables).

In accordance with the previous sections a decoupled representation of the strain-energy function is used. The change of the potential from the reference to the current configuration within a isothermal transformation is then given by

$$\Psi(\mathbf{C}, \mathbf{\Gamma_1}, \dots, \mathbf{\Gamma_m}) = U^\infty(J) + \bar{\Psi}^\infty(\bar{\mathbf{C}}) + \sum_{\alpha=1}^{m} \Upsilon_\alpha(\bar{\mathbf{C}}, \mathbf{\Gamma}_\alpha) \tag{2.61}$$

The first two terms, $U^\infty(J)$ and $\bar{\Psi}^\infty$, describe the equilibrium state of the solid. According to (2.41), they represent the volumetric and the isochoric part of the elastic response as $t \to \infty$, respectively. The additional term represents the 'dissipative' viscoelastic contribution.
A common assumption, based on experimental evidence, is that the time-dependent properties are function only of the isochoric part of the deformation. Thus, the volumetric part remains fully elastic and can be described with the equation introduced in section 2.4.1. The viscoelastic behaviour instead is function of the modified right Cauchy-Green tensor $\bar{\mathbf{C}}$ and it is modelled as the superposition of $\alpha = 1, \dots, m$ viscoelastic processes, each characterized by a particular *relaxation time* $\tau_\alpha \in (0, \infty)$, which characterizes the rate of decay of stress and strain. The condition of non-negative internal dissipation, required by the second law of thermodynamics, can be enforced using the Coleman-Noll procedure (for a complete description the reader is referred to [25]), which leads to the following expressions for the

Second Piola-Kirchhoff stress tensor and the internal dissipation:

$$\mathbf{S} = 2\frac{\partial \Psi(\mathbf{C}, \boldsymbol{\Gamma}_\mathbf{1}, \ldots, \boldsymbol{\Gamma}_\mathbf{m})}{\partial \mathbf{C}} = \mathbf{S}_{vol}^{\infty} + \bar{\mathbf{S}}^{\infty} + \sum_{\alpha=1}^{m} \bar{\mathbf{S}}_{\alpha}^{V} \tag{2.62}$$

$$\mathcal{D}_{int} = -\sum_{\alpha=1}^{m} 2\frac{\partial \Upsilon_\alpha(\bar{\mathbf{C}}, \boldsymbol{\Gamma}_\alpha)}{\partial \boldsymbol{\Gamma}_\alpha} : \frac{1}{2}\dot{\boldsymbol{\Gamma}}_\alpha \geq 0 \tag{2.63}$$

where the tensor variables $\bar{\mathbf{S}}_{\alpha}^{V}$ have been introduced, which represent non-equilibrium stresses. This quantity is defined in analogy with (2.48)

$$\bar{\mathbf{S}}_{\alpha}^{V} = J^{-2/3}\mathbb{P} : \tilde{\mathbf{S}}_{\alpha}^{V} \qquad \text{with} \quad \tilde{\mathbf{S}}_{\alpha}^{V} = 2\frac{\partial \Upsilon_\alpha(\bar{\mathbf{C}}, \boldsymbol{\Gamma}_\alpha)}{\partial \bar{\mathbf{C}}} \tag{2.64}$$

where the fictitious non-equilibrium stress $\tilde{\mathbf{S}}_{\alpha}^{V}$ is introduced. Based on the equilibrium equation for a linear viscoelastic solid, the non-equilibrium stresses can be related to the strain-like quantities $\boldsymbol{\Gamma}_\alpha$ resulting in an equivalent expression for the internal dissipation:

$$\bar{\mathbf{S}}_{\alpha}^{V} = -2\frac{\partial \Upsilon_\alpha(\bar{\mathbf{C}}, \boldsymbol{\Gamma}_\alpha)}{\partial \boldsymbol{\Gamma}_\alpha} \qquad \Rightarrow \qquad \mathcal{D}_{int} = \sum_{\alpha=1}^{m} \bar{\mathbf{S}}_{\alpha}^{V} : \frac{\dot{\boldsymbol{\Gamma}}_\alpha}{2} \geq 0 \tag{2.65}$$

Additional equations of evolution must be defined in order to satisfy the inequality (2.63) (i.e. the condition of local entropy production). An extension of the evolution equations for the linear case leads to

$$\dot{\bar{\mathbf{S}}}_{\alpha}^{V} + \frac{\bar{\mathbf{S}}_{\alpha}^{V}}{\tau_\alpha} = \dot{\bar{\mathbf{S}}}_{\alpha} \,, \quad \alpha = 1, \ldots, m \tag{2.66}$$

which is valid for a semi-open time interval $t \in (0, T]$. The values of the internal variables at initial time $t = 0$ are assumed to be zero, since a stress-free reference configuration is considered. The tensor $\bar{\mathbf{S}}_\alpha$ is the isochoric second Piola-Kirchhoff stress corresponding to the system related to the α-relaxation process with relaxation time $\tau_\alpha \in (0, \infty)$. $\bar{\mathbf{S}}_\alpha$ is defined according to equation (2.48) as

$$\bar{\mathbf{S}}_\alpha = J^{-2/3}\mathbb{P} : \tilde{\mathbf{S}}_\alpha \tag{2.67}$$

where $\tilde{\mathbf{S}}_\alpha = 2\partial\bar{\Psi}_\alpha/\partial\bar{\mathbf{C}}$ is a (fictitious) isochoric second Piola-Kirchhoff stress.

The set of linear equations (2.66) has a physical basis, provides a good approximation of the behaviour of real materials under large deformation and it is also suitable for efficient numerical time integration scheme.

Finally, disregarding an instantaneous response at $t = 0$ the closed form solution of equations

(2.66) is given by the convolution integrals

$$\bar{\mathbf{S}}_{\alpha}^{V} = \int_{t=0}^{t=T} \exp\left\{\frac{-(T-t)}{\tau_{\alpha}}\right\} \dot{\bar{\mathbf{S}}}_{\alpha}(t)\,\mathrm{d}t \tag{2.68}$$

The integral (2.68) defines a so-called *quasi-linear* viscoelastic response: compared to a standard linear viscoelastic model, the relation between stress and strain becomes non-linear due to finite deformations but the linearity in the time domain is preserved.

2.6 Elasticity tensor

In order to compute the solution of non-linear problems in finite elasticity, a sequence of linearised problem is derived using Newton-like techniques, and solved instead. Hence, from the computational point of view it is important to derive a linearisation of the constitutive relations defined above.

The non-linear second Piola-Kirchhoff stress tensor $\mathbf{S}$ is assumed to be solely a tensor-valued function of one tensorial variable, in particular the right Cauchy-Green tensor $\mathbf{C}$. A first order Taylor expansion of $\mathbf{S}$ around $\mathbf{C}$ then gives

$$\mathbf{S}(\mathbf{C} + \mathrm{d}\mathbf{C}) = \mathbf{S}(\mathbf{C}) + \mathrm{d}\mathbf{S} + O(\mathrm{d}\mathbf{C}) \tag{2.69}$$

with

$$\mathrm{d}\mathbf{S} = \frac{\partial \mathbf{S}(\mathbf{C})}{\partial \mathbf{C}} : \mathrm{d}\mathbf{C} = 2\frac{\partial \mathbf{S}(\mathbf{C})}{\partial \mathbf{C}} : \frac{1}{2}\mathrm{d}\mathbf{C} \tag{2.70}$$

where

$$\mathbb{C} = 2\frac{\partial \mathbf{S}(\mathbf{C})}{\partial \mathbf{C}} \quad \text{or} \quad C_{IJKL} = 2\frac{\partial S_{IJ}}{\partial C_{KL}} \tag{2.71}$$

is known as *elasticity tensor* and represent the derivative of $\mathbf{S}$ relative to $\mathbf{C}$ and it is therefore a fourth order tensor. The elasticity tensor relates the work conjugate pairs of stress and strain tensors, measuring the change of stress resulting from a change in strain.

It should be emphasized that for hyperelastic materials $\mathbb{C}$ possesses minor and major symmetries. The minor symmetries can be expressed in index form as

$$\mathrm{C_{IJKL}} = \mathrm{C_{JIKL}} = \mathrm{C_{IJLK}} \tag{2.72}$$

and they arise from the symmetries of $\mathbf{S}$ and $\mathbf{C}$. Therefore they are typical of all elastic

materials and they do not require the existence of a hyperelastic potential.
On the other hand, the major symmetries hold if a hyperelastic strain-energy functionΨ is defined. Using the definition of the second Piola-Kirchhoff with respect to the potential energy (2.42) it is possible to write

$$\mathbb{C} = 2\frac{\partial}{\partial \mathbf{C}}\left[2\frac{\partial \Psi(\mathbf{C})}{\partial \mathbf{C}}\right] = 4\frac{\partial^2 \Psi(\mathbf{C})}{\partial \mathbf{C}\partial \mathbf{C}} \quad \text{or} \quad C_{IJKL} = 4\frac{\partial^2 \Psi}{\partial C_{IJ}\partial C_{KL}} \tag{2.73}$$

which directly provides the symmetry relation

$$\mathbb{C} = \mathbb{C}^{\mathrm{T}} \quad \text{or} \quad \mathrm{C_{IJKL}} = \mathrm{C_{KLIJ}} \tag{2.74}$$

Due to the symmetries, the elasticity tensor $\mathbb{C}$ has only 21 independent components. The major symmetries are particularly important from a numerical point of view as they guarantee the symmetry of the tangent stiffness matrix in a finite element formulation.
The elasticity tensor in spatial reference is computed through an inverse Piola transformation (sometimes in the literature a normal push-forward operation is used instead):

$$\mathbb{c} = J^{-1}\chi_*[\mathbb{C}] \quad \text{or} \quad c_{ijkl} = J^{-1}F_{iI}F_{jJ}F_{kK}F_{lL}C_{IJKL} \tag{2.75}$$

Minor and major symmetries hold also in the spatial reference (the latter only if hyperelastic potential can be defined).

According to the decoupled definition of the second Piola-Kirchhoff stress tensor (2.42) the elasticity tensor in material reference can be written as

$$\mathbb{C} = 2\frac{\partial \mathbf{S_{vol}}(\mathbf{C})}{\partial \mathbf{C}} + 2\frac{\partial \bar{\mathbf{S}}(\bar{\mathbf{C}})}{\partial \bar{\mathbf{C}}} = \mathbb{C}_{vol} + \bar{\mathbb{C}} \tag{2.76}$$

Using arguments introduced in previous sections, a straightforward but lengthy calculation that for brevity is not reported here (see e.g. [25]) leads to the following expression for volumetric and isochoric contribution:

$$\mathbb{C}_{vol} = J\tilde{p}\mathbf{C}^{-1} \otimes \mathbf{C}^{-1} - 2Jp\mathbb{I}_{\mathbf{C}^{-1}} \tag{2.77}$$

$$\bar{\mathbb{C}} = J^{-4/3}\mathbb{P} : \tilde{\mathbb{C}} : \mathbb{P} + \frac{2}{3}\mathrm{Tr}(J^{-2/3}\bar{\mathbf{S}})\tilde{\mathbb{P}} - \frac{2}{3}(\mathbf{C}^{-1} \otimes \bar{\mathbf{S}} + \bar{\mathbf{S}} \otimes \mathbf{C}^{-1}) \tag{2.78}$$

where the scalar function $\tilde{p} = p + J(\mathrm{d}p/\mathrm{d}J)$, the referential isochoric (fictitious) elasticity tensor $\tilde{\mathbb{C}} = 4\partial^2\bar{\Psi}/\partial\bar{\mathbf{C}}^2$ and the fourth order tensor $[\mathbb{I}_{\mathbf{C}^{-1}}]_{\mathrm{IJKL}} = \frac{1}{2}(C^{-1}_{IK}C^{-1}_{JL} + C^{-1}_{IL}C^{-1}_{JK})$ are introduced. Moreover, the referential trace operator $\mathrm{Tr}[\cdot] := [\cdot] : \mathbf{C}$ and the referential fourth order projection tensor $\tilde{\mathbb{P}} = \mathbb{I}_{\mathbf{C}^{-1}} - \frac{1}{3}(\mathbf{C}^{-1} \otimes \mathbf{C}^{-1})$ are utilized.

An inverse Piola transformation of (2.76) gives the definition of the decoupled elasticity tensor in the spatial configuration

$$\mathbb{c} = J^{-}1\chi_*[\mathbb{C}] = \mathbb{c}_{vol} + \bar{\mathbb{c}} \tag{2.79}$$

with

$$\mathbb{C}_{vol} = \tilde{p}\mathbf{I} \otimes \mathbf{I} - 2p\mathbb{I} \tag{2.80}$$

$$\bar{\mathbb{C}} = J^{-4/3}\mathbb{p} : \tilde{\mathbb{c}} : \mathbb{p} + \frac{2}{3}J^{-2/3}\mathrm{tr}(\tilde{\boldsymbol{\sigma}})\mathbb{p} - \frac{2}{3}[\mathbf{I} \otimes \bar{\boldsymbol{\sigma}} + \bar{\boldsymbol{\sigma}} \otimes \mathbf{I}] \tag{2.81}$$

where $\tilde{\mathbb{c}} = J^{-1}\chi_*[\tilde{\mathbb{C}}]$ is the spatial isochoric (fictitious) elasticity tensor and the spatial trace operator $\mathrm{tr}[\cdot] := [\cdot] : \mathbf{I}$ is utilized.

The equations above are compact notations for the material and spatial tensors, but an efficient finite element implementation requires these expressions to be elaborated for a particular constitutive model.

Chapter 3

Methods

In this chapter the constitutive equations and the relative numerical implementation are described. It is assumed that fibres are continuously distributed throughout the material so that the continuum theory of fibre reinforced composite materials (see section 2.4.3, or [25] for a complete discussion) is the constitutive theory of choice. The elastic strain energy function of a material with statistical fibre distribution is obtained from that of a composite material with a family of perfectly aligned fibres by using a directional average of the structure tensor (2.58) and suitably modified to account for tension compression asymmetry of collagen fibres. The stress and elasticity tensors are computed as the first and second derivatives of the elastic potential with respect to a suitable strain measure. A probability distribution function is also proposed and its use in the model is discussed. Finally, the main aspects of the finite element implementation are outlined and some illustrative examples are described.

3.1 Structure tensor

Soft tissues with fibre reinforcement are often modelled using the superposition method and including the directional information of each family of fibres into a structure tensor (see section 2.4.3). However, the complex three-dimensional network of collagen that characterizes AC can be more effectively modelled as one family of fibres statistically distributed around a polar axis.

To account for such configuration, it was proposed in [13] to define a generalized structure tensor by calculating the directional average of the structure tensor (2.58). For completeness and continuity, the derivation of this tensor is reported below, as it represents the foundation of the one introduced in section 3.2 for the specific case of AC.

Following [13], an orthonormal basis of the *Eulerian* space $\mathbb{R}^3$ is considered. The choice of the basis is arbitrary, but for sake of simplicity the canonical basis ($\{\hat{\mathbf{e}}_\mathbf{1}, \hat{\mathbf{e}}_\mathbf{3}, \hat{\mathbf{e}}_\mathbf{3}\}$) is used. A generic unit vector $\mathbf{M}$ ($|\mathbf{M}| = 1$) can be expressed in polar coordinates as function of the co-latitude Θ from the polar axis $\mathbf{K}$ (without loss of generality $\mathbf{K} = \hat{\mathbf{e}}_\mathbf{3}$ is chosen) and longitude Φ from the $\hat{\mathbf{e}}_\mathbf{1} - \hat{\mathbf{e}}_\mathbf{3}$ plane as

$$\mathbf{M}(\Theta, \Phi) = \sin\Theta\cos\Phi\,\hat{\mathbf{e}}_1 + \sin\Theta\sin\Phi\,\hat{\mathbf{e}}_2 + \cos\Theta\,\hat{\mathbf{e}}_3. \tag{3.1}$$

where $\Theta \in [0, \pi]$ and $\Phi \in [0, 2\pi]$ (see Figure 3.1). For each $\mathbf{M}$, $-\mathbf{M}$ is also included in the ranges of the *Eulerian* angles.

A probability distribution $\rho(\mathbf{M})$ is introduced, that characterizes the distribution of fibres in the reference configuration Ω_0. The distribution is defined such that $\rho(\mathbf{M}(\Theta, \Phi))\sin\Theta d\Theta d\Phi$ represents the number of fibres with orientation in the range $[(\Theta, \Theta + d\Theta), (\Phi, \Phi + d\Phi)]$ (see Figure 3.1). Moreover, it has to obey the symmetry condition $\rho(\mathbf{M}) \equiv \rho(-\mathbf{M})$ and to be normalized over the unit sphere such that

$$\frac{1}{4\pi}\int_{\mathbb{S}^2} \rho(\mathbf{M}(\Theta, \Phi))\, dS = \frac{1}{4\pi}\int_0^{2\pi}\int_0^{\pi} \rho(\Theta, \Phi)\sin\Theta\, d\Theta\, d\Phi = 1 \tag{3.2}$$

where $\mathbb{S}^2$ is the unit sphere and the polar representation of $\mathbf{M}$ was used to express the probability distribution as a function of Θ and Φ.

The directional average of any function $f(\mathbf{M})$ is then given by

$$\langle f \rangle = \frac{1}{4\pi}\int_{\mathbb{S}^2} \rho(\mathbf{M}) f(\mathbf{M})\, dS = \frac{1}{4\pi}\int_0^{2\pi}\int_0^{\pi} \rho(\Theta, \Phi) f(\mathbf{M}(\Theta, \Phi))\sin\Theta\, d\Theta\, d\Phi \tag{3.3}$$

Due to the symmetry requirement on the density function, only general orthotropic distributions are suitable to represent the fibres. In particular, a transversely isotropic distribution around the polar axis $\mathbf{K} = \hat{\mathbf{e}}_\mathbf{3}$ is chosen, that is sufficient to describe the fibre arrangement characterizing the three zones of AC (see section 1.2). Hence, the distribution is independent of the longitude Φ and the normalization condition becomes

$$\int_0^{\pi} \rho(\Theta)\sin\Theta\, d\Theta = 2 \tag{3.4}$$

Following [13], a (symmetric) generalized structure tensor of second order can then be in-

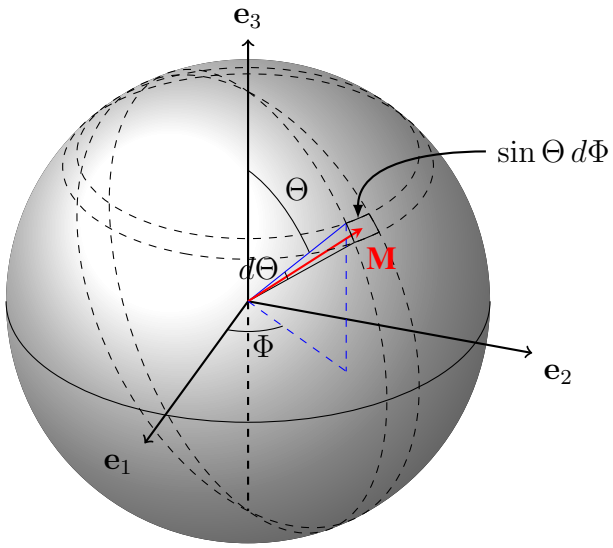

Figure 3.1: Representation of the unit sphere and the typical pyramidal element and characterization of an arbitrary unit direction vector **M** in polar coordinates. The fibres distribution can be seen as a smaller pyramidal element whose base is determined by $\rho(\mathbf{M})$ as a fraction of $dA = \sin\Theta d\Theta d\Phi$.

troduced, which represents the fibre distribution:

$$\mathbf{H} = \frac{1}{4\pi}\int_0^{2\pi}\int_0^{\pi} \rho(\Theta)\mathbf{M}(\Theta,\Phi)\otimes\mathbf{M}(\Theta,\Phi)\sin\Theta\, d\Theta\, d\Phi = \frac{1}{4\pi}\int_{\mathbb{S}^2}\rho(\mathbf{M})\mathbf{A}(\mathbf{M})\, dS \quad (3.5)$$

where $\mathbf{A}(\mathbf{M}) = \mathbf{M}\otimes\mathbf{M}$ is the contribution to the structure tensor associated with direction $\mathbf{M}$.

3.2 Anisotropic viscoelastic formulation at finite strains

A free energy potential was formulated based on the decoupled form of the potential described in section 3.2. The tissue was assumed to be incompressible. This assumption, supported by the high water content in biological tissue and by experimental evidence, it is fundamental when the decoupled potential is used to study fibre reinforced composite materials, in order to avoid non-physical behaviour of the model [19]. Moreover, the traditional definition of a free energy function, as is adopted here, requires the use of a stress-free reference configuration.

Firstly, the equilibrium potential is considered (i.e. viscoelasticity is disregarded).
Due to the incompressibility assumption, a function U of the volumetric deformation J (2.41)

does not need to be defined. Moreover, it is assumed that the isochoric part of the free energy function can be expressed as the superposition of an isotropic potential $\bar{\Psi}_g^\infty$ related to the ground matrix and and a potential $\bar{\Psi}_f^\infty$ due to the collagen fibre distribution

$$\bar{\Psi}^\infty(\bar{\mathbf{C}}, \mathbf{H}) = \phi_g \bar{\Psi}_g^\infty(\bar{\mathbf{C}}) + \phi_f \bar{\Psi}_f^\infty(\bar{\mathbf{C}}, \mathbf{H}) \tag{3.6}$$

where $\mathbf{H}$ is defined in accordance with (3.5) and depends on a concentration parameter and the Cauchy-Green tensor, as will be explained in more details below.
Several works, e.g. [24] [13] [1], model the ground matrix as an incompressible isotropic *neo-Hookean* material. Due to the complexity of the composition of AC (see section 1.2), this might be a too restrictive simplification. Nevertheless, in view of its simplicity, this assumption is adopted here. Hence the free energy function associated with the matrix reads

$$\bar{\Psi}_g^\infty(\bar{\mathbf{C}}) = \frac{1}{2} c_0 (\bar{I}_1 - 3) \tag{3.7}$$

where c_0 denotes the *neo-Hookean* parameter (i.e. the shear modulus of the matrix) and $\bar{I}_1$ is the standard definition of the first invariant of $\bar{\mathbf{C}}$

$$\bar{I}_1 = \bar{\mathbf{C}} : \mathbf{I} = tr(\bar{\mathbf{C}}) \tag{3.8}$$

The fibre contribution is split into an isotropic contribution, that accounts for the different 'passive' mechanical properties with respect to the ground matrix, and an anisotropic contribution that accounts for the transversely isotropic properties of the fibres.

$$\bar{\Psi}_f^\infty(\bar{\mathbf{C}}, \mathbf{H}) = \bar{\Psi}_{f_i}^\infty(\bar{\mathbf{C}}) + \bar{\Psi}_{f_a}^\infty(\bar{\mathbf{C}}, \mathbf{H}) \tag{3.9}$$

For simplicity, the isotropic contribution is modelled as a *neo-Hookean* material characterized by a parameter $c_{f_i} \neq c_0$, i.e.

$$\bar{\Psi}_{f_i}^\infty(\bar{\mathbf{C}}) = \frac{1}{2} c_{f_i} (\bar{I}_1 - 3) \tag{3.10}$$

As described in section 1.2, collagen fibres are wavy in the reference configuration and the load required to straighten them can be neglected when compared to the load that they transmit once stretched (i.e. collagen fibres are assumed to transmit load only if stretched beyond the point where undulations disappear). This phenomenon can be effectively modelled by

means of a non-linear expression for the potential and such solution was adopted in this work. It is reported in the literature that a quadratic function may be sufficient to effectively reproduce the behaviour of AC in different cases of interest, e.g. immature or engineered cartilage, that do not exhibit strong non-linearity at large deformations [51]. Hence, the second-order polynomial form

$$\bar{\Psi}^{\infty}_{f_a}(\bar{\mathbf{C}}, \mathbf{H}) = \frac{1}{2} c_{f_a} \bar{E}^2 = \frac{1}{2} c_{f_a} (\bar{I}_4 - 1)^2 \tag{3.11}$$

is proposed to particularize the fibre contribution, where $c_{f_a} > 0$ is a stress-like parameter to be determined from mechanical tests of the tissue and $\bar{I}_4$ denotes an invariant of the symmetric generalized structure tensor (see [56] for a general discussion of invariants of this kind), defined as

$$\bar{I}_4 = \mathbf{H} : \bar{\mathbf{C}} \tag{3.12}$$

The same invariant can be defined for each component of the structure tensor, i.e

$$\bar{I}_4^{\mathbf{M}} = \mathbf{A} : \bar{\mathbf{C}} = (\mathbf{M} \otimes \mathbf{M}) : \bar{\mathbf{C}} = \mathbf{M} \cdot \bar{\mathbf{C}}\mathbf{M} = \bar{\lambda}^2_{\mathbf{M}} \tag{3.13}$$

where it is clearly shown that the distorsional invariant $\bar{I}_4^{\mathbf{M}}$ represents the squared stretch in the direction $\mathbf{M}$, i.e. the distortional fibre stretch under the hypothesis of perfect bonding between fibres and matrix. Note that $\mathbf{A} : \mathbf{I} = \mathbf{H} : \mathbf{I} = 1$. $\bar{I}_4$ can be interpreted as an extension of (3.13) and it is used to define the Green-Lagrange strain-like quantity $\bar{E} = \mathbf{H} : \bar{\mathbf{C}} - 1$, which characterizes the weighted averaged strain of the fibres at the material point.

Finally, it is assumed that collagen fibres would buckle under the smallest compressive load (i.e. they are characterized by zero compressive modulus) [34]. This modelling assumption, common for the representation of soft tissues with fibre reinforcement, is not only based on physical reasons and experimental evidence, but also essential for stability [22] [13] [9]. It is therefore assumed that the fibres contribute to the anisotropic potential $\bar{\Psi}^{\infty}_{f_a}$ only if the strain in their axial direction is positive, i.e. if $\bar{I}_4^{\mathbf{M}} > 1$.

In biological tissues in which families of fibres can be identified, it is sufficient to check the preferred orientation assuming that if the fibres in that direction are stretched, then all the fibres at that point are stretched as well [13], while the dispersion about the polar axis modulates the level of response. This assumption is not valid for the network of collagen in AC. Under physiological load, the depth-dependent stiffness of the tissue generates a complex three-dimensional deformation state such that at each point in the continuum some

of the fibres are stretched while other are compressed.
This has two important implications: firstly, the stretch must be evaluated in every direction and the definition (3.5) of the structure tensor $\mathbf{H}$ should be modified to include only the contribution of stretched fibres; secondly, at each loading step the integration must be performed at each material point.

3.2.1 Modified structure tensor

The expression of the structure tensor must be suitably modified so that the contribution $\mathbf{A}(\mathbf{M})$ associated with compressed fibres does not affect the anisotropic fibre contribution.
The idea is that the strain-like quantity $\bar{E}$ in the energy expression should be zero in the initial configuration Ω_0, which is assumed to be stress-free, and also in every configuration where fibres are either compressed or undeformed. Moreover, when fibres are stretched in some directions and compressed in others, only the stretched bundles should affect the potential.

A solution often adopted in the literature is the introduction of a Heaviside function that completely eliminates the contribution of compressed bundles [13] [51] [9], thus defining an effective volume fraction. This approach is effective when an ensemble fibre potential is considered, i.e. when the potential associated with each direction is computed independently and then integrated over the sphere [9], but it leads to non-physical results when used in the directional average for the structure tensor, as it is shown with an example below. The difference is that in the former case the step function is directly applied on the energy contribution making it null, whereas in the latter case it acts on a stretch measure ($\mathbf{H} : \bar{\mathbf{C}}$) that should always be greater than zero.
The contribution to the structure tensor in the direction of compressed fibres should be such that it generates a unit stretch under the current deformation state. Hence, this contribution cannot be computed *a priori* but has to be related to the deformation tensor.
In particular, the definition of the contribution to the structure tensor associated with each direction $\mathbf{M}$ was modified as

$$\mathbf{A} = \begin{cases} \frac{1}{3}\bar{\mathbf{C}}^{-\mathbf{1}} & \text{if } \bar{\lambda}^2_{\mathbf{M}} \leq 1 \\ \mathbf{M} \otimes \mathbf{M} & \text{if } \bar{\lambda}^2_{\mathbf{M}} > 1 \end{cases} \tag{3.14}$$

It can be easily showed that the new definition of $\mathbf{A}(\bar{\lambda}_M^2 \leq 1)$ fulfils the requirements as

$$\bar{I}_4^{\mathbf{M}}(\bar{\lambda}_{\mathbf{M}}^2 \leq 1) = \mathbf{A} : \bar{\mathbf{C}} = \frac{1}{3}\bar{\mathbf{C}}^{-\mathbf{1}} : \bar{\mathbf{C}} = \frac{1}{3}tr(\bar{\mathbf{C}}^{-\mathbf{T}}\bar{\mathbf{C}}) = \frac{1}{3}tr(\mathbf{I}) = 1$$

so that the strain-like quantity associated with the considered direction becomes $\bar{E}^{\mathbf{M}} = 0$ and the anisotropic contribution to the potential vanishes for configurations where no fibres are stretched.

Compared to the use of a step function, the definition introduced above has also the advantage of ensuring the continuity of the integrand function, which in turn leads to the continuity of $\bar{I}_4^M$ with respect to the stretch $\lambda_{\mathbf{M}}$ (see Figure 3.2), and more in general of the averaged quantity $\bar{I}_4$, e.g. for the initial configuration Ω_0:

$$\bar{I}_4(\Omega_0) = \mathbf{H} : \bar{\mathbf{C}} = \langle \mathbf{A}(\bar{\lambda}_{\mathbf{M}}^{\mathbf{2}} = \mathbf{1}) \rangle : \bar{\mathbf{C}} = 1$$
$$\bar{I}_4(\Omega_0^+) = \mathbf{H} : \bar{\mathbf{C}} = \langle [\mathbf{M} \otimes \mathbf{M}](\bar{\lambda}_{\mathbf{M}}^{\mathbf{2}} = \mathbf{1}^+) \rangle : \bar{\mathbf{C}} = \langle \bar{\lambda}_{\mathbf{M}}^2 \rangle = 1$$

This is important for the numerical implementation of the model as it improves the stability and it spares the use of smoothing functions sometimes required for convergence.

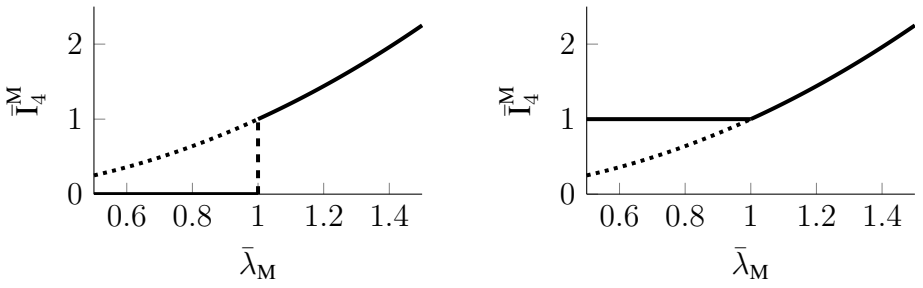

(a) $\mathbf{A}(\bar{\lambda}_{\mathbf{M}}^2 \leq 1) = 0$ **(b)** $\mathbf{A}(\bar{\lambda}_{\mathbf{M}}^2 \leq 1) = \frac{1}{3}\bar{\mathbf{C}}^{-\mathbf{1}}$

Figure 3.2: If compressed fibres are simply disregarded $\bar{I}_4^M$ is not a continuous function of $\bar{\lambda}_M$ (left). The proposed definition of $\bar{I}_4^M$ ensures continuity (right). The dotted lines represent the original definition of the structure tensor.

An alternative approach would be to integrate the structure tensor (3.5) over an effective surface on the unit sphere that includes only stretched fibres and to weight the result for the strain with the density fraction of stretched fibres:

$$\mathrm{E}_{\mathrm{eff}} = \left\{ \left[\frac{1}{\rho_t} \int_{\mathbb{S}_t^2} \rho(\mathbf{M}) \mathbf{M} \otimes \mathbf{M} \, \mathrm{dS} \right] : \mathbf{C} - 1 \right\} \frac{\rho_t}{\rho_{tot}} \tag{3.15}$$

where ρ_t is the density of stretched fibres and ρ_{tot} is the total fibre density, i.e. the result of the integration of the density function over the unit sphere (in this case 4π).

It can be shown that the two approaches are equivalent:

$$\begin{aligned} \mathrm{E}^* &= \left\{ \frac{1}{\rho_{tot}} \left[\int_{\mathbb{S}_t^2} \rho(\mathbf{M}) \mathbf{M} \otimes \mathbf{M} \, \mathrm{dS} + \int_{\mathbb{S}_c^2} \rho(\mathbf{M}) \frac{1}{3} \mathbf{C}^{-1} \, \mathrm{dS} \right] \right\} : \mathbf{C} - 1 \\ &= \left[\frac{1}{\rho_{tot}} \int_{\mathbb{S}_t^2} \rho(\mathbf{M}) \mathbf{M} \otimes \mathbf{M} \, \mathrm{dS} \right] : \mathbf{C} + \frac{\rho_c}{\rho_{tot}} - 1 \\ &= \left[\frac{1}{\rho_{tot}} \int_{\mathbb{S}_t^2} \rho(\mathbf{M}) \mathbf{M} \otimes \mathbf{M} \, \mathrm{dS} \right] : \mathbf{C} - \frac{\rho_t}{\rho_{tot}} = \mathrm{E}_{\mathrm{eff}} \end{aligned} \tag{3.16}$$

The definition of the contribution (3.14) has two advantages: it does not require the redefinition of the integration surface and it encloses all the information in the structure tensor without the need to operate on the strain definition.

Example

In order to clearly show the effect of the modified contribution for compressed fibres in the structure tensor, a simplified example is analysed. Consider the configuration sketched in Figure 3.3: a cube of incompressible hyperelastic material is constrained in direction x_3 and it is stretched along direction x_1. The material is reinforced by a three dimensional network of fibres, which can be interpreted as the limit case of a distribution in which one third of the fibres is aligned in the direction of each of the three axes of a Cartesian basis x_1, x_2, x_3. A first configuration (denoted by 'A')is considered, with applied stretch $\lambda_1 = \lambda_A > 1$.

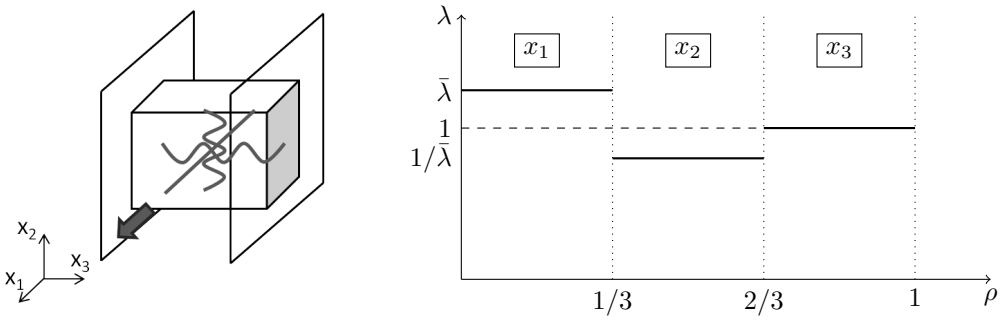

Figure 3.3: Cube of incompressible hyperelastic material reinforced by a three dimensional fibre network under tension (left); one-dimensional representation of stretch level in the fibres (right).

Given the simple configuration of boundary conditions and loads and the fibres orientation, the stretches along the Cartesian basis axes represent the principal stretches for the problem.

Hence, the deformation gradient is simply given by the diagonal matrix:

$$F = \begin{bmatrix} \lambda_1 & 0 & 0 \\ 0 & \lambda_2 & 0 \\ 0 & 0 & \lambda_3 \end{bmatrix} \tag{3.17}$$

Incompressibility prevents volume changes. According to (2.7) this can be expressed as

$$J = \det(\mathbf{F}) = \lambda_1\lambda_2\lambda_3 = 1 \tag{3.18}$$

which immediately leads to the stretch in direction x_2

$$\lambda_2 = \frac{1}{\lambda_1\lambda_3} = \frac{1}{\lambda_A} \tag{3.19}$$

where $\lambda_1 = \lambda_A$ and $\lambda_3 = 1$ due to the constraint in direction x_3.
Assuming perfect bonding between fibres and matrix, the principal stretches can be directly associated to the fibres in the corresponding direction. The stretch level in the fibres can therefore be schematically represented as in Figure 3.3. Clearly, only the fibres in direction x_1 are stretched, and therefore they are the only ones that should contribute to the energy, such that $\Psi = f(\mathrm{E}_1)$, where $\mathrm{E}_1 = \lambda_1^2 - 1$ is a measure of the strain in direction x_1, defined in analogy with $\bar{E}$.

Using an approach similar to the one described in section 3.1, the averaged squared stretch (corresponding to $\mathbf{H} : \bar{\mathbf{C}}$) is used to compute the fibre contribution to the energy through the strain measure $E = \langle\lambda^2\rangle - 1$.
The calculations are performed (i) according to the definition of H as in (3.5), (ii) applying the Heaviside function to eliminate the contribution of the compressed fibres and (iii) modifying $\mathbf{H}$ as described above in this section. The results are, respectively:

$$\begin{aligned} \mathrm{E}_A &= \lambda_A^2\frac{1}{3} + 1\cdot\frac{1}{3} + \frac{1}{\lambda_A^2}\frac{1}{3} - 1 = \frac{(\lambda_A^2-1)^2}{3\lambda_A^2} \\ \mathrm{E}_A^H &= \lambda_A^2\frac{1}{3} - 1 \\ \mathrm{E}_A^* &= \lambda_A^2\frac{1}{3} + \frac{2}{3} - 1 = \frac{\lambda_A^2-1}{3} \end{aligned} \tag{3.20}$$

A second configuration (denoted by 'B') is then considered, in which the stretch λ_1 is such

that the strain in direction x_1 is k times the corresponding strain in configuration (A) with $k > 1$, i.e.

$$\mathrm{E}_1^B = k\mathrm{E}_1^A \quad \Rightarrow \quad \lambda_1^B = \lambda_B = \sqrt{k\lambda_A^2 - k + 1} \tag{3.21}$$

The energy contribution in this configuration is then expected to be $\Psi^B = f(\mathrm{E}_1^B) = f(k\mathrm{E}_1^A)$. Once again the averaged squared stretch is used to compute the energy associated with this configuration. The results for the three cases defined above are

$$\begin{aligned}
\mathrm{E}_B &= \frac{k\lambda_A^2 - k + 1}{3} + \frac{1}{3} + \frac{1}{3(k\lambda_A^2 - k + 1)} - 1 = \dots \\
&= \frac{\lambda_A^2 k^2}{\lambda_A^2 k - k + 1} \frac{(\lambda_A^2 - 1)^2}{3\lambda_A^2} = \frac{\lambda_A^2 k^2}{\lambda_B^2} \mathrm{E}_A \\
\mathrm{E}_B^H &= \frac{k\lambda_A^2 - k + 1}{3} - 1 = k(\frac{\lambda_A^2}{3} - 1) + \frac{2}{3}(k-1) = k\mathrm{E}_A^H - \frac{2}{3}(k-1) \\
\mathrm{E}_B^* &= \frac{k\lambda_A^2 - k + 1}{3} - \frac{1}{3} = k\frac{\lambda_A^2 - 1}{3} = k\mathrm{E}_A^*
\end{aligned} \tag{3.22}$$

The comparison of the results for the two configurations shows that only the modification described in this work leads to the correct representation of the energy contribution. In particular the original definition of λ^2 is such that the change in the compression of the fibres in direction x_2 (that should not influence the energy) modulates the change of the strain measure, whereas the introduction of the Heaviside function alters the expected energy contribution with a term related to the change of strain in the stretched fibres direction. Moreover, it should be noted that the potential defined in (3.11) is a quadratic function of the strain-like quantity E, so that $\Psi(E) = \Psi(|E|)$. Thus, the introduction of the Heaviside function results in a clearly non-physical behaviour for all the cases where $k\lambda < \sqrt{3}$, since the contribution for configuration (B), where the fibres are more stretched, is lower than the one for configuration (A):

$$|\mathrm{E}_A^H| = -\mathrm{E}_A^H \quad \Rightarrow \quad |\mathrm{E}_B^H| = k|\mathrm{E}_A^H| - \frac{2}{3}(k-1) \tag{3.23}$$

where $2/3(k-1)$ is always positive as $k > 1$.

Finally, the example confirms that the approach suggested in this work provides the same results as an effective strain computed through the average of the stretch only over an effective area on the spherical surface (in this limit case direction x_1) and weighted with the density

fraction of the stretched fibres (in this case 1/3):

$$\mathrm{E}_{\mathrm{eff}} = (\lambda^2 - 1) \cdot \frac{1}{3} = \frac{\lambda^2 - 1}{3} = \mathrm{E}_A^* \tag{3.24}$$

Once again it is emphasized that the problem analysed above is indeed a strong simplification of the case considered in this work and cannot be directly assumed as a general proof of the correct behaviour of the model proposed here, but it serves the purpose of clearly showing the advantages of the chosen approach with respect to other possible solutions.

3.2.2 Viscoelastic contribution

The viscoelastic response was modelled using the concept of internal variables described in section 2.5, i.e. as the superposition of an elastic equilibrium response and a number of non-equilibrium viscous processes. Accordingly, it was assumed that viscoelasticity is associated only with the isochoric part of the deformation, as it is well established in the literature (see [25] for a complete discussion).

Moreover, since it has been observed also in tensile tests, where fluid pressure is negligible as well as the contribution from the proteoglycan matrix (see section 1.2), the intrinsic viscoelasticity of AC must be mainly determined by the collagen fibres and their cross-links. Hence, in the current work collagen fibres are considered viscoelastic, but the matrix is elastic similarly to [34].

Finally, following [21] the viscoelastic potentials $\bar{\Psi}_\alpha$ were expressed as a function of the isochoric elastic strain-energy $\bar{\Psi}^\infty$, which is responsible for the equilibrium response at $t \to \infty$:

$$\bar{\Psi}_\alpha(\bar{\mathbf{C}}) = \beta_\alpha^\infty \bar{\Psi}^\infty(\bar{\mathbf{C}}) \ , \quad \alpha = 1, \dots, m \tag{3.25}$$

where $\beta_\alpha^\infty \in [0, \infty)$ are non-dimensional strain energy factors associated with τ_α.

In accordance with the assumptions above, the complete form of the isochoric potential energy reads

$$\bar{\Psi} = \bar{\Psi}_g(\bar{\mathbf{C}}) + (1 + \sum_{\alpha=1}^{m} \beta_\alpha^\infty)[\bar{\Psi}_{f_i}^\infty(\bar{\mathbf{C}}) + \bar{\Psi}_{f_a}^\infty(\bar{\mathbf{C}}, \mathbf{H})] \tag{3.26}$$

where the non-dimensional constant $\beta_\alpha^\infty \in [0, \infty)$ relates the elastic and the viscous representations. It should be noted that this assumption is only valid close to the thermodynamic equilibrium.

This relation is immediately extended to the stress tensors, leading to the following rate equation for the viscous over-stress

$$\dot{\bar{\mathbf{S}}}_{\alpha}^{V} + \frac{\bar{\mathbf{S}}_{\alpha}^{V}}{\tau_{\alpha}} = \beta_{\alpha}^{\infty}[\dot{\bar{\mathbf{S}}}_{f_i}^{\infty} + \dot{\bar{\mathbf{S}}}_{f_a}^{\infty}] = \beta_{\alpha}^{\infty}\dot{\bar{\mathbf{S}}}_{f}^{\infty} \tag{3.27}$$

Disregarding an instantaneous stress response at $t = 0$, the closed form solution of equation (3.27) is given by the convolution integral [52]

$$\bar{\mathbf{S}}_{\alpha}^{V} = \beta_{\alpha}^{\infty} \int_{T=0}^{T=t} \exp\left\{\frac{-(t-T)}{\tau_{\alpha}}\right\} \dot{\bar{\mathbf{S}}}_{f}^{\infty} \, \mathrm{d}T \tag{3.28}$$

The integral (3.28) describes the viscous over-stress related to a α-relaxation process with relaxation time $\tau_{\alpha} \in (0, \infty)$, and corresponds to the contribution of a single element in the generalized Maxwell model, which is the most general representation for the linear case. This approach takes into account that the relaxation does not occur at a single time, but at a distribution of times. It is possible to define as many relaxation processes (i.e. spring-dashpot elements in the Maxwell model) as are necessary to accurately represent the distribution. In this work three elements were defined, as in many cases this is sufficient to approximate correctly the time dependent behaviour shown by AC in experimental tests [35] [58].

As explained in section 2.5, the relation (3.28) defines a quasi-linear viscoelastic model, which implies that in a relaxation test the relaxation function (i.e. stress normalized on the maximum stress at the end of the loading ramp) is independent of the level of applied deformation. Experimental tests on AC have shown that this assumption is not verified [2], indicating that a non-linear viscoelastic model is necessary to fully capture the time evolution of the mechanical response. However, the superposition of an elastic matrix and a quasi-linear viscoelastic reinforcement leads to a non-linear viscoelastic response for the tissue, as was suggested in [62] for a mixture of quasi-linear viscoelastic components characterized by different relaxation functions.

Following [62], it is possible to illustrate this effect considering the special case of stress relaxation under a uniaxial loading condition along the longitudinal direction parallel to the collagen fibre. At any given time $\bar{t}$ during the relaxation period it is possible to define the *relaxation ratio* as the ratio between the stress at time $\bar{t}$ and the stress at the end of the loading ramp, which equals the elastic solution for the limit case of a step load. Expressing the stress carried by the fibre as a fraction of the stress borne by the matrix dependent on the

strain level, the total relaxation ratio reads:

$$\mathrm{R}^{(\bar{t})} = \frac{\sigma_m^{(\bar{t})} + \sigma_f^{(\bar{t})}}{\sigma_m^e + \sigma_f^e} = \left\{\sigma_f^e = \alpha(\varepsilon)\sigma_m^e\right\} = \frac{\sigma_m^{(\bar{t})} + \sigma_f^{(\bar{t})}}{\sigma_m^e(1+\alpha(\varepsilon))} \tag{3.29}$$

Having assumed that only the fibres are viscoelastic, it is possible to define different relaxation ratios for the components, and in particular to set $\mathrm{R}_m^{(\bar{t})} = 1$:

$$\sigma_m^{(\bar{t})} = \mathrm{R}_m^{(\bar{t})}\sigma_m^e = \sigma_m^e\,; \qquad \sigma_f^{(\bar{t})} = \mathrm{R}_f^{(\bar{t})}\sigma_f^e = \mathrm{R}_f^{(\bar{t})}\alpha(\varepsilon)\sigma_m^e \tag{3.30}$$

Finally, substituting (3.30) into (3.29), it is possible to write the total relaxation ratio as a function of the strain:

$$\mathrm{R}^{(\bar{t})}(\varepsilon) = \frac{\sigma_m^e + \mathrm{R}_f^{(\bar{t})}\alpha(\varepsilon)\sigma_m^e}{\sigma_m^e(1+\alpha(\varepsilon))} = \frac{1 + \mathrm{R}_f^{(\bar{t})}\alpha(\varepsilon)}{1+\alpha(\varepsilon)} \tag{3.31}$$

which defines a non-linear viscoelastic behaviour.
At low strain levels, where the response is dominated by the matrix, the viscoelastic effect is low, while it progressively increases to higher strain levels where more fibres are active and the load is mostly carried by collagen.

3.3 Illustrative fibre distribution

In this section the specific probability function used in this work to describe the distribution of collagen fibres in AC is introduced.
Following the procedure proposed in [13] [9] the π-periodic von Mises distributions $\bar{\rho}(\Theta)$ centred at $\Theta = \pi/2$ and $\Theta = 0$ were considered:

$$\bar{\rho}_A\left(\Theta; \frac{\pi}{2}, b\right) = \frac{\exp[b\cos(2\Theta - \pi)]}{2\pi I_0(b)} \tag{3.32a}$$

$$\bar{\rho}_B(\Theta; 0, b) = \frac{\exp[b\cos(2\Theta)]}{2\pi I_0(b)} \tag{3.32b}$$

where $b > 0$ is a concentration parameter describing the dispersion about the polar axis (see Figure 3.4) and I_0 denotes the modified Bessel function of the first kind of order zero, given by

$$I_0(b) = \frac{1}{\pi}\int_0^\pi \exp(b\cos\Theta)\, d\Theta \tag{3.33}$$

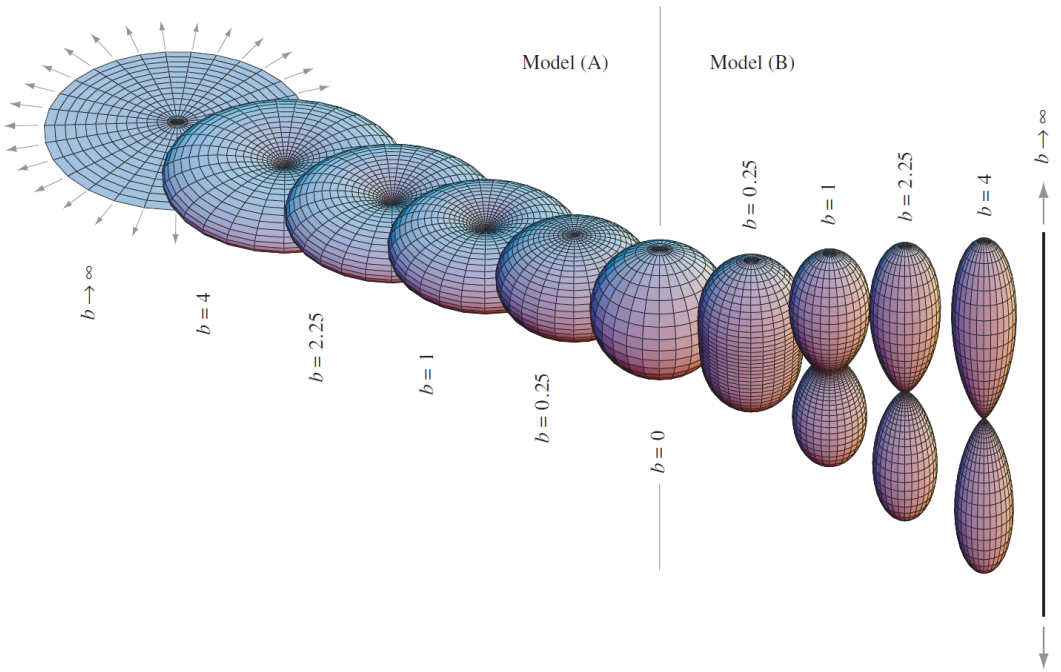

Figure 3.4: Three-dimensional graphical representation of the orientation of collagen fibres based on the transversely isotropic density functions ρ_A and ρ_B. Surface plots are defined by the vector $\rho(\boldsymbol{\Theta})\mathbf{M}$, where ρ is given by (3.34a) for model (A) and by (3.34b) for model (B). Image reproduced from [9].

The von Mises distribution is a close approximation to the wrapped normal distribution, which is the circular analogue of the normal distribution. As $b \to \infty$, it tends to a Dirac delta distribution with the same centre, so that $\bar{\rho}_A$ and $\bar{\rho}_B$ represent the limit cases of fibres randomly oriented in the transverse plane and fibres perfectly aligned in the polar direction, respectively.

According to the normalization condition (3.4) the expressions

$$I_A \equiv \frac{1}{2}\int_0^\pi \bar{\rho}_A(\Theta)\sin\Theta\, d\Theta \equiv \frac{1}{2}\frac{\exp(b)}{2\sqrt{2\pi b}}\frac{erf(\sqrt{2b})}{I_0(b)}$$
$$I_B \equiv \frac{1}{2}\int_0^\pi \bar{\rho}_B(\Theta)\sin\Theta\, d\Theta \equiv \frac{1}{2}\frac{\exp(-b)}{2\sqrt{2\pi b}}\frac{erfi(\sqrt{2b})}{I_0(b)}$$

are defined and used to normalize $\bar{\rho}$ resulting in

$$\rho_A(\Theta) = \frac{\bar{\rho}_A}{I_A} = 4\sqrt{\frac{b}{2\pi}}\frac{\exp[b(\cos(2\Theta-\pi)-1)]}{\operatorname{erf}(\sqrt{2b})} \tag{3.34a}$$

$$\rho_B(\Theta) = \frac{\bar{\rho}_B}{I_B} = 4\sqrt{\frac{b}{2\pi}}\frac{\exp[b(\cos(2\Theta)+1)]}{\operatorname{erfi}(\sqrt{2b})} \tag{3.34b}$$

where $\mathrm{erfi}(x) = -\mathrm{ierf}(x)$ is the imaginary error function [65], the error function itself being

$$\mathrm{erfi}(x) = \frac{2}{\sqrt{\pi}} \int_0^{\pi} \exp(-t^2)\, dt$$

The density functions (3.34) can be interpreted as a projection of the normal distribution onto the unit sphere [10]. A graphical representation of the density functions (3.34) is provided in Figure 3.4, in which the surface defined by the apex of the vector $\rho(\mathbf{M})\mathbf{M}$ is plotted with respect to the Eulerian angles Θ and Φ. Note that for both the distributions $b \to 0$ represents isotropy.

Due to the symmetry about the polar axis, the density functions (3.34) can also be represented by means of a two-dimensional plot, which is frequently used in the literature to present histological data, e.g. experimentally determined collagen distributions for planar collagenous tissues [50].

It is important to note that using this approach it is only necessary to know the orientation of the fibres in the reference configuration, since the new orientation in the current configuration is given by the push forward of the reference direction ($\mathbf{m} = \mathbf{F}\mathbf{M}$).

3.4 Spatial isochoric structure tensor

The solution of the governing equations is computed in an Eulerian setting. Hence, to include the structure tensor (3.5) in the numerical implementation, it is necessary to derive the corresponding expression in the spatial reference.

The spatial isochoric fibre direction can be computed as the push-forward of $\mathbf{M}$ through the isochoric deformation ($\bar{\chi}_*[\cdot]$):

$$\bar{\mathbf{m}} = \bar{\chi}_*[\mathbf{M}] = J^{-1/3}\mathbf{F}\mathbf{M} = \bar{\mathbf{F}}\mathbf{M} \tag{3.35}$$

Similarly, the spatial isochoric structure tensor related to the fibre bundle in direction $\mathbf{M}$ becomes

$$\begin{aligned} \bar{\mathbf{a}} &= \bar{\chi}_*[\mathbf{M} \otimes \mathbf{M}] = J^{-2/3}\mathbf{F}(\mathbf{M} \otimes \mathbf{M})\mathbf{F}^{\mathrm{T}} = \bar{\mathbf{F}}(\mathbf{M} \otimes \mathbf{M})\bar{\mathbf{F}}^{\mathrm{T}} \\ &= \bar{\mathbf{F}}\mathbf{M} \otimes \bar{\mathbf{F}}^{\mathrm{T}}\mathbf{M} = \bar{\mathbf{m}} \otimes \bar{\mathbf{m}} \end{aligned} \tag{3.36}$$

which in turn leads to the following definition of the spatial isochoric averaged structure

tensor $\bar{\mathbf{h}}$

$$\bar{\mathbf{h}} = \bar{\mathbf{F}}\mathbf{H}\bar{\mathbf{F}}^{\mathrm{T}} = \frac{1}{4\pi}\int_{\mathbb{S}^2} \rho(\bar{\mathbf{m}})\bar{\mathbf{a}}(\bar{\mathbf{m}})\, dS \tag{3.37}$$

The trace of the spatial tensor $\bar{\mathbf{a}}$ can be related to the stretch in direction $\mathbf{M}$:

$$\begin{aligned} \mathrm{tr}(\bar{\mathbf{a}}) &:= \bar{\mathbf{a}} : I = (\bar{\mathbf{m}} \otimes \bar{\mathbf{m}}) : \mathbf{I} = \bar{\mathbf{m}} \cdot \bar{\mathbf{m}} = \bar{\mathbf{F}}\mathbf{M} \cdot \bar{\mathbf{F}}\mathbf{M} = (\bar{\mathbf{F}}^{\mathrm{T}}\bar{\mathbf{F}}) : (\mathbf{M} \otimes \mathbf{M}) \\ &= \bar{\mathbf{C}} : (\mathbf{M} \otimes \mathbf{M}) = \bar{I}_4^{\mathbf{M}}(\mathbf{C}, \mathbf{M}) = \bar{\lambda}^2_{\mathbf{M}} \end{aligned} \tag{3.38}$$

Hence, the positivity of $\mathrm{tr}(\bar{\mathbf{a}})$ can be used to check whether a fibre bundle is stretched. Moreover, the Green-Lagrange strain like quantity $\bar{E}$ can be written with respect to the spatial configuration as

$$\bar{e} = \bar{\mathbf{h}} : \mathbf{I} - 1 \tag{3.39}$$

Thus, in the spatial reference the correct modification of the structure tensor contribution in direction $\bar{\mathbf{m}}$ is given by

$$\bar{\mathbf{a}}^* = \bar{\mathbf{F}}\mathbf{A}^*\bar{\mathbf{F}}^{\mathrm{T}} = \begin{cases} \frac{1}{3}\mathbf{I} & \text{if } \mathrm{tr}(\bar{\mathbf{a}}) \leq 1 \\ \bar{\mathbf{m}} \otimes \bar{\mathbf{m}} & \text{if } \mathrm{tr}(\bar{\mathbf{a}}) > 1 \end{cases} \tag{3.40}$$

where the Eulerian contribution for compressed fibre corresponds to the isochoric push-forward of the Lagrangian contribution:

$$\bar{\chi}_*[\bar{\mathbf{C}}^{-1}] = \bar{\mathbf{F}}\bar{\mathbf{C}}^{-1}\bar{\mathbf{F}}^{\mathrm{T}} = \bar{\mathbf{F}}(\bar{\mathbf{F}}^{-1}\bar{\mathbf{F}}^{\mathrm{T}})\bar{\mathbf{F}}^{\mathrm{T}} = \mathbf{I} \tag{3.41}$$

3.5 Cauchy stress tensor and spatial elasticity tensor

Specific expressions for the stress and the elasticity tensors in the spatial configuration must be derived to compute the numerical solution of the governing equations (see section 2.6). This can be done introducing the particularized free-energy function defined in section 3.2 into the continuum mechanical framework discussed in chapter 2.

Given the decoupled form of the potential used in this work and the incompressibility assumption, only the isochoric contribution needs to be considered. Moreover, the following analysis is limited to the equilibrium stress and tangent elasticity tensors, as the viscous contributions can be immediately computed as a function of the elastic results.

Firstly, the ground matrix is considered. It is convenient to introduce first and second derivative of the first isochoric invariant relative to the isochoric right Cauchy-Green tensor:

$$\frac{\partial \bar{I}_1}{\partial \bar{\mathbf{C}}} = \frac{\partial(\bar{\mathbf{C}} : \mathbf{I})}{\partial \bar{\mathbf{C}}} = \mathbf{I} \tag{3.42}$$

$$\frac{\partial^2 \bar{I}_1}{\partial \bar{\mathbf{C}}^2} = \frac{\partial(\mathbf{I})}{\partial \bar{\mathbf{C}}} = \mathbb{0} \tag{3.43}$$

According to the definition of $\bar{\boldsymbol{\sigma}}$ in (2.51) and the expression of the neo-Hookean potential (3.7), the isochoric Cauchy stress associated with the matrix is given by

$$\tilde{\boldsymbol{\sigma}}_g^{\infty} = 2J^{-1}\mathbf{F}\left[\frac{\partial \bar{\Psi}_g}{\partial \bar{\mathbf{C}}}\right]\mathbf{F}^{\mathrm{T}} = 2J^{-1/3}\bar{\mathbf{F}}\left[\frac{c_0}{2}\mathbf{I}\right]\bar{\mathbf{F}}^{\mathrm{T}} = J^{-1/3}[c_0\bar{\mathbf{b}}] \tag{3.44}$$

$$\bar{\boldsymbol{\sigma}}_g^{\infty} = J^{-2/3}\mathbb{p} : \tilde{\boldsymbol{\sigma}}_g^{\infty} = J^{-1}\mathbb{p} : [c_o\bar{\mathbf{b}}] \tag{3.45}$$

where $\mathbb{p}$ is the deviatoric operator and $\bar{\mathbf{b}}$ is the isochoric left Cauchy Green tensor defined in (2.39).

Hence, the contribution to the elasticity tensor can be computed immediately, as the first term in (2.81), i.e. $J^{-4/3}\mathbb{p} : \tilde{\mathbb{c}} : \mathbb{p}$, vanishes in accordance with the definition of $\tilde{\mathbb{c}}$ and the result for the second derivative of the potential relative to the isochoric right Cauchy-Green tensor (3.43), whereas the second and third terms $\frac{2}{3}J^{-2/3}\mathrm{tr}(\tilde{\boldsymbol{\sigma}})\mathbb{p}$ and $\frac{2}{3}[\mathbf{I} \otimes \bar{\boldsymbol{\sigma}} + \bar{\boldsymbol{\sigma}} \otimes \mathbf{I}]$ are directly computed from (3.44) and (3.45). These are well known result in the literature, see for example [39] [13].

The same arguments can be used for the isotropic fibre contribution, which is also modelled as a neo-Hookean material, simply substituting c_{f_i} to c_0. Hence, the isochoric Cauchy stress associated with the isotropic fibre contribution reads

$$\bar{\boldsymbol{\sigma}}_{f_i}^{\infty} = J^{-1}\mathbb{p} : [c_{f_i}\bar{\mathbf{b}}] \tag{3.46}$$

Once again, this expression leads directly to the expression for the elasticity tensor.

Similarly to [64] [9] the anisotropic fibre potential is assumed to be a function solely of the Green-Lagrange strain like quantity $\bar{E}$. According to the particularized expression of the potential (3.11) it is then possible to compute the scalar quantities

$$\psi'_{f_a} = \frac{d\bar{\Psi}_{f_a}^{\infty}}{d\bar{E}} = c_{f_a}\bar{E} \tag{3.47}$$

$$\psi''_{f_a} = \frac{d^2\bar{\Psi}^{\infty}_{f_a}}{d\bar{E}} = c_{f_a} \tag{3.48}$$

Also, it is convenient to report the derivative of $\bar{E}$ with respect to $\bar{\mathbf{C}}$

$$\frac{\partial \bar{E}}{\partial \bar{\mathbf{C}}} = \frac{\partial(\bar{\mathbf{C}} : \mathbf{H} - 1)}{\partial \bar{\mathbf{C}}} = \mathbf{H} \tag{3.49}$$

Using the arguments in section 2.4.1 and the equations (3.47) (3.49)

$$\frac{\partial \bar{\Psi}^{\infty}_{f_a}}{\partial \bar{\mathbf{C}}} = \frac{\partial \bar{\Psi}^{\infty}_{f_a}}{\partial \bar{E}} \frac{\partial \bar{E}}{\partial \bar{\mathbf{C}}} = \psi'_{f_a} \mathbf{H} \tag{3.50}$$

$$\tilde{\boldsymbol{\sigma}}^{\infty}_{f_a} = 2\psi'_{f_a} J^{-1} \mathbf{F}\mathbf{H}\mathbf{F}^{\mathrm{T}} = 2\psi'_{f_a} J^{-1/3} \bar{\mathbf{F}}\mathbf{H}\bar{\mathbf{F}}^{\mathrm{T}} = 2\psi'_{f_a} J^{-1/3} \bar{\mathbf{h}} \tag{3.51}$$

where the spatial isochoric structure tensor $\bar{\mathbf{h}}$ is introduced according to (3.37). Finally, the isochoric Cauchy stress reads

$$\bar{\boldsymbol{\sigma}}^{\infty}_{f_a} = 2\psi'_{f_a} J^{-1} \mathbb{p} : \bar{\mathbf{h}} \tag{3.52}$$

In order to particularize the expression of the spatial isochoric elasticity tensor, it is only necessary to particularize the first part of (2.81), i.e. $J^{-4/3}\mathbb{p} : \tilde{\mathbb{c}} : \mathbb{p}$, as the contributions from the second and third terms $\frac{2}{3} J^{-2/3} \mathrm{tr}(\tilde{\boldsymbol{\sigma}})\mathbb{p}$ and $\frac{2}{3}[\mathbf{I} \otimes \bar{\boldsymbol{\sigma}} + \bar{\boldsymbol{\sigma}} \otimes \mathbf{I}]$ can be obtained immediately by using the results in (3.51) (3.52).

The second derivative of the anisotropic fibre potential relative to $\bar{\mathbf{C}}$ is given by

$$\frac{\partial^2 \bar{\Psi}^{\infty}_{f_a}}{\partial \bar{\mathbf{C}}^2} = \frac{\partial[\psi'_{f_a} \mathbf{H}]}{\partial \bar{\mathbf{C}}} = \frac{\partial \psi'_{f_a}}{\partial \bar{E}} \frac{\partial \bar{E}}{\partial \bar{\mathbf{C}}} \otimes \mathbf{H} + \psi'_{f_a} \frac{\partial H}{\partial \bar{\mathbf{C}}} = \psi''_{f_a} \mathbf{H} \otimes \mathbf{H} \tag{3.53}$$

where the derivative of the structure tensor $\mathbf{H}$ relative to $\bar{\mathbf{C}}$ is assumed to be the null fourth order tensor $\mathbb{0}$. According to its definition, the structure tensor is indeed dependent on the isochoric deformation that determines the amount of fibres that contribute to the potential. Nevertheless, this is the correct assumption based on the numerical implementation of the model (details are given in section 3.6).

According to the definition $\tilde{\mathbb{c}}^{\infty} = J^{-1} \chi_* [4\partial^2 \bar{\Psi} / \partial \bar{\mathbf{C}}^2]$, the spatial isochoric (fictitious) elasticity tensor is given by

$$\begin{aligned} [\tilde{\mathbb{c}}]^{\infty}_{ijkl} &= 4J^{-1} F_{iI} F_{jJ} F_{kK} F_{lL} [\psi''_{f_a} \mathbf{H} \otimes \mathbf{H}] = 4J^{1/3} \bar{F}_{iI} \bar{F}_{jJ} \bar{F}_{kK} \bar{F}_{lL} [\psi''_{f_a} \mathbf{H} \otimes \mathbf{H}] \\ &= 4J^{1/3} [\psi''_{f_a} \bar{\mathbf{h}} \otimes \bar{\mathbf{h}}] \end{aligned} \tag{3.54}$$

Hence, the first contribution to the spatial isochoric elasticity tensor becomes

$$J^{-4/3}\mathbb{p} : \tilde{\mathbb{c}}^{\infty} : \mathbb{p} = 4J^{-1}\psi''_{fa}(\mathbb{p} : \bar{\mathbf{h}}) \otimes (\mathbb{p} : \bar{\mathbf{h}}) \tag{3.55}$$

With the major and minor symmetries of the elasticity tensor (see section 2.6) contributions accounted for, these relations can be efficiently implemented into a finite element code.

3.6 Numerical implementation

Due to complex geometries, material properties and loading conditions, in general it is not possible to find an analytical solution for the model presented in the previous sections and numerical methods are required. In this section the numerical implementation of the model is analysed, with focus on the assumptions and procedures adopted to solve the equations in the framework of Finite Element Analysis.

The Finite Element Method has proven to be particularly effective in the modelling of biological tissues and has been used routinely in the literature. A description of this method is out of the scope of this work and for a detailed discussion the reader is referred to [69]. The general purpose finite element package FEAP[1] was chosen to perform the analysis since it allows the use of custom materials through user-defined subroutines and it has been reported to be effective in modelling soft biological tissues [13] [21] and also specifically AC [9].

3.6.1 Structure tensor

To implement the structure tensor defined in (3.37), it is necessary to evaluate the strain in all directions for every integration point in each element of the mesh.

The system of non-linear equation representing the problem cannot be solved directly, but some iterative procedure is required. At each solution step a number of linearised sub-steps is performed until converged solution is achieved (see section 3.7.2). The deformation is computed at each sub step, so that the number and location of stretched collagen bundles might change within the iterations.

This means that on the error reduction path towards a converged solution, the configuration of stretched fibres (and therefore the associated anisotropic energy contribution) might suddenly

[1]FEAP-A Finite Element Analysis Program version 8.2. Berkeley, California: R. L. Taylor, 2008

change, so that the exact solution changes as well. Thus, the iterative method needs to start a path towards the new solution.

Even if the solution of the previous sub-step (that is used as starting point for the new iterative process) is likely to be in the so-called *region of attraction* of the new solution (i.e. to be close enough to the new solution to prevent that the iterative method converges to a different solution), every configuration change affects the rate of convergence and multiple changes might prevent the achievement of a converged solution before the chosen maximum number of iteration is reached.

Therefore, at each solution step the stretch is kept constant during the Newton iterations. In particular, the value computed at the previous step is used, assuming that time and load variations are small enough to make the difference negligible. The check is anyway performed at each sub-step and the value of $\bar{\mathbf{I}}_4^M$ computed at the last sub-step (i.e. the one that gives converged solution) is then use at the next solution step. This approach is not ideal, as it requires the definition of history variables to store the stretch information when the solution is updated.

On the other hand, as mentioned in section 3.5, it simplifies the derivation of stress and elasticity tensor. The structure tensor $\mathbf{H}$ is not independent of the right Cauchy-Green tensor $\mathbf{C}$ because the deformation determines the number and position of fibres bundles that are stretched at a particular solution step. However, at each the step n the derivation of the energy function Ψ is relative to the current deformation state (i.e. $\bar{\mathbf{C}}_n$), but the value of $\mathbf{H}_{n-1}$ of the previous step is used, which is indeed dependent on the deformation up to $\bar{\mathbf{C}}_{n-1}$ but constant with respect to $\bar{\mathbf{C}}_n$.

3.6.2 Spherical integration

Following [9], the structure tensor (3.5) was integrated using a spherical *t*-design, consisting of a set of *N* points on the unit sphere $\{\mathbf{M}^{(1)}, \dots, \mathbf{M}^{(N)}\} \in \mathbb{S}^2$ (i.e. a set of N directions), such that, as $S(\mathbb{S}^2) = 4\pi$ is the surface measure of the unit sphere in $\mathbb{R}^3$, the equality

$$\int_{\mathbb{S}^2} f(\mathbf{M})\, dS = \frac{4\pi}{N} \sum_{\alpha=1}^{N} f(\mathbf{A}^{(\alpha)}) \tag{3.56}$$

holds for polynomials f of degree $k \leq t$ [17]. Hence, using (3.5) the structure tensor can be computed as

$$\mathbf{H} = \frac{1}{N} \sum_{\alpha=1}^{N} \rho(\mathbf{M}^{(\alpha)}) \mathbf{A}^{(\alpha)} \tag{3.57}$$

The degree *t* required to guarantee the desired precision depends on the form of the probability density function ρ. Therefore, in the case of the transversely isotropic distribution used in this work, the integration order is defined by the concentration parameter *b*, that has a specific value for each element. In particular *t* should be increased as *b* increases, i.e. when the fibres are more concentrated about the polar axis.

Indeed, it would be possible to define an empirical relation between *b* and *t* as in [9] [15] and to set the order in each element depending on its value of *b*. In this work though the same order was used for all the elements, as the corresponding number of points *N* on the unit sphere was necessary to initialize the history variables required to store the value of $\overline{\mathbf{I}}_4^M$ at each solution step, which are globally defined for all the elements. Numerical compression experiments were performed increasing *t* until convergence was achieved and the minimum sufficient value was found to be $t = 21$, corresponding to the $N = 240$ integration points[2] plotted in Figure 3.5.

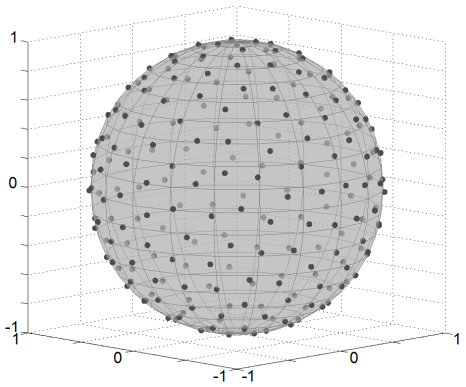

Figure 3.5: Graphical representation of the spherical *t*-design with $t = 21$, corresponding to 240 points on the unit sphere.

It should be noted that increasing the order of the spherical integration also increases the size of the problem and the computational cost: for every additional integration point on the unit sphere (note that the number of points required for a one-order improvement increases with *t*), a total of $n \times gp$ new operations are required to compute the structure tensor, and $n \times gp$ new history variables need to be stored, where n is the number of elements in the

[2]The coordinates of all the points are reported at http://neilsloane.com/sphdesigns/

mesh and gp is the number of Gauss points for each element. The total number of history variables allowed in the problem depends on the memory of the machine used for the simulations. Hence, higher integration orders reduce the maximum size (i.e. the maximum number of nodes) allowed for the problem, which can be a limitation when standard personal computers are used. In this work an optimization algorithm available in FEAP [59] was used for the numbering of the unknowns, which improves the use of the memory and therefore the performance of the code and the maximum size allowed.

3.6.3 Numerical integration of the evolution equation

The update algorithm for stress and elasticity tensors follows an approach well established in the literature for viscoelasticity at finite strain [60] [21] [14]. The main task is the discretisation of the convolution integral (3.28).

It is assumed that at certain times t_n and t_{n+1} all relevant kinematic quantities are given, as well as the equilibrium isochoric second Piola-Kirchhoff stresses associated with the collagen fibres $\bar{\mathbf{S}}_n^{\infty}$ and $\bar{\mathbf{S}}_{n+1}^{\infty}$, uniquely defined by the constitutive equation.

Firstly, the convolution integral (3.28) is split into

$$\beta \int_{t=0}^{t=t_n} \exp\left\{-\frac{t_{n+1}-t}{\tau}\right\} \dot{\bar{\mathbf{S}}}_f^{\infty}(t)\,\mathrm{d}t + \beta \int_{t=t_n}^{t=t_{n+1}} \exp\left\{-\frac{t_{n+1}-t}{\tau}\right\} \dot{\bar{\mathbf{S}}}_f^{\infty}(t)\,\mathrm{d}t \tag{3.58}$$

Secondly, the quantities

$$\Delta t_{n+1} = t_{n+1} - t_n \quad \text{and} \quad t_{n+0.5} = (t_{n+1} + t_n)/2 \tag{3.59}$$

are introduced, where Δt is the time increment and $t_{n+0.5}$ approximates the time variable in a second-order accurate mid-point integration scheme. Hence, using (3.58) and the standard property of exponential function

$$\exp\{-(\Delta t + \beta)/\tau\} = \exp\{-\Delta t/\tau\} \exp\{-\beta/\tau\} \tag{3.60}$$

the viscoelastic overstress at time t_{n+1} can be written as

$$\begin{aligned} \bar{\mathbf{S}}_{n+1}^{V} =& \beta \exp\left\{\frac{-\Delta t_{n+1}}{\tau}\right\} \int_{t=0}^{t=t_n} \exp\left\{-\frac{t_n - t}{\tau}\right\} \dot{\bar{\mathbf{S}}}_f^{\infty}(t)\,\mathrm{d}t + \\ &+ \beta \exp\left\{\frac{-\Delta t_{n+1}}{2\tau}\right\} \int_{t=t_n}^{t=t_{n+1}} \dot{\bar{\mathbf{S}}}_f^{\infty}(t)\,\mathrm{d}t \end{aligned} \tag{3.61}$$

Introducing the dimension-less parameter $\xi_{n+1} = \exp\{-\Delta t_{n+1}/2\tau\}$,

$$\bar{\mathbf{S}}^V_{n+1} = \xi^2_{n+1}\bar{\mathbf{S}}^V_n + \beta\xi_{n+1}(\bar{\mathbf{S}}^\infty_{f_{n+1}} - \bar{\mathbf{S}}^\infty_{f_n}) \tag{3.62}$$

Finally, (3.62) can be rearranged as

$$\begin{aligned} \bar{\mathbf{S}}^V_{n+1} &= \beta\xi_{n+1}\bar{\mathbf{S}}^\infty_{f_{n+1}} + \mathcal{H}_n \\ \mathcal{H}_n &= \xi^2_{n+1}\bar{\mathbf{S}}^V_n - \beta\xi_{n+1}\bar{\mathbf{S}}^\infty_{f_n} \end{aligned} \tag{3.63}$$

where $\mathcal{H}_n$ is a stress-like tensor storing the history of the problem.
The viscoelastic contribution to the elasticity tensor is then given immediately by the derivative of the viscous overstress with respect to the isochoric deformation tensor at the same time

$$\bar{\mathbb{C}}^V_{n+1} = \beta\xi_{n+1}\bar{\mathbb{C}}^\infty_{f_{n+1}} \tag{3.64}$$

where the derivative of the history term is clearly zero since it depends only on the deformation up to time t_n.
Performing an inverse Piola transformation and introducing the set of superimposed Maxwell elements defining the generalized Maxwell model, the viscous contribution in terms of Cauchy stress and spatial elasticity tensor (used in the finite element implementation) reads

$$\begin{aligned} \bar{\boldsymbol{\sigma}}^V_{n+1} &= \sum_{k=1}^{3} \beta^k \xi^k_{n+1}\bar{\boldsymbol{\sigma}}^\infty_{f_{n+1}} + \mathfrak{h}^k_n \\ \bar{\mathbb{c}}^V_{n+1} &= \bar{\xi}_{n+1}\bar{\mathbb{c}}^\infty_{f_{n+1}} \end{aligned} \tag{3.65}$$

where $\bar{\xi}_{n+1} = \sum_{k=1}^{3} \beta^k \xi^k_{n+1}$ and the history term in spatial reference can be written as

$$\mathfrak{h}^k_n = (\xi^k_{n+1})^2\bar{\boldsymbol{\sigma}}^{V^k}_n - \beta^k\xi^k_{n+1}\bar{\boldsymbol{\sigma}}^\infty_{f_n} \tag{3.66}$$

The algorithm used in the finite element implementation of the isochoric potential is reported in Table 3.1.

Table 3.1: Finite element implementation of the isochoric potential.

given

isochoric deformation gradient	$\bar{\mathbf{F}} = J^{-1/3}\mathbf{F}$
orientation distribution data	$\mathbf{K}, b, \rho = \begin{cases} \text{Model (A)} \\ \text{Model (B)} \end{cases}$
viscous parameters	$\beta^{(i)}, \tau^{(i)}, i \in \{1 \dots k\}$
integration order	$t(b)$
time step	Δt

algorithm

load spherical design	$\mathbf{M}^{(\alpha)}, \alpha \in \{1 \dots N\}$
load history variables	$\bar{I}^M_{4_{n-1}}, \bar{\boldsymbol{\sigma}}^{\infty}_{f_{n-1}}, \bar{\boldsymbol{\sigma}}^{V^{(i)}}_{n-1}, i \in \{1 \dots k\}$
initialize stress and elasticity tensors	$\bar{\boldsymbol{\sigma}} \leftarrow \boldsymbol{o}, \bar{\mathbb{C}} \leftarrow \mathbb{0}$
initialize stretched fibres boolean	flag = FALSE

DO $\alpha = 1, N$

compute spatial isochoric fibre direction	$\bar{\mathbf{m}}^{(\alpha)} = \bar{\mathbf{F}}\mathbf{M}^{(\alpha)}$
compute co-latitude angle	$\boldsymbol{\Theta}^{(\alpha)} = \arccos(\mathbf{K} \cdot \mathbf{M}^{(\alpha)})$
compute orientation density function	$\rho^{(\alpha)} = \begin{cases} 4\sqrt{\frac{b}{2\pi}}\frac{\exp[b(\cos(2\Theta-\pi)-1)]}{\text{erf}(\sqrt{2b})} & \text{(A)} \\ 4\sqrt{\frac{b}{2\pi}}\frac{\exp[b(\cos(2\Theta)+1)]}{\text{erfi}(\sqrt{2b})} & \text{(B)} \end{cases}$

IF ($\rho^{(\alpha)} > \varepsilon$) THEN

compute spatial isochoric structure tensor contribution	$\bar{\mathbf{a}}^{(\alpha)} = \bar{\mathbf{m}}^{(\alpha)} \otimes \bar{\mathbf{m}}^{(\alpha)}$
compute stretch in fibre direction	$\bar{I}^4_M = \bar{\mathbf{m}}^{(\alpha)} \cdot \bar{\mathbf{m}}^{(\alpha)}$

IF ($\bar{I}^4_{M_{n-1}} \leq 1$) THEN

modify spatial isochoric structure tensor contribution	$\bar{\mathbf{a}}^{(\alpha)} = \frac{1}{3}\mathbf{I}$

ELSE

turn on anisotropic contribution to potential	flag = TRUE

ENDIF

update spatial isochoric structure tensor	$\bar{\mathbf{h}} = \bar{\mathbf{h}} + \frac{1}{N}\rho^{(\alpha)}\bar{\mathbf{a}}^{(\alpha)}$

ENDIF

ENDO

IF (flag = TRUE) THEN

compute $\bar{\Psi}_{f_a}$ contribution to stress and elasticity tensors

$\bar{\boldsymbol{\sigma}}_{f_a} = J^{-1} 2\psi'_{f_a} \mathbb{P} : \bar{\mathbf{h}}$

$\bar{\mathbb{C}}_{f_a} = J^{-1} 4\psi''_{f_a} (\mathbb{P} : \bar{\mathbf{h}}) \otimes (\mathbb{P} : \bar{\mathbf{h}}) + J^{-1} \frac{4}{3}\psi'_{f_a} \bar{I}_4 \mathbb{P} - \frac{2}{3}(\mathbf{I} \otimes \bar{\boldsymbol{\sigma}}_{f_a} + \bar{\boldsymbol{\sigma}}_{f_a} \otimes \mathbf{I})$

update stress and elasticity tensor $\quad \bar{\boldsymbol{\sigma}} \leftarrow \bar{\boldsymbol{\sigma}} + \phi_f \bar{\boldsymbol{\sigma}}_{f_a}, \quad \bar{\mathbb{C}} \leftarrow \bar{\mathbb{C}} + \phi_f \bar{\mathbb{C}}_{f_a}$

ENDIF

Continued on next page

Table 3.1: (continued)

add $\bar{\Psi}_{f_i}$ contribution to stress and elasticity tensors (neo-hookean)
$\bar{\boldsymbol{\sigma}} \leftarrow \bar{\boldsymbol{\sigma}} + \phi_f \bar{\sigma}_{f_i}$
$\bar{\mathbb{C}} \leftarrow \bar{\mathbb{C}} + \phi_f \bar{\mathbb{C}}_{f_i}$

store elastic fibre contribution $\bar{\sigma}_f^{\infty} \leftarrow \bar{\sigma}$
DO $i = 1, k$
compute viscous parameters
$\xi^{(i)} = \exp[-\Delta t/2\tau^{(i)}]$
$\bar{\xi} \leftarrow \bar{\xi} + \xi^{(i)}$
compute viscous overstress
$\bar{\sigma}^{V^{(i)}} = \beta^{(i)}\xi^{(i)}\bar{\boldsymbol{\sigma}} + [(\xi^{(i)})^2 \bar{\boldsymbol{\sigma}}_{n-1}^{V^{(i)}} - \beta^{(i)}\xi^{(i)}\bar{\boldsymbol{\sigma}}_{f_{n-1}}^{\infty}]$
$\bar{\boldsymbol{\sigma}}^{V} \leftarrow \bar{\boldsymbol{\sigma}}^{V} + \bar{\boldsymbol{\sigma}}^{V^{(i)}}$
ENDDO
compute viscous contribution to elasticity tensor $\bar{\mathbb{C}}^{V} = \bar{\xi}\bar{\mathbb{C}}$
update stress and elasticity tensor $\bar{\boldsymbol{\sigma}} \leftarrow \bar{\boldsymbol{\sigma}} + \bar{\boldsymbol{\sigma}}^{V}, \quad \bar{\mathbb{C}} \leftarrow \bar{\mathbb{C}} + \bar{\mathbb{C}}^{V}$

add $\bar{\Psi}_g$ contribution to stress and elasticity tensors (neo-hookean)
$\bar{\boldsymbol{\sigma}} \leftarrow \bar{\boldsymbol{\sigma}} + \phi_g \bar{\boldsymbol{\sigma}}_g$
$\bar{\mathbb{C}} \leftarrow \bar{\mathbb{C}} + \phi_g \bar{\mathbb{C}}_g$

history update (if converged solution is achieved)
$\bar{I}_M^4 \rightarrow \bar{I}_{M_{n-1}}^4$
$\bar{\boldsymbol{\sigma}}_f^{\infty} \rightarrow \bar{\boldsymbol{\sigma}}_{f_{n-1}}^{\infty}$
$\bar{\boldsymbol{\sigma}}^{V^{(i)}} \rightarrow \bar{\boldsymbol{\sigma}}_{n-1}^{V^{(i)}}$

3.7 Representative numerical examples

Three numerical examples were analysed to demonstrate the physical behaviour of the constitutive relations defined above[3]. Experimental studies selected from the literature were used to validate the results. In this section these examples and the solution procedure adopted are discussed in details.

The probability density function defined in 3.3 was used in the example studies and the concentration parameter b was changed linearly across the thickness. In a full-thickness

[3] All the computations were performed on a standard personal computer (Dell optiplex GX790).

specimen the arrangement of collagen fibres is assumed to vary from nearly aligned perpendicular to the bone in deep zone (Model (B), *b*=5), to randomly distributed in the middle zone (Model (A/B), *b*=0) and nearly planar parallel to the articular surface in the superficial zone (Model (A), *b*=5). These values were not computed from experimental data but represent qualitatively the collagen fibre distribution in AC [41]. However, it is important to note that the generality of the model allows the definition of different distributions, e.g. tabulated functions based on experimental studies [5] [45].

Elastic constants of matrix and fibres and their volume fractions were also qualitatively estimated rather than computed from experimental data; the values used in the examples are reported in Table 3.2.

The mesh and the collagen distribution data for each element were developed in MATLAB[4]. The examples considered are all rotationally symmetric but the whole problem was modelled as the use of symmetry boundary conditions might suppress the development of instabilities.

Parameters used by (3.6)	$c_g = 0.5$ MPa	$\phi_g = 0.8$
	$c_{f_i} = 2$ MPa	$\phi_f = 0.2$
	$c_{f_a} = 90$ MPa	

Table 3.2: Elastic constants (c_α) and volume fractions(ϕ_α) relative to ground matrix and collagen fibres.

3.7.1 Incompressibility constraint

As stated above, AC was modelled as an incompressible material. This assumption can cause numerical problems: when Poisson's ratio approaches 0.5, the value of the bulk modulus shoots to infinity determining an overly stiff behaviour of the model. At each integration point of an element the volume remains almost constant and thus it over-constraints the kinematically admissible displacement field, resulting in over-constraining of the mesh, also known as 'locking' [28].

A finite element formulation which is free from locking for nearly incompressible material can be obtained with a mixed variational approach [70] [6]. In FEAP the mixed formulation elements are based on the Hu-Washizu variational principle [53], which introduces separated approximations for the pressure and the volumetric deformation (**u**-p-θ model).

[4]MATLAB R2012A, THE MATHWORKS, INC.

For the present study the Q1-P0 element available in FEAP was used, which is a large deformation finite element based on the Hu-Washizu variational formulation. It uses linear shape functions for the deformation field related to the deviatoric kinematical variables and constant ansatz functions to discretise the pressure and volumetric strain. The volumetric variables are eliminated on the element level.
Finite elements that are derived from mixed methods have to fulfil the so-called *BB-condition* to guarantee the stability of the formulation [68]. The Q1-P0 element does not fulfil this condition in the geometrical linear theory, which implies that it can generate unstable solution for the pressure under particular loads or boundary conditions. Nevertheless, it has been observed in many practical application that it is robust for finite elasticity problems involving quasi-incompressible material, and therefore it is commonly used in commercial software.

Enforcing correctly the incompressibility constraint is also crucial to avoid non-physical behaviour of the model when the decoupled form of the potential is used for fibre reinforced composites [19].
This can be done using a penalty method. However, the use of large penalty parameters can make the iterative method unable to converge. On the other hand, if the penalty parameter value is reduced much in order to achieve convergence of the solution, the constraint is not sufficiently enforced.
In the following examples, incompressibility was enforced using an augmented Lagrangian solution strategy based on the Uzawa algorithm [70], which is available in FEAP. If a penalty value v_p is calculated from the equation

$$v_p = K \cdot c(u) \tag{3.67}$$

where K is a material parameter and c(u) is a constraint to be made close to zero, then the augmented Lagrangian parameter update is computed as

$$v_a = v_a + \mathit{augf} \cdot v_p. \tag{3.68}$$

where *augf* is the augmentation factor. At each solution step, after a converged solution is computed, the update is performed and the solution is computed again. The iteration continues until incompressibility is enforced up to a given tolerance of accuracy. Using this solution the value of the penalty parameter has to be just one or two orders of magnitude

larger than the conventional stiffness terms, instead of the six or seven that are required in the basic penalty method. This method is computationally expensive and the number of iterations should be kept low. In order to do this, the augmentation factor can be increased as well as the initial value of the bulk modulus. Numerical tests were performed with configurations similar to the examples described below and finally two augmentation iterations were used in the solution procedure.

3.7.2 Solution procedure

As mentioned above, the solution of a non-linear problem cannot be approached directly, but some iterative procedure is required and the choice of a particular method is problem-dependent. For the example problems studied in this work the Newton-Raphson method was used, in which the asymptotic rate of convergence is quadratic. However, the numerical solution can only approximately be achieved: since finite precision arithmetic is used in all computer calculations, one can never achieve a better solution than the round-off limit of the calculations. Hence, it is necessary to set some kind of tolerance on the solution to terminate the iteration. Every iterative method aims to reduce the residual, which is defined as

$$\mathbf{R} = \mathbf{K}_T \boldsymbol{\Delta}\mathbf{U} \tag{3.69}$$

where K_T is the stiffness matrix and $\boldsymbol{\Delta}\mathbf{U}$ is the displacement parameter change. Thus, it is convenient to define the convergence criteria based on a norm of the residual, or similarly on a norm of the energy, defined as

$$\|E_i\| = (\boldsymbol{\Delta}\mathbf{U}_i \cdot \mathbf{R}_i)^{1/2} \tag{3.70}$$

In FEAP the energy of the first iteration in the current solution step is used as a basis and the limit is expressed as some tolerance of its norm: $\|E_i\| = \varepsilon\|E_0\|$, where ε is the tolerance.
Once a criterion is defined it is still necessary to choose an appropriate value for ε. The tolerance was chosen at half the machine precision (i.e. $\varepsilon = 10^{-8}$), since quadratic convergence assure that the next residual (disregarding round-off error) would achieve full precision.
It was observed that the rate the Newton-Raphson method did not achieve quadratic convergence for relatively high level of compressive deformation, so that many iterations were necessary to guarantee the chosen precision. This was not surprising as the progressive buckling

of the fibres in compression is likely to generate instabilities that in turn make convergence more difficult to achieve. This idea is supported by the evidence that such problem did not occur in tension. It would have been possible to use larger tolerance values (as it is often done when other methods with lower convergence rate are used, e.g. the modified Newton method). However, the value was not altered because instabilities in the solution may appear if the convergence tolerance is too large. Moreover, the use of a line search method, which is sometimes useful to achieve faster convergence when quadratic rate is not assured, did not provide any significant improvement.

The set of linear algebraic equations resulting from the use of the Newton-Raphson method was solved for the incremental solution values by mean of an iterative conjugate gradient solution scheme with diagonal preconditioning. The system of linear equation is written in a form analogous to (3.69), and once again it is necessary to choose a value for the tolerance. In this case the norm of the residual is used and the relative error is computed with respect to the first iteration:

$$(\mathbf{R}^T\mathbf{R})_i^{1/2} \leq \varepsilon(\mathbf{R}^T\mathbf{R})_0^{1/2} \tag{3.71}$$

where ε is the tolerance, that was chosen at $\varepsilon = 10^{-8}$ (default value in FEAP).

A summary of the solution procedure is given in Figure 3.6

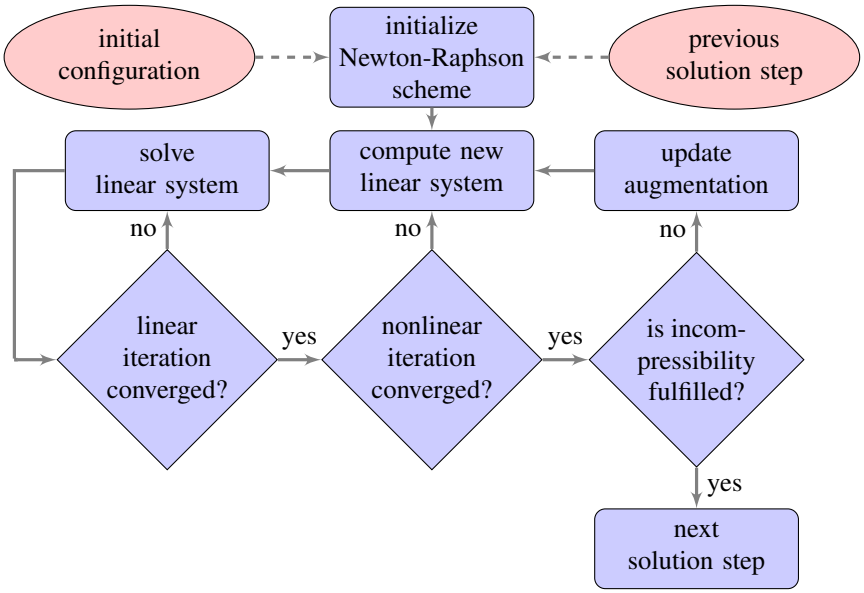

Figure 3.6: Flowchart of the solution procedure adopted for the numerical example.

3.7.3 Problems specification

In the following, details are given about geometrical characteristics, loading configuration and structural and viscous parameters chosen for the representative examples, together with information about the numerical settings for the analyses.

Relaxation tests

Relaxation tests were conducted on cylindrical AC samples of 3.65 mm in diameter and 1.13 mm in thickness. The dimensions were taken from [35] and in accordance with that study, a layer of subchondral bone was assumed to constrain the radial deformation of the lower boundary of the AC specimen.

The stepwise relaxation test was conducted both in traction and compression using the same loading configuration. In particular a ramp displacement of 6.8 μm was prescribed at the articular surface with a ramp velocity of 1 $\mu\mathrm{m/s}$. After the ramp is complete, the displacement is kept constant until a second ramp, similar to the first one, starts at $t = 565s$. When the second ramp ends, the displacement is again kept constant for about 560 seconds. The interval allowed for relaxation was estimated from the results shown in [35] and complete relaxation of the specimen should be observed. Geometry and load are summarized in Figure 3.9.

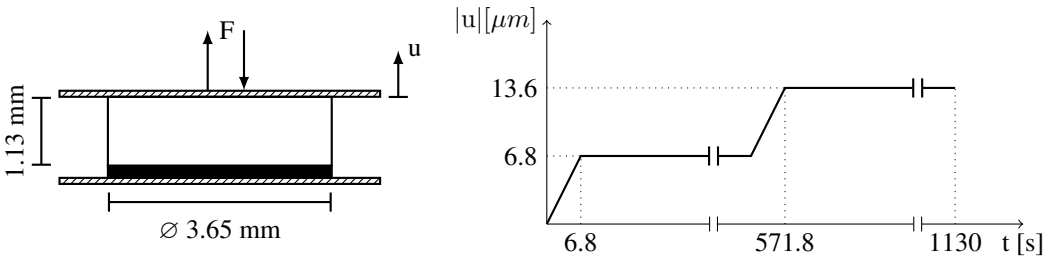

Figure 3.7: Geometry and load for the relaxation tests on full thickness specimen with layer of subchondral bone.

The viscoelastic parameters used in the example were determined by fitting the experimental relaxation tests reported in [35] and they are given in Table 3.3.

A mesh composed of 20 layers across the thickness of the specimen was defined, for a total of 20580 nodes. In order to correctly capture the response of the material, which is supposed to show fast variations during and immediately after the loading ramp, the time steps were set to 0.2 seconds for the 30 seconds intervals following the start of each loading ramp, to 0.5 for the following 50 seconds intervals and to 1 second for the rest of the test. According to [35] the specimen was assumed to be glued to the loading platen and the radial displacement

was constrained at the upper boundary, as well as at the lower boundary due to the layer of subchondral bone mentioned above.

	Tests I and II		Test III	
Parameters used by (3.65)	$\beta_1^\infty = 0.5$	$\tau_1 = 10$ s	$\beta_1^\infty = 0.1$	$\tau_1 = 0.1$ s
	$\beta_2^\infty = 2$	$\tau_2 = 100$ s	$\beta_2^\infty = 0.5$	$\tau_2 = 1.0$ s
	$\beta_3^\infty = 0.1$	$\tau_3 = 1000$ s	$\beta_3^\infty = 1.2$	$\tau_3 = 10$ s

Table 3.3: Constitutive parameters describing the time-dependent effects of AC, i.e. the constitution of the generalized Maxwell model.

Unconfined compression of full thickness specimen

This example aims at investigating the stress state within a cylindrical AC specimen of 3.0 mm in diameter and of 1.83 mm in height, with focus on the anisotropic and depth-depending response due to the fibre reinforcement. According to [11] the full thickness was modelled and the AC sample was assumed to be attached to a layer of subchondral bone.

A displacement linearly increasing over time from 0 to 0.35 mm in the direction of the thickness was prescribed at the articular surface. The ramp duration was set to one second. Geometry and load are summarized in Figure 3.8.

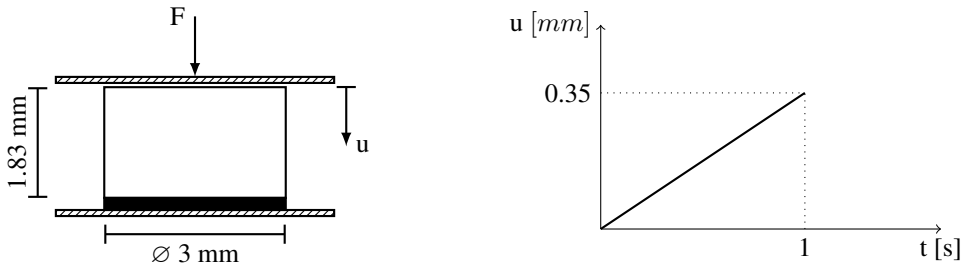

Figure 3.8: Geometry and load for the unconfined compression of full thickness specimen with layer of subchondral bone.

The viscoelastic parameters estimated fitting the relaxation tests in [35] were used also in this example, as reported in Table 3.3.

Given the goal of the test, the number of layers through the thickness was increased to 28, for a total of 28420 nodes. The radial displacement was constrained at the lower boundary as the AC sample is attached to the bone, which is assumed to be rigid under the present test configuration. The time step was set to 0.05 seconds for the first half of the loading ramp and to 0.01 seconds afterwards to improve convergence, since problems arose in achieving converged solutions for high level of compression, as mentioned in section 3.7.2.

Unconfined compression of reduced thickness specimen

The goal of this example is to analyse the non-linear viscoelastic response of the model (i.e. the dependence of the response on the loading frequency). A cylindrical AC specimen was tested under unconfined compression. Dimensions are similar to those of the previous example and were taken from test specimens used in [44]. However, in accordance with that study, a 0.5 mm thick layer of the deep zone was removed, such that Model (B) with $b = 2.85$ describes the collagen distribution at the deepest zone of the test specimen.
The sinusoidal loads used in the experimental study were approximated by triangular loads with the same mean value and the same cycle frequency. Two tests were performed with loading frequencies of 0.1 Hz (i.e. 5 seconds loading ramp plus 5 seconds unloading ramp) and 1 Hz (i.e. 0.5 seconds loading ramp plus 0.5 seconds unloading ramp), respectively. Moreover, the analysis was conducted under displacement-control (that ensure easier convergence of the finite element implementation) whereas in the reference experimental tests load-control was used. Hence, the results reported in [44] were used as input in the simulations to ease the comparison of the results. Accordingly, in the first test a displacement of 0.366 mm in the direction of thickness, corresponding to a 20% deformation, was prescribed at the articular surface, whereas for the second test the displacement was reduced to 0.275 mm, corresponding to a 15% deformation. These values correspond to physiologically relevant AC strains [44]. Geometry and load are summarized in Figure 3.9.

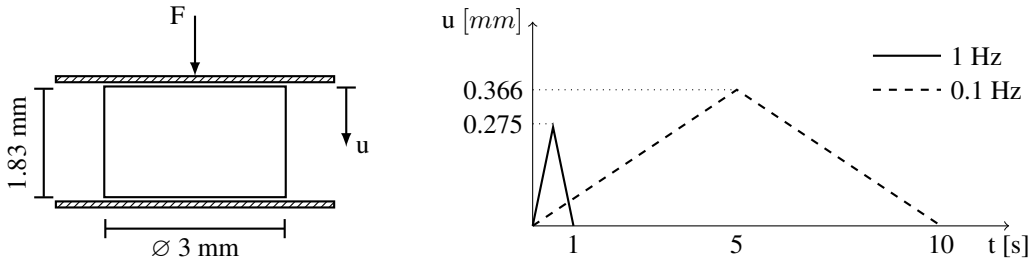

Figure 3.9: Geometry and load for the unconfined compression of reduced thickness specimen.

The viscoelastic constants were estimated from the results shown in [44] and are reported in Table 3.3. Indeed, the experimental results include the effect of fluid flow through the poroelastic matrix, that are not negligible in compression. The comparison with the viscoelastic parameters used for the relaxation tests immediately reveals that the chosen values are not suitable to describe the intrinsic viscoelastic behaviour of AC. However, they were meant to compensate the contribution of fluid flow viscoelasticity (see sections 1.2 and 3.2.2) that is not explicitly modelled in this work.

Given the reduced thickness (i.e. the limited range of the distribution parameter b), 20 layers were defined in the specimen for a total of 20580 nodes. Similarly to the previous example, for the first test the time steps were set to 0.25 seconds and 0.05 seconds for the lower and the higher half of each ramp, respectively. For the second test these value were reduced of an order of magnitude due to the one order increase in the load frequency. According to [44] unconfined compression was assumed.

Chapter 4

Results

In this chapter the results of the representative numerical tests described in section 3.7.3 are presented. A qualitative comparison with experimental data from the literature is meant to demonstrate the physical behaviour of the model, while a quantitative analysis, required to fully validate the results for each specific case, is out of the objective of this work.

4.1 Relaxation tests

A typical stress relaxation response from the model prediction is shown in Figure 4.1 for a AC disk subjected to axial tension and compression. The model predicts an asymmetric tension-compression behaviour, with a stiffer response in tension due to the action of the collagen fibre reinforcement, in accordance with experimental evidence (see section 1.2).

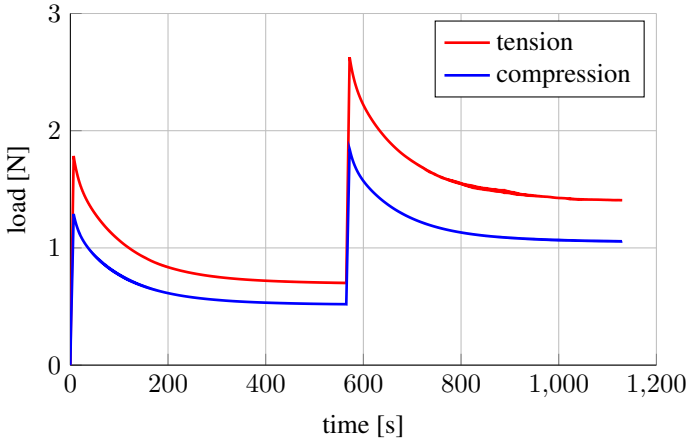

Figure 4.1: Simulation of a two-steps relaxation test of a full-thickness specimen of AC in tension and compression using the model. The results are given as external load vs time.

Figure 4.2 shows a comparison between model prediction and experimental results for the

same tests reported in [35]. In order to ease the comparison, tensile and compressive stresses shown are the total nominal axial stresses, computed from the external load and the cross section area of the specimen in the reference configuration. The stress values computed for the tensile test are similar to those reported in [35], while the compressive stress appears overestimated. As a consequence, the tension-compression asymmetry is less pronounced than in [35]. With regard to the time-dependent response, the results for the tensile test are in very good agreement with the experimental data: after 565 seconds relaxation is completed and the peak stress is reduced by about 60%. A similar time evolution is predicted for the compressive test, while experimental data show a higher viscous contribution in this case due to the effect of fluid flow, not modelled in this work. Moreover, 565 seconds were again sufficient to reach complete relaxation, but this was not the case in the experimental tests. In order to get a better fitting the viscous parameters of the collagen fibres could be altered in the simulation of the compressive test.

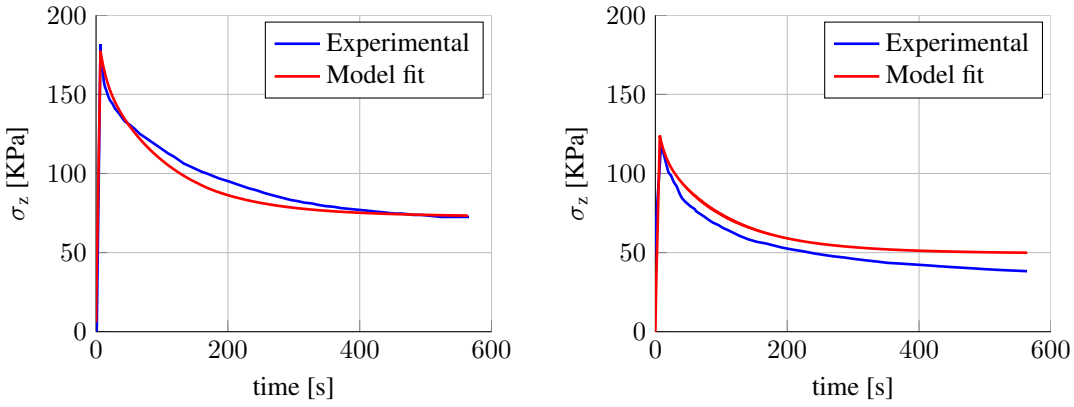

(a) Tension **(b)** Compression

Figure 4.2: Comparison between model prediction and experimental data reported in [35] for both tensile (a) and compressive (b) relaxation tests. The results are given as axial engineering stress vs time.

Following the assumption that collagen is the only viscoelastic component, the contribution of the fibres to the time-dependent response in compression is not negligible, in contrast with what suggested by the numerical model used in [35], described in [34]. Indeed, it seems more realistic that the compressive time-dependent behaviour is affected by the fibres [9] [4], since some of them are active under axial tension due to the complex orientation distribution through the thickness. However, the fibre contribution to the viscoelastic behaviour in compression appears too close to the one computed in tension and is probably overestimated, which also explains the high values of compressive stress in Figure 4.2.

In order to test if the model can reproduce the non-linearity of the viscoelastic response of the tissue, the tensile relaxation test was repeated with a maximum displacement of $45\mu m$, corresponding to a 4% maximum strain. Figure 4.3a shows the evolution of the axial nominal stress normalized over the peak value. Relaxation is faster at lower load, demonstrating a strain-dependent viscous response. This behaviour can be interpreted as an experimental evidence of non-linear viscoelasticity, since the response of linear viscoelastic materials is by definition independent of the strain level (see 3.2.2). The same concept is expressed in Figure 4.3b using the relaxation rate n, i.e. the slope obtained from curve fitting the data with a single-term power law t^n in time (dotted line). Note that the results are presented in logarithmic scale. A quasi-linear viscoelastic fit (dashed line) based on 0.6% strain predicts the same rate for the second test, hence it is not suitable for capturing the dependence of rate on strain. Similar results, with lower relaxation rates at higher maximum displacements are reported in [48] for ligaments. It is again emphasized that this non-linearity is not explicitly modelled by means of non-linear viscoelastic constitutive equations, but emerges as the result of the mixture of structure elements having different time-dependent characteristics. Thus, the model can effectively account for the viscoelastic non-linearity observed in experimental tests on AC [2].

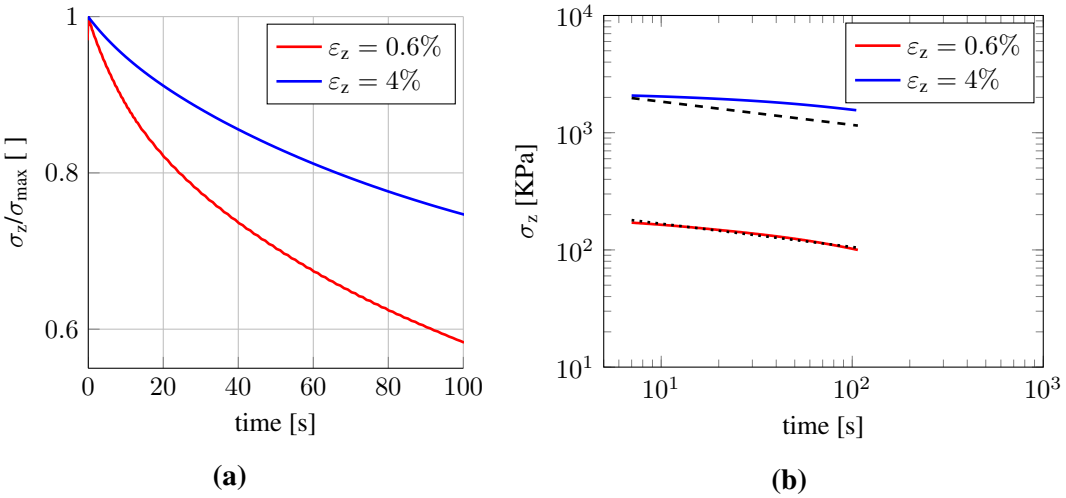

Figure 4.3: **(a)** Time evolution of normalized axial nominal stress for two tensile relaxation tests with different maximum displacement. **(b)** A QLV fit (dashed line) based on a power law fit (dotted line) of the results at low strain cannot reproduce stress relaxation at higher level of strain. The axes are in logarithmic scale.

The axial stress distribution at the end of the relaxation test is shown in Figure 4.4 for both tension (a) and compression (b). The complex stress state reveals again tension-compression

asymmetry. Note that the pattern of radial displacement is different for the two cases, even if the deformation is small due to the small displacement prescribed on the articular surface. During the tensile test, the fibres in the superficial zone, radially distributed, buckle due to the Poisson effect and the negative radial deformation is concentrated in the upper half of the specimen (note that the upper surface is undeformed as it is glued to the loading platen). On the other hand, during the compressive test the fibres in the superficial zone are subjected to positive stretch and try to counteract the effect of the axial displacement. Hence, the radial deformation is localized in the lower half of the specimen, where the fibres are mostly oriented perpendicularly to the subchondral bone (i.e. in the direction of the compressive load), and thus buckle and do not restrain the lateral expansion. The radial displacement is again zero at the lower surface as the deformation is constrained by the subchondral bone).

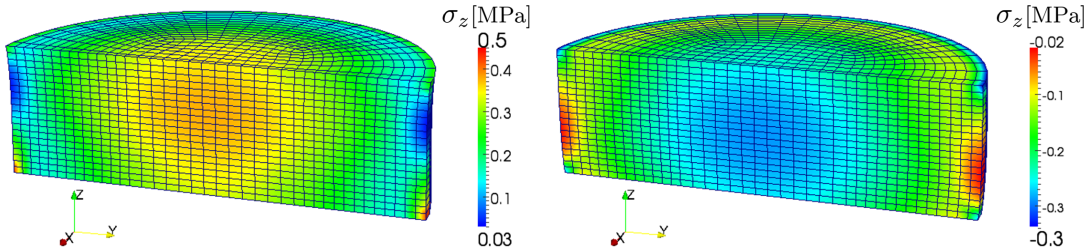

(a) tensile test **(b)** compressive test

Figure 4.4: Axial Cauchy stress distribution in deformed specimen at the end of the relaxation test ($t = 1200$s) for tension (a) and compression(b).

In relation to the mechanical response of the fibres described above, the overestimation of the fibre contribution in compression that emerges from Figure 4.2 can be related to the particular distribution of collagen fibres orientations used in this work. In particular the linear variation of the polar direction through the thickness leads to equally thick superficial and deep zones, whereas in harvested specimen the superficial zone is usually thinner. This implies that there are more fibres lying parallel to the articular surface and acting in compression, and accordingly less fibres are active in tension in the deep zone.

4.2 Unconfined compression of full thickness specimen

The main goal of this test is the analysis of the effect of the collagen fibres and their thickness-dependent distribution under compressive load. The axial load required during compression is plotted in Figure 4.5 against the prescribed compressive displacement on

the upper surface. The results show a non-linear response with a quadratic trend, which can clearly be related to the fibre contribution (if the response was dominated by the matrix, the plot would be similar to that of a neo-Hookean material). Also, they are in good agreement with experimental results from similar tests [44], which reinforce the idea that fibre contribution in compression should be taken into account. At the final displacement of 0.35 mm, the compressive load is equal to 49.9 N.

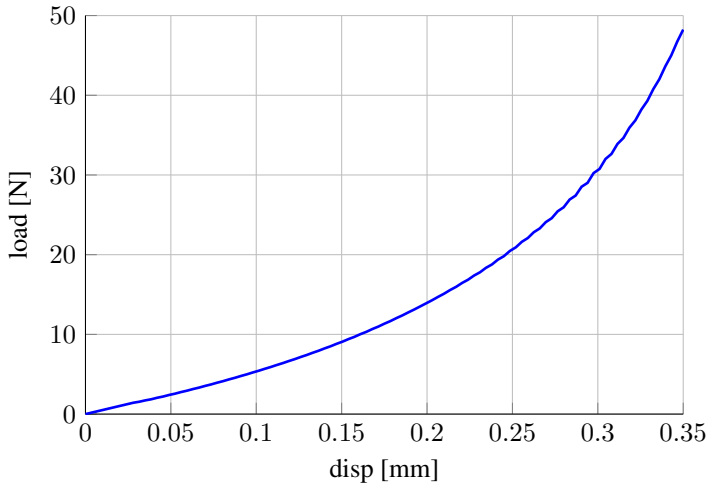

Figure 4.5: Load vs displacement for the unconfined compression of a full-thickness specimen of AC.

The Cauchy stress distribution in the deformed specimen is given in Figure 4.6. The structural inhomogeneity across the thickness, described by the structure tensor H, causes an inhomogeneous deformation. In accordance with [11], the displacement increases towards the deep zone and finally decreases at the bottom due to the constraint imposed by the subchondral bone. Even if the upper surface is not constrained in the radial direction, the action of the fibres, mainly distributed parallel to the articular surface in the superficial zone, limits the radial displacement, that consequently shows a non-linear profile along the thickness. The stress distribution confirms that the fibres of the superficial zone distributed in the radial direction are active in tension.

Moreover, Figure 4.6 shows how the deformation modifies the symmetries of the problem. In the reference configuration the problem is axial symmetric due to the geometry of the specimen and the fact that the fibre distribution varies across the thickness but is the same for all the points lying on the same transversal plane, and that the polar axis of the distribution does not violate the symmetry. In addition, the material is transversely isotropic as a result of the local transverse isotropy around the polar axis guaranteed by the chosen probability

function.

Due to the depth-dependent stiffness of the tissue, under compression the push-forward direction of the polar axis $\mathbf{k} = \mathbf{FK}$ is rotated with respect to its reference direction $\mathbf{K}$. Hence, the symmetry axis of the distribution is no longer aligned with the load. This in turn implies that the pattern of fibres activation and buckling is no longer symmetric with respect to $\mathbf{k}$ and local transverse isotropy is lost.

Nevertheless, the rotational symmetry of geometry, load and boundary conditions forces this rotation to be axial symmetric across each transverse section and global axial symmetry of the solution is preserved. In particular this prevents the rotation of the polar axis at each point lying on the axis of symmetry of the system. Thus, at these points the local transverse isotropy of the material is conserved during the deformation, as shown by the values of first and second principal Cauchy stresses in Figure 4.6 (note that the polar axis coincides with the axis of symmetry of the specimen).

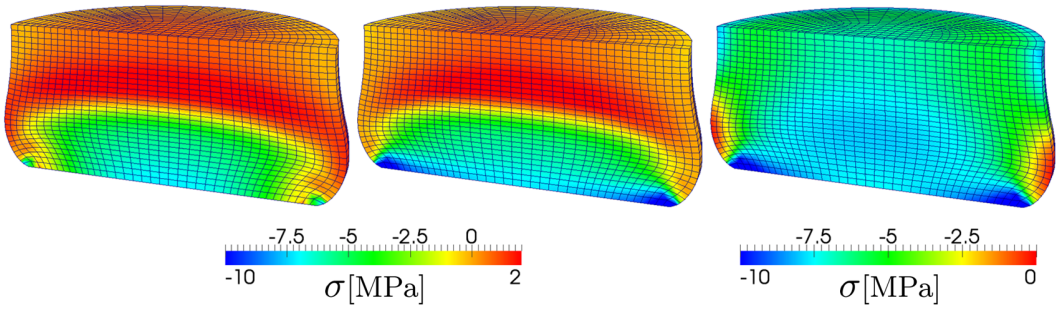

Figure 4.6: Distribution of first, second and third principal Cauchy stresses in a full-thickness cylindrical AC specimen under unconfined compression at maximum displacement $u = 0.35$mm. The articular surface is the upper surface, and the lower surface is attached to a layer of subchondral bone.

4.3 Unconfined compression of reduced thickness specimen

This test analyses the effect of loading frequency on the model response. The load versus displacement curves of the specimen are presented in Figure 4.7 at both the loading frequencies tested. The response has a quadratic trend similar to the one in Figure 4.5. The load values are lower as the specimen is not radially constrained at the bottom surface. The maximum loads registered are in the same range as those used in [44] to generate the same values of maximum displacement in a force-controlled test. In accordance with the reference study, the material is stiffer at higher loading frequency, while the trend remains quadratic in accor-

dance with the expression of the free energy. The reverse point of the cycle, where the unload phase starts, is sharper than in [44]. This is due to the fact that the sinusoidal loading used in the experiments was approximated imposing a triangular displacement. This also reduces the hysteresis area, i.e. the area between the loading and the unloading curves, which represents the energy loss due to viscoelastic dissipation (in regime of elasticity the unloading curve overlaps the loading curve). Nevertheless, a comparison with the results in [44] reveals that increasing the value of the viscoelastic parameter associated with the response at 0.1 Hz was not sufficient to compensate the effect of fluid flow, which is not modelled in this work and dominates the viscoelastic response at that frequency. Accordingly, changing the relaxation times to reproduce short time response of the material is not sufficient to reproduce the frequency dependent influence of the fluid. However, the results of the computations show lower hysteresis at higher frequency, in accordance with the values of the viscoelastic parameters and qualitatively with the curves in [44]. Moreover, the results at 1 Hz are in better agreement with the experimental study as the cycle is too fast for fluid exudation and AC starts behaving like an incompressible material.

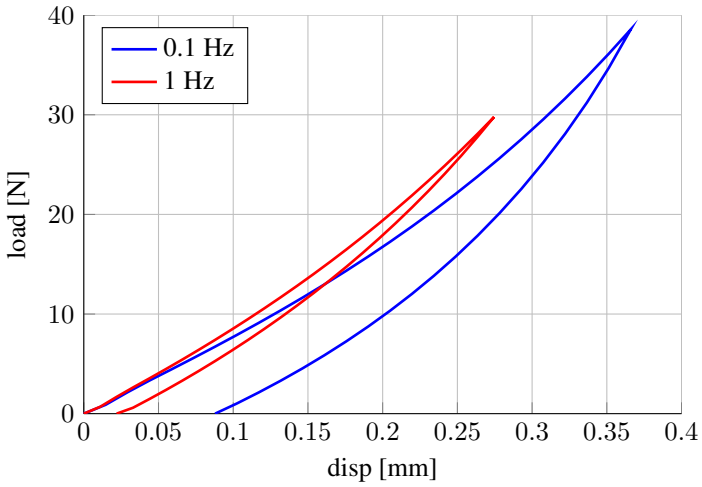

Figure 4.7: Load cycle versus displacement for the unconfined compression of a reduced thickness specimen of AC at two loading frequencies.

Figure 4.8 shows the principal Cauchy stresses distribution in the specimen corresponding to the maximum displacement in the test at 1 Hz. The largest deformation is at the bottom surface, which is free to deform radially. This is in accordance with the fact that in the deep zone most of the fibres are oriented in the direction of the load and buckle, while only a limited number of fibres can actively counteract the radial deformation. The lower load

required in this test compared to the one in section 4.2 is reflected in lower negative stresses than in Figure 4.6. The stress distribution is also sensibly different due to the change in the boundary conditions.

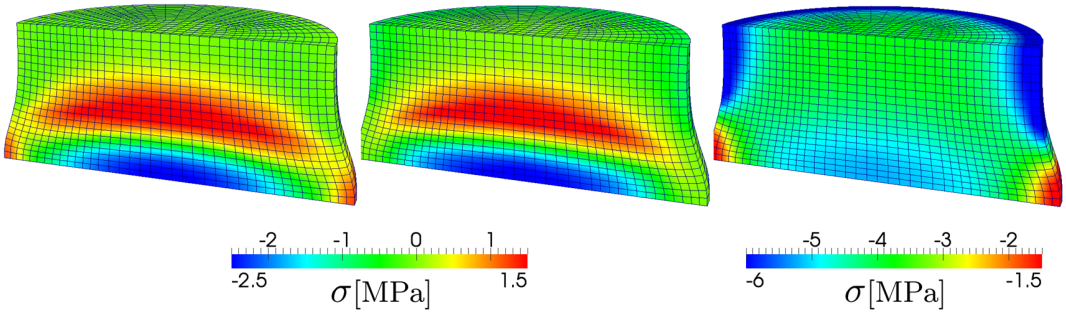

Figure 4.8: Distribution of the first, second and third principal Cauchy stresses in a cylindrical AC specimen under unconfined compression. Upper (articular) and lower surfaces are both unconstrained in the radial direction.

Using the specimen geometry and the force-displacement curves it is possible to compute the dynamic modulus, similarly to [44], as the ratio between the Cauchy normal stress, assumed homogeneous in this context to ease the comparison with the reference results in [44], and the stretch ratio ($\sigma_{33} = hF/(h_0 A_0)$, $\lambda_3 = h/h_0$). While the homogeneity of the normal stress across the thickness is an oversimplified assumption, the results can be interpreted as depth-averaged properties of the articular layer.

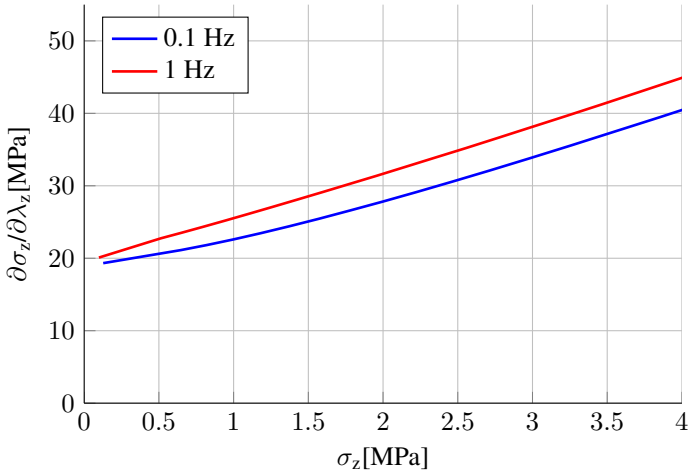

Figure 4.9: Dynamic modulus $\frac{\partial \sigma_z}{\partial \lambda_z}$ versus Cauchy normal stress σ_z

The incremental dynamic modulus is plotted in figure Figure 4.9 as a function of the Cauchy normal stress. The results are in agreement with the curves in Figure 4.7 and show that the dynamic modulus increases at higher loads. Moreover, the increment is higher at higher frequencies while the starting modulus has similar values. These trends, as well as the range

of computed values, are in good agreement with [44]. Moreover, the results support the hypothesis that the non-linear stiffening of collagen fibrils in tension regulates the dynamic properties in compression [55] through the mechanism described in the previous example.

Chapter 5

Conclusions

The present work developed a non-linear anisotropic viscoelastic constitutive model for AC, whose characteristics were illustrated by mean of three representative numerical examples.

The first objective was to define a structural quantity that represents the distributed collagen fibres in a continuum sense and that accounts for their directional characteristics. This was achieved through the computation of the directional average of the structure tensor at each material point. The use of averaging integrals it is not affected by the limitations of a finite number of fibres and on the computational side it does not require to store the information related to the fibre directions, but only the parameters of the distribution that represent them. The proposed definition for the structural contribution of compressed fibres effectively accounts for their distribution without influencing the value of the potential, according to the assumption that only stretched fibres can bear load. To the author's knowledge, such contribution represents an element of innovation in the study of biological tissues with statistical fibre orientation.

The generalized structure tensor introduced in this work extends the range of applicability of the averaged structure tensor presented in [13] to the modelling of tissues with inhomogeneous mechanical properties and fibre reinforcements without a preferential direction. The downside is represented by an increased computational cost of the model: the amount and direction of fibres that contributes to the structure tensor must be determined at each loading step, which in turn implies that the averaging integration has to be repeated for each material point. The increased level of complexity is anyway necessary to model AC, while it could be required in other applications to get more accurate predictions.

It should be noted that the developed structure representation does not account either for

shear interactions between matrix and fibres or fibre-fibre interaction due to entanglement, which can occur when fibre orientation has a statistical distribution. Such contributions are often disregarded and they would require the definition of additional generalized invariants to be included in the elastic potential.
The proposed approach is very general: it is compatible with any expression of the elastic potential that accounts for the presence of a structure tensor as well as any fibre distribution function, either in an analytical form as a probability density function or in a tabular form from experimental data. Hence, this work provides the framework for the development of more complex constitutive models. Moreover, AC represents only one of the possible applications of the model, which could be applied also to other tissues with statistical fibre orientation (e.g. the adventitial layer of the arterial walls).
The results of the numerical test show that the model can effectively account for the role of the fibre reinforcement in the response of AC. It reproduces the inhomogeneous and depth-dependent mechanical properties of the tissue and it accounts for the contribution of collagen under compressive load, suggesting that it should not be neglected. The computed deformation pattern is in agreement with theoretical predictions and experimental results from the literature.

The second objective was to introduce a formulation of the intrinsic viscoelastic properties of AC. A quasi-linear viscoelastic relation was chosen for collagen fibres, while the rest of the solid phase was assumed to be elastic. This is a partial limitation as other constituents (e.g. proteoglycans) are known to be viscoelastic. However, they play only a secondary role in the intrinsic time-dependent response.
The results of the numerical tests show that the model can effectively reproduce the response of AC observed in tension. On the other hand, the attempt to reproduce the viscoelastic behaviour in compression did not provide acceptable results, suggesting a dominant role of fluid-related viscoelastic response.
Nevertheless, the results demonstrate the expected frequency-related response, indicating that the model can be tuned using the viscoelastic parameters to reproduced specific experimental tests. In addition, the relaxation function was found to be strain-dependent, indicating that the model can reproduce the non-linear viscoelastic nature of the solid phase of AC.

The last goal was to develop a suitable numerical implementation for the model. The expres-

sion of the structure tensor in the spatial configuration was derived as well as those of the Cauchy stress and the elasticity tensor. These quantities where included into a finite element implementation based on efficient numerical schemes from the literature. In particular the evolution equations where integrated according to [21], while the directional average of the structure tensor is computed using a spherical design as in [9].
On the other hand, the dependence of the structure tensor on the deformation was disregarded in the derivation of the elasticity tensor as the value of the stretch in each direction (that discriminates between the two definitions for the contribution to the structure tensor) is taken from the previous solution step. This requires the definition of a high number of history variables to store the stretch values, which slows the calculation of the solution and can be a limitation for the maximum size of the problem, especially on regular personal computers. Moreover, a decrease in the rate of convergence of the solution scheme was experienced for relatively high compressive load. This can be related to instabilities generated by the progressive buckling of the fibres in compression, as the problem does not arise in tension.

It should also be noted that the particular choice of the strain energy potential is not based on experimental data. However, the quadratic function used in this work accounts for the non-linearity in the stress-strain curve due to fibre engagement and it is reported in the literature that a second order function can be sufficient to describe cases of interest such as immature or engineered cartilage. Moreover, it is again emphasized that the generality of the model allows the use of a function of higher order or of a different class (e.g. exponential) without the need to modify the implementation of the generalized structure tensor.
Similarly, the proposed fibre distribution density function is not based on experimental data but can qualitatively reproduce the depth-dependent arrangement of collagen reported in the literature. A drawback of the chosen distribution, which is based on a dispersion parameter that varies linearly through the thickness, is that it defines equally thick superficial and deep zones, whereas histological data indicate that the former should be thinner than the latter. This is reflected in an overestimation of the fibre contribution in the superficial layer to the compressive modulus of the tissue.

The last two remarks imply that a direct, quantitative comparison of the results of the model with published experimental results is not possible. However, the developed constitutive model for the solid phase of AC demonstrates correct physical behaviour and produces re-

sults qualitatively in agreement with the literature. In particular, it is capable of predicting the response of the tissue under tensile load both in terms of local stress and deformation and in terms of viscoelastic behaviour. The model is also able to account for the fibre contribution in compression, but at the current state it is not suitable for the analysis of the time-dependent response of AC in such configuration due to the important role of fluid flow, not included in the model.

Further enhancements include the use of experimental data for the definition of the expressions for the potential and the fibre distribution, as well as for the choice of the viscoelastic parameter. On the numerical side, the derivation of a consistent linearisation that accounts for the dependence of the structure tensor on the deformation would improve the performance of the model. Finally and most importantly, a formulation of the poroelastic phenomena arising from the presence of interstitial fluid should be added to the model in order to make it suitable to describe the time-dependent response of AC in compression.

References

[1] A. Agianniotis, R. Rezakhaniha, and N. Stergiopulos. A structural constitutive model considering angular dispersion and waviness of collagen fibres of rabbit facial veins. *BioMedical Engineering OnLine*, 10:18, 2011.

[2] G.A. Ateshian and S. Park. Dynamic response of immature bovine articular cartilage in tension and compression, and nonlinear viscoelastic modeling of the tensile response. *ASME Journal of biomechanical engineering*, 128:623–630, 2006.

[3] G.A. Ateshian, V. Raja, N.O. Chahine, C.E. Canal, and C.T. Hung. Modeling the matrix of articular cartilage using a continuous fiber angular distribution predicts many observed phenomena. *ASME Journal of Biomechanical Engineering*, 131:061003–10, 2009.

[4] D.L. Bader, G.E. Kempson, J. Egan, W. Gilbey, and A.J. Barrett. The effects of selective matrix degradation on the short-term compressive properties of adult human articular cartilage. *Biochimica et Biophysica Acta*, 1116(2):147–154, 1992.

[5] S. Below, S.P. Arnoczky, J. Dodds, C. Kooima, and N.J. Walter. The split-line pattern of the distal femur: a consideration in the orientation of autologous cartilage grafts. *Journal of Arthroscopic and Related Surgery*, 18:613–617, 2002.

[6] F. Brezzi and M. Fortin. *Mixed and hybrid Finite Element Methods*. Springer-Verlag, 1991.

[7] J. Buckwalter, H. Mankin, and A. Grodzinsky. Articular cartilage and osteoarthritis. *AAOS Instructional Course Lectures*, 54:465–480, 2005.

[8] Y. Cheng, J. Hootman, L. Murphy, G. Langmaid, and C. Helmick. Prevalence of doctor-diagnosed arthritis and arthritis-attributable activity limitation. *CDC: Morbidity and Mortality Weekly Report*, 59(39):1261–1265, 2010.

[9] S. Federico and T.C. Gasser. Nonlinear elasticity of biological tissues with statistical fibre orientation. *Journal of the Royal Society Interface*, 7(47):955–966, 2010.

[10] N. I. Fisher, T. L. Lewis, and B. J. J. Embleton. *Statistical analysis of spherical data.* Cambridge: Cambridge University Press, 1987.

[11] M. Fortin, M. D. Buschmann, M. J. Bertrand, F.S. Foster, and J. Ophir. Dynamic measurement of internal solid displacement in articular cartilage. *Journal of Biomechanics*, 29:340–360, 2003.

[12] Y.C. Fung. Biorheology of soft tissues. *Biorheology*, 10:139–155, 1973.

[13] T. Gasser, R.W. Ogden, and G.A. Holzapfel. Hyperelastic modelling of arterial layers with distributed collagen fibre orientations. *Journal of the Royal Society Interface*, 3(6):15–35, 2006.

[14] T.C. Gasser and C. Forsell. The numerical implementation of invariant-based viscoelastic formulations at finite strains. an anisotropic model for the passive myocardium. *Computer Methods in Applied Mechanics and Engineering*, 200(49):3637–3645, 2011.

[15] T.C. Gasser and G. Martufi. A constitutive model for vascular tissue that integrates fibril, fiber and continuum levels with application to the isotropic and passive properties of the infrarenal aorta. *Journal of Biomechanics*, 44:2544–2550, 2011.

[16] A. Getgood, T. Bhullar, and N. Rushton. Current concepts in articular cartilage repair. *Orthopaedics and Trauma*, 23:189–200, 2009.

[17] R. H. Hardin and N. J. A. Sloane. Mclaren's improved snub cube and other new spherical designs in three dimensions. *Discrete Computational Geometry*, 15:429–441, 1996.

[18] W. Hayes and L. Mockros. Viscoelastic properties of human articular cartilage. *Journal of Applied Physiology*, 31(4):562–568, 1971.

[19] J. Helfenstein, M. Jabareen, E. Mazza, and Govindjee S. On non-physical response in models for fiber-reinforced hyperelastic materials. *International Journal of Solids and Structures*, 47:2056–2061, 2010.

[20] G. Holzapfel. On large strain viscoelasticity: Continuum formulation and finite element applications to elastomeric structures. *Intenational Journal of Numerical Methods in Engineering*, 39:3903–3926, 1996.

[21] G. A. Holzapfel and T. C. Gasser. A viscoelastic model for fiber-reinforced composites at finite strains: continuum basis, computional aspects and applications. *Computater Methods in Applied Mechanics and Engineering*, 190:4397–4403, 2001.

[22] G. A. Holzapfel, T. C. Gasser, and R. W. Ogden. A new constitutive framework for arterial wall mechanics and a comparative study of material models. *Journal of Elasticity*, 61:1–48, 2000.

[23] G. A. Holzapfel, T. C. Gasser, and M. Stadler. A structural model for the viscoelastic behavior of arterial walls: continuum formulation and finite element analysis. *European Journal of Mechanics A/Solids*, 21:441–463, 2002.

[24] G. A. Holzapfel and H. W. Weizsäcker. Biomechanical behavior of the arterial wall and its numerical characterization. *Computational biology and medicine*, 28:377–392, 1998.

[25] G.A. Holzapfel. *Nonlinear Solid Mechanics: A Continuum Approach for Engineering*. Wiley, 2000.

[26] C. Huang, V.C. Mow, and G.A. Ateshian. The role of flow-independent viscoelasticity in the biphasic tensile and compressive responses of articular cartilage. *ASME Journal of Biomechanical Engineering*, 123:410–417, 2001.

[27] C.Y. Huang, M.A. Soltz, M. Kopacz, V.C. Mow, and G.A. Ateshian. Experimental verification of the roles of intrinsic matrix viscoelasticity and tension-compression nonlinearity in the biphasic response of cartilage. *ASME Journal of Biomechanical Engineering*, 125:84–93, 2003.

[28] U. Hueck, B. Reddy, and Wriggers P. On the stabilization of the rectangular fournode quadrilateral element. *Communications in Applied Numerical Methods*, 10:555–563, 1994.

[29] J. D. Humphrey. Continuum biomechanics of soft biological tissues. *Proceedings of the Royal Society A*, 459:1–44, 2003.

[30] E. B. Hunziker. Articular cartilage repair: basic science ad clinical progress. a review of the current status and prospects. *Osteoarthritis and Cartilage*, 10:432–463, 2002.

[31] S. M. Klisch. A bimodular polyconvex anisotropic strain energy function for articular cartilage. *ASME Journal of Biomechanical Engineering*, 129:250–258, 2007.

[32] S.M. Klisch, R.L. Sah, P. Vena, A. Asanbaeva, and G.C. Thomas. A nonlinear constituent based viscoelastic model for articular cartilage and analysis of tissue remodeling due to altered glycosaminoglycan-collagen interactions. *ASME Journal of Biomechanical Engineering*, 131:101002, 2009.

[33] Y. Lanir. Constitutive equations for fibrous connective tissues. *Journal of Biomechanics*, 16:1–12, 1983.

[34] L.P. Li and W. Herzog. The role of viscoelasticity of collagen ffiber in articula cartilage: Theory and numerical formulation. *Biorheology*, 41:181–194, 2004.

[35] L.P. Li, W. Herzog, R.K. Korhonen, and J.S. Jurvelin. The role of viscoelasticity of collagen ffiber in articular cartilage: axial tension versus compression. *Medical Engineering & Physics*, 27:51–57, 2005.

[36] M. Lilledahl, D. Pierce, T. Ricken, G. Holzapfel, and C. de Lange Davies. Structural analysis of articular cartilage using multiphoton microscopy: input for biomechanical modeling. *IEEE Transactions on Medical Imaging*, 30(9):1635–1648, 2011.

[37] F. Maceri, M. Marino, and G. Vairo. A unified multiscale mechanical model for soft collagenous tissues with regular fiber arrangement. *Journal of Biomechanics*, 43:355–363, 2010.

[38] J.M. Mansour. *Kinesiology: the mechanics and pathomechanics of human movement*, chapter Biomechanics of cartilage. Lippincott Williams & Wilkins, 2004.

[39] C. Miehe. Multisurface thermoplasticity for single crystals at large strains in terms of eulerian vector updates. *International Journal of Solids and Structures*, 33:3103–3130, 1996.

[40] R.J. Minns and F.S. Steven. The collagen fiber organization in human articular cartilage. *Journal of Anatomy*, 123(2):437–457, 1977.

[41] J. Mollenhauer, M. Aurich, C. Muehleman, G. Khelashvilli, and T.C. Irving. X-ray diffraction of the molecular substructure of human articular cartilage. *Connective Tissue Research*, 44:201–207, 2003.

[42] V. C. Mow, A. Ratcliffe, and A.R. Poole. Cartilage and diarthrodial joints as paradigms for hierarchical materials and structures. *Biomaterials*, 13:67 – 97, 1992.

[43] S. Park and G. A. Ateshian. Dynamic response of immature bovine articular cartilage in tension and compression, and nonlinear viscoelastic modeling of the tensile response. *ASME Journal of Biomechanical Engineering*, 128(4):623–630, 2006.

[44] S. Park, C. Hung, and G. A. Ateshian. Mechanical response of bovine articular cartilage under dynamic unconfined compression loading at physiological stress levels. *Osteoarthritis and Cartilage*, 12:65–73, 2004.

[45] D. Pierce, W. Trobin, J. Raya, S. Trattnig, H. Bischof, C. Glaser, and G. Holzapfel. Dt-mri based computation of collagen fiber deformation in human articular cartilage: a feasibility study. *Annals of Biomedical Engineering*, pages 2447–2463, 2010.

[46] D. Pierce, W. Trobin, S. Trattnig, H. Bischf, and G. Holzapfel. A phenomenological approach toward patient-specific computational modeling of articular cartilage including collagen fiber tracking. *Journal of Biomechanical Engineering*, 131:091006–1:12, 2009.

[47] D.M. Pierce, T. Ricken, and G.A. Holzapfel. A hyperelastic biphasic fibre-reinforced model of articular cartilage considering distributed collagen fibre orientations: continuum basis, computational aspects and applications. *Computer Methods in Biomechanics and Biomedical Engineering*, pages 1–18, 2012.

[48] P. Provenzano, R. Lakes, T. Keenan, and R.J. Vanderby. Nonlinear ligament viscoelasticity. *Annals of Biomedical Engineering*, 29:908–914, 2001.

[49] J. Rieppo, M.M. Hyttinen, E. Halmesmaki, H. Ruotsalainen, A. Vasara, I. Kiviranta, J.S. Jurvelin, and H.J. Helminen. Changes in spatial collagen content and collagen network architecture in porcine articular cartilage during growth and maturation. *Osteoarthritis and Cartilage*, 17(4):448–455, 2009.

[50] M. Sacks. Incorporation of experimentally-derived fiber orientation into a structural constitutive model for planar collagenous tissues. *ASME Journal of Biomechanical Engineering*, 125:280–287, 2003.

[51] R. Shirazi, P. Vena, R.L. Sah, and S.M. Klisch. Modeling the collagen fibril network of biological tissues as a nonlinearly elastic material using a continuous volume fraction distribution function. *Mathematics and Mechanics of Solids*, 16(7):706–715, 2011.

[52] J.C. Simo. On a fully three-dimensional finite-strain viscoelastic damage model: formulation and computational aspects. *Computer Methods in Applied Mechanics and Engineering*, 60:153–173, 1987.

[53] J.C. Simo, R.L. Taylor, and K.S. Pister. Variational and projection methods for the volume constraint in finite deformation elastoplasticity. *Computer Methods in Applied Mechanics and Engineering*, 51:177–208, 1985.

[54] M.A. Soltz and G.A. Ateshian. A cone wise linear elasticity model for the analysis of tension-compression nonlinearity of articular cartilage. *ASME Journal of Biomechanical Engineering*, 122(5):576–586, 2000.

[55] J. Soulhat, M. D. Buschmann, and Shirazi-Adl A. A fibril-network-reinforced biphasic model of cartilage in unconfined compression. *ASME Journal of Biomechanical Engineering*, 121:340–347, 1999.

[56] A. J. M. Spencer. Constitutive theory for strongly anisotropic solids. in continuum theory of the mechanics of fibre-reinforced composites. *CISM Courses and Lectures*, 282:1–32, 1984.

[57] J. K. Suh and S. Bai. Finite element formulation of biphasic poroviscoelastic model for articular cartilage. *ASME Journal of Biomechanical Engineering*, 120:195–201, 1998.

[58] J.K. Suh and M.R. Di Silvestro. Biphasic poroviscoelastic behavior of hydrated biological soft tissue. *ASME Journal of Biomechanical Engineering*, 66:528–535, 1999.

[59] R. L. Taylor. *FEAP - a finite element analysis program, version 8.2 user manual.* Berkeley, CA: University of California at Berkeley, 2007.

[60] R.L. Taylor, K.S. Pister, and G.L. Goudreau. Thermomechanical analysis of viscoelastic solids. *International Journal of Numerical Methods*, 2:45–59, 1970.

[61] M.C van Turnhout, M.B. Haazelager, M. A. L. Gijsen, H. Schipper, S. Kranenbarg, and J. L. van Leeuwen. Quantitative description of collagen structure in the articular

cartilage of the young and adult equine distal metacarpus. *Animal Biology*, 58:353–370, 2008.

[62] P. Vena, D. Gastaldi, and R. Contro. A constituent-based model for the nonlinear viscoelastic behavior of ligaments. *ASME Journal of Biomechanical Engineering*, 128(3):449–457, 2006.

[63] T. Vos, A.D. Flaxman, M. Naghavi, and R. Lozano. Years lived with disability (ylds) for 1160 sequelae of 289 diseases and injuries 1990–2010: a systematic analysis for the global burden of disease study 2010. *Lancet*, 380 (9859):2163–96, 2012.

[64] J. A. Weiss, B. N. Maker, and S. Govindjee. Finite element implementation of incompressible, transversely isotropic hyperelasticity. *Computater Methods in Applied Mechanics and Engineering*, 135:107–128, 1996.

[65] E. W. Weisstein. Erfi, see http://mathworld.wolfram.com/erfi.html, 2005.

[66] W. Wilson, C.C. van Donkelaar, R. van Rietbergen, and R. Huiskes. The role of computational models in the search for the mechanical behavior and damage mechanisms of articular cartilage. *Medical engineering and Physics*, 27:810–826, 2005.

[67] S.L.Y. Woo, B.R. Simon, S.C. Kuei, and W.H. Akeson. Quasi-linear viscoelastic properties of normal articular cartilage. *ASME Journal of Biomechanical Engineering*, 102:85–90, 1980.

[68] P. Wriggers. *Nonlinear Finite Element Methods*. Springer, 2008.

[69] O.C. Zienkiewicz and R.L. Taylor. *The Finite Element Method: Basis and Fundamentals*. Butterworth-Heinemann, 2000.

[70] O.C. Zienkiewicz and R.L. Taylor. *The Finite Element Method: Solid Mechanics*, volume 2. Butterworth-Heinemann, 5 edition, 2000.